U.S. Department of Transportation
Federal Railroad Administration

An Experimental Investigation of the Discharge of a Flashing Liquid from a Finite Reservoir

Office of Research and Development
Washington, D.C. 20590

A Fundamental Study of the Two-Phase Flow Phenomena Occurring During Venting from Rail Tank Cars

S.R. Rod
M. Gühler
D.W. Sallet

Department of Mechanical Engineering
University of Maryland
College Park, Maryland 20742

DOT/FRA/ORD-85/05

January 1985
Final Report

NOTICE

This document is disseminated under the sponsorship of the Department of Transportation in the interest of information exchange. The United States Government assumes no liability for its contents or use thereof.

NOTICE

The United States Government does not endorse products or manufacturers. Trade or manufacturers' names appear herein solely because they are considered essential to the object of this report.

Technical Report Documentation Page

1. Report No.	2. Government Accession No.	3. Recipient's Catalog No.

4. Title and Subtitle
An Experimental Investigation of the Discharge of a Flashing Liquid from a Finite Reservoir: A Fundamental Study of the Two-Phase Flow Phenomena Occurring During Venting from Rail Tank Cars

5. Report Date
August 1984

6. Performing Organization Code

8. Performing Organization Report No.

7. Author(s)
S. R. Rod, M. Gühler and D. W. Sallet*

9. Performing Organization Name and Address
Department of Mechanical Engineering
University of Maryland
College Park, MD 20742

10. Work Unit No. (TRAIS)

11. Contract or Grant No.
D.O.T.-FR-64181

13. Type of Report and Period Covered
Final Report
August 1975-August 1984

12. Sponsoring Agency Name and Address
U.S. Department of Transportation
Federal Railroad Administration
Office of Research and Development
Washington, D.C. 20590

14. Sponsoring Agency Code

15. Supplementary Notes
* Comments or discussion relating to the contents of this report should be addressed to the Project Director of this investigation, Professor D.W. Sallet, Department of Mechanical Engineering, The University of Maryland, College Park, MD 20742.

16. Abstract

The design of pressure relief valves for railroad tank cars containing pressurized liquid commodities is dependent on knowledge of venting rates during accidents. In turn, development of an appropriate theoretical model requires knowledge of many properties which affect the venting rates of vapor, liquid and two-phase mixtures.

Previous reports and technical papers on this phenomenon published by members of the Mechanical Engineering Department of the University of Maryland as part of the D.O.T. sponsored project have described experimental investigations of the blowdown of flashing liquids from finite vessels. In these studies the system mass, pressure, vertical temperature profile and mass flow rate were measured. This report describes experiments which expand upon previous studies to include measurements of horizontal temperature variations, quality of the two-phase mixture, bubble rise velocities and growth rates, fluid flow patterns and boiling phenomena during the blowdown.

Venting tests were conducted with three different orifice sizes, four liquid fill fractions and two wall materials of different thermal conductivity. From this new data a detailed description of the two-phase blowdown is presented, including boiling and heat transfer effects. The essential visual features of the two phase flow and boiling were recorded with a high speed 16 mm movie camera. An edited film was produced and is available for future review of the phenomena described in this report.

17. Key Words	18. Distribution Statement
Two-Phase Flow, Pressure Vessel, Blowdown, Rail-Tank Car Venting, Two-Phase Boiling, Flashing Flow, Venting of Compressed Liquified Vapor	This document is available to the public through the National Technical Information Service, Springfield, VA 22161

19. Security Classif. (of this report)	20. Security Classif. (of this page)	21. No. of Pages	22. Price
Unclassified	Unclassified	131	

METRIC CONVERSION FACTORS

Approximate Conversions to Metric Measures

Symbol	When You Know	Multiply by	To Find	Symbol
LENGTH				
in	inches	*2.5	centimeters	cm
ft	feet	30	centimeters	cm
yd	yards	0.9	meters	m
mi	miles	1.6	kilometers	km
AREA				
in^2	squere inches	6.5	square centimeters	cm^2
ft^2	squere feet	0.09	squere meters	m^2
yd^2	square yards	0.8	square meters	m^2
mi^2	square miles	2.6	square kilometers	km^2
	acres	0.4	hecteres	ha
MASS (weight)				
oz	ounces	28	grams	g
lb	pounds	0.45	kilograms	kg
	short tons (2000 lb)	0.9	tonnes	t
VOLUME				
tsp	teaspoons	5	milliliters	ml
Tbsp	tablespoons	16	milliliters	ml
fl oz	fluid ounces	30	milliliters	ml
c	cups	0.24	liters	l
pt	pints	0.47	liters	l
qt	quarts	0.95	liters	l
gal	gallons	3.8	liters	l
ft^3	cubic feet	0.03	cubic meters	m^3
yd^3	cubic yards	0.76	cubic meters	m^3
TEMPERATURE (exact)				
°F	Fahrenheit temperature	5/9 (after subtracting 32)	Celsius temperature	°C

*1 In. = 2.54 cm (exactly). For other exact conversions and more detail tables see NBS Misc. Publ. 286, Units of Weight and Measures. Price $2.25 SD Catalog No. C13 10 286.

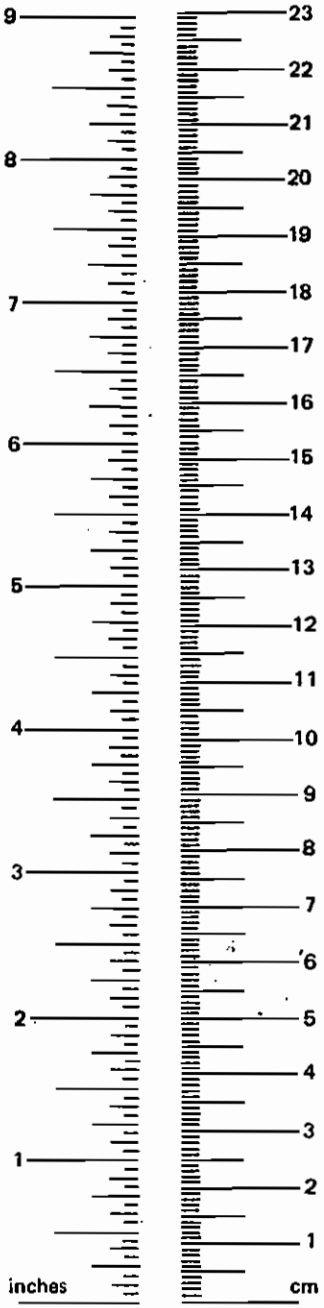

Approximate Conversions from Metric Measures

Symbol	When You Know	Multiply by	To Find	Symbol
LENGTH				
mm	millimeters	0.04	inches	in
cm	centimeters	0.4	inches	in
m	meters	3.3	feet	ft
m	meters	1.1	yards	yd
km	kilometers	0.6	miles	mi
AREA				
cm^2	square centimeters	0.16	square inches	in^2
m^2	square meters	1.2	square yerds	yd^2
km^2	square kilometers	0.4	square miles	mi^2
he	hectares (10,000 m^2)	2.5	acres	
MASS (weight)				
g	grams	0.035	ounces	oz
kg	kilograms	2.2	pounds	lb
t	tonnes (1000 kg)	1.1	short tons	
VOLUME				
ml	milliliters	0.03	fluid ounces	fl oz
l	liters	2.1	pints	pt
l	liters	1.06	querts	qt
l	liters	0.26	gallons	gal
m^3	cubic meters	36	cubic feet	ft^3
m^3	cubic meters	1.3	cubic yards	yd^3
TEMPERATURE (exact)				
°C	Celsius temperature	9/5 (then add 32)	Fahrenheit temperature	°F

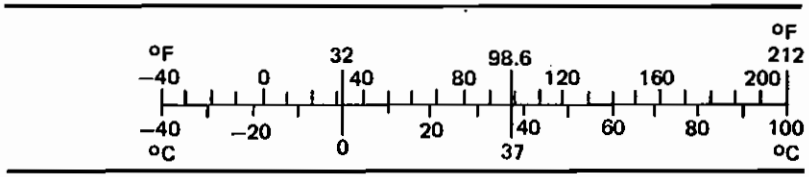

TABLE OF CONTENTS

CHAPTER		PAGE
I.	INTRODUCTION	1
II.	EXPERIMENTAL APPARATUS AND PROCEDURE	6
	Experimental Apparatus	6
	Instrumentation	11
	Experimental Procedure	15
	Data Reduction	17
III.	INITIAL TRANSIENTS	21
	General Description	21
	Comparison of Individual Tests	23
IV.	THE BLOWDOWN FOLLOWING INITIAL TRANSIENTS	40
	General Description	40
	Pressure Decay	41
	Liquid Temperature Profiles	50
	Vapor Superheat	58
	System Mass and Mass Discharge Rate	68
	Boiling Characteristics	75
	Two-Phase Column Characteristics	87
V.	THE BLOWDOWN PROCESS MODEL	92
	Heat Transfer Effects	92
	The Computer Simulation	97
	Comparison of Individual Tests	109
VI.	CONCLUSION	111
REFERENCES		113
APPENDIX A:	Governing Formulas of the Blowdown Model	115
APPENDIX B:	Application of the Martin-Hou Equation of State to the Generation of Pressure-Volume-Temperature Data for a Pure Saturated Vapor	118
APPENDIX C:	Listing of the Computer Program	123

LIST OF TABLES

TABLE		PAGE
1.	List of Tests Conducted	5
2.	Initial Mass Flow Rates	24
3.	Initial Decompression and Recovery	25
4.	Vapor Region Temperatures and Thermal Gradients	66
5.	Comparison of Some Measured Bubble Rise Velocities to Theory	86
6.	Maximum Two-Phase Column Quality and Void Fraction	90
7.	Thermophysical Properties of Plexiglas and Aluminum	94
8.	Properties of the Experimental Vessel	94
B-1.	Results of the First Set of Trial Optimizations	121

LIST OF FIGURES

Figure		Page
1.	The Instrumented Sections.	7
2.	The Orifice and Exit Section.	8
3.	Cross Section of Experimental Chamber.	8
4.	The Assembled Test Stand.	9
5.	Schematic of Pressure Vessel with Locations of Thermocouples.	10
6.	The Pressure Probe Piston Assembly.	12
7.	Initial Pressure Transients.	26
8.	Initial Temperature Transients.	27
9.	Boiling Patterns at the Beginning of the Initial Transient.	31
10.	Boiling Patterns at the End of the Initial Transient: 100% Liquid Fill Tests.	33
11.	Boiling Patterns at the End of the Initial Transient: 75% Liquid Fill Tests.	34
12.	Boiling Patterns at the End of the Initial Transient: 50% Liquid Fill Tests.	35
13.	Boiling Patterns at the End of the Initial Transient: 25% Liquid Fill Tests.	36
14.	Pressure Decay Curve: 1.59mm Orifice Plexiglas Wall Tests.	42
15.	Pressure Decay Curve: 1.59mm Orifice Aluminum Wall Tests.	43
16.	Pressure Decay Curve: 3.18mm Orifice Plexiglas Wall Tests.	44
17.	Pressure Decay Curve: 3.18mm Orifice Aluminum Wall Tests.	45
18.	Pressure Decay Curve: 4.76mm Orifice Plexiglas Wall Tests.	46
19.	Pressure Decay Curve: 4.76mm Orifice Aluminum Wall Tests.	47
20.	Temperature Decay Curve: 1.59mm Orifice Plexiglas Wall Tests.	51
21.	Temperature Decay Curve: 1.59mm Orifice Aluminum Wall Tests.	52

LIST OF FIGURES (CONTINUED)

Figure		Page
22.	Temperature Decay Curve: 3.18mm Orifice Plexiglas Wall Tests.	53
23.	Temperature Decay Curve: 3.18mm Orifice Aluminum Wall Tests.	54
24.	Temperature Decay Curve: 4.76mm Orifice Plexiglas Wall Tests.	55
25.	Temperature Decay Curve: 4.76mm Orifice Aluminum Wall Tests.	56
26.	Liquid Superheat at the Beginning of the 100% Liquid Fill Tests.	57
27.	The Thermal Gradient in the Superheated Vapor Region: 1.59mm Orifice, 100% Liquid Fill, Plexiglas Wall Test.	59
28.	The Thermal Gradient in the Superheated Vapor Region: 1.59mm Orifice, 100% Liquid Fill, Aluminum Wall Test.	60
29.	The Thermal Gradient in the Superheated Vapor Region: 1.59mm Orifice, 87% Liquid Fill, Aluminum Wall Test.	61
30.	The Thermal Gradient in the Superheated Vapor Region: 1.59mm Orifice, 75% Liquid Fill, Aluminum Wall Test.	62
31.	The Thermal Gradient in the Superheated Vapor Region: 1.59mm Orifice, 50% Liquid Fill, Aluminum Wall Test.	63
32.	Vapor Superheat Profile in the Pressure Vessel.	65
33.	Discharged Mass: 1.59mm Orifice Plexiglas Wall Tests.	69
34.	Discharged Mass: 1.59mm Orifice Aluminum Wall Tests.	70
35.	Discharged Mass: 3.18mm Orifice Plexiglas Wall Tests.	71
36.	Discharged Mass: 3.18mm Orifice Aluminum Wall Tests.	72
37.	Discharged Mass: 4.76mm Orifice Plexiglas Wall Tests.	73
38.	Discharged Mass: 4.76mm Orifice Aluminum Wall Tests.	74
39.	Instantaneous Mass Discharge Rate: 1.59mm Orifice Plexiglas Wall Tests.	76

LIST OF FIGURES (CONTINUED)

Figure		Page
40.	Instantaneous Mass Discharge Rate: 1.59mm Orifice Aluminum Wall Tests.	77
41.	Instantaneous Mass Discharge Rate: 3.18mm Orifice Plexiglas Wall Tests.	78
42.	Instantaneous Mass Discharge Rate: 3.18mm Orifice Aluminum Wall Tests.	79
43.	Instantaneous Mass Discherge Rate: 4.76mm Orifice Plexiglas Wall Tests.	80
44.	Instantaneous Mass Discharge Rate: 4.76mm Orifice Aluminum Wall Tests.	81
45.	Histogram of Measured Bubble Rise Velocities.	84
46.	Average Quality of the Two-Phase Column Versus Time for the 100% Fill Tests.	88
47.	Average Void Fraction of the Two-Phase Column Versus Time for the 100% Fill Tests.	89
48.	Total Theoretical Heat Input to Fluid Versus Time for the 100% Liquid Fill Tests.	99
49.	Theoretical and Experimental Pressure Decay: 1.59mm Orifice, 100% Liquid Fill Tests.	100
50.	Theoretical and Experimental Temperature Decay: 1.59mm Orifice, 100% Liquid Fill Tests.	101
51.	Theoretical and Experimental Mass Discharge: 1.59mm Orifice, 100% Liquid Fill Tests.	102
52.	Theoretical and Experimental Pressure Decay: 3.18mm Orifice, 100% Liquid Fill Tests.	103
53.	Theoretical and Experimental Temperature Decay: 3.18mm Orifice, 100% Liquid Fill Tests.	104
54	Theoretical and Experimental Mass Discharge: 3.18mm Orifice, 100% Liquid Fill Tests.	105
55.	Theoretical and Experimental Pressure Decay: 4.76mm Orifice, 100% Liquid Fill Tests.	106

LIST OF FIGURES (CONTINUED)

Figure		Page
56.	Theoretical and Experimental Temperature Decay: 4.76mm Orifice, 100% Liquid Fill Tests.	107
57.	Theoretical and Experimental Mass Discharge: 4.76mm Orifice, 100% Liquid Fill Tests.	108
C-1.	Flowchart of the Blowdown Process Model.	124

NOMENCLATURE

c	specific heat, J/kg°C	
d	diameter, m	
E	total system energy, J	
g	gravitational acceleration, 9.80 m/s^2	
g_c	gravitational conversion factor, 1 $Ns^2/kg \cdot m$	
H	height, m	
h	specific enthalpy, J/kj	see context
h	heat transfer coefficient, $J/m^2s°C$	see context
k	thermal conductivity, $J/m \cdot s°C$	
L_c	characteristic length, m (defined in text)	
m	mass, kg	
P	pressure, N/m^2	
Q	total heat transfer, J	
q	heat transfer per unit area, J/m^2	
R	radius, m	
T	temperature, °C	
T_i	thermocouple #i (i = integer)	
t	time, s	
V	velocity, m/s	
v	specific volume, m^3/kg	
W	work, J	see context
W	width, m	see context
x	quality, nondimensional	
z	elevation, m	

α	thermal diffusivity, m^2/s	see context
α	void fraction, nondimensional	
μ	viscosity, $kg/m \cdot s$	
ρ	density, kg/m^3	
σ	surface tension, N/m	

Superscripts

$-$	average value
$\cdot$	$\frac{d}{dt}$, first derivative with respect to time

Subscripts

a	air boundary layer
b	bubble
e	exit
f	liquid
fg	difference between vapor and liquid value
g	gas or vapor
l	liquid
o	initial
p	constant pressure

I. INTRODUCTION

Safety considerations in the design of many current hydraulic systems require knowledge of the behavior of saturated liquids subjected to sudden depressurization. Such accidents as steam line breaks in pressurized water nuclear reactors or the puncture of tanks containing compressed liquid commodities involve the rapid depressurization of the container through the venting of its contents.

One aspect of the pressurized liquid venting problem is of particular concern to the railroad industry. Many flammable, volatile and toxic substances such as propane, chlorine and ammonia are shipped by rail as liquids in pressurized tank cars. In derailments some cars may immediately rupture, spilling burning liquids. Other cars can then rupture explosively as heat input from surrounding fires raises their cargo's vapor pressure past the bursting point of the tank. The goal of safety design, therefore, is to relieve the internal pressure by controlled venting through valves actuated at some pressure below the tank's burst pressure.

Early safety valve design was based on the assumption of pure vapor flow. However, recent studies have demonstrated that the violent boiling which occurs during depressurization can result in liquid flow through the valve. Furthermore, entrained liquid in the exit flow has the effect of reducing the pressure relieving capability of the valve.

The necessary analysis of two-phase discharge becomes complex. Consideration must be made of heat transfer and boiling characteristics of the system, exit flow quality and any non-equilibrium effects such as liquid or vapor superheat or a non-unity slip ratio. That the entire

process is unsteady complicates the analysis further.

Several investigations, both experimental and theoretical, have been made of the unsteady blowdown of flashing liquids from pressurized containers. Tanger, Vachon and Pollard [1] studied the response of pool boiling in water to sudden depressurization. Ordin, Weiss and Christenson [2] performed similar studies on liquid hydrogen, while Clark, Van Wylen and Fenster [3] studied liquid nitrogen. These and other related reports make similar observations of pressure and temperature histories of venting systems, but they do not look into the important two-phase flow characteristics of the systems.

Researchers at the Mechanical Engineering Department at the University of Maryland, supported by the U. S. Department of Transportation, have begun a basic and detailed study of two-phase discharge from finite vessels. Publications by Sallet et al [4], [5] & [6] describe experiments which concurrently measured system pressure and mass, vertical temperature distribution and instantaneous mass flow rate during the blowdown of propane and Freon-12 (dichlorodifluoromethane). The results are consistent with similar studies of other liquids, but one previously unreported phenomenon was observed. A strong thermal gradient developed in the vapor space above the boiling liquid surface. The temperature at the top of the vessel became as much as 40°C (72°F) above the liquid temperature at late times in the blowdown. The mechanism generating the gradient is as yet unexplained.

This report describes an experimental investigation of two-phase discharge which expands upon those carried out earlier at the University of Maryland. The purpose is to significantly enlarge the experimental data base on individual tests to include heat transfer, boiling and two-

phase flow data as well as pressure, temperature and mass discharge rate measurements. The additional data will support a more detailed theoretical model of the blowdown process.

A small (1.1 liter, 0.039 ft^3) vessel is filled with Freon-12 at ambient temperature and is allowed to discharge through a square-edged orifice at the top of the chamber. System pressure and mass are continuously monitored. A vertical array of 6 thermocouples and a horizontal array of 3 thermocouples measure local temperatures and provide data on horizontal as well as vertical thermal gradients. High speed motion pictures (300 frames/second) are taken to record details of boiling phenomena (bubble nucleation sizes, growth rates and rise velocities) and of the two-phase flow (liquid entrainment in the exit flow, two-phase column height and void fraction). When combined, the accumulated data give additional information on liquid superheat or subcooling, quality of the two-phase column, vapor superheat and instantaneous mass discharge rate.

Thirty-three fully instrumented blowdowns are conducted. They are grouped according to the diameter of the orifice, the initial mass of Freon-12 (i.e. initial percentage fill of liquid) and the composition of the vessel's side walls (aluminum or plexiglas). A summary of the tests is given as Table 1.

Three orifice diameters. 1.59 mm (1/16 in), 3.18 mm (1/8 in) and 4.76 mm (3/16 in) are employed to evaluate the effect of the rate of mass discharge on the boiling characteristics and the blowdown process. Similarly, several percentage fills are used to determine the effect that different proportions of vapor and liquid (implying not only variations in initial mass but also in initial internal energy) have on

the blowdown in general and especially on the two-phase characteristics of the exit flow. The two wall materials are used to determine the effect of heat transfer from the environment on the blowdown. The thermal conductivity (k) of aluminum is about 1200 times that of plexiglas and the thermal diffusivity (α) of aluminum is about 800 times that of plexiglas at the temperatures at which the tests are run. Some duplicate tests are run to check reproducibility, which is indeed verified.

Descriptions of the visible phenomena are presented for the distinct initial transient, which lasts about 1.5 seconds, and for the remainder of the blowdown. The pressure and temperature decay rates and the mass flow rates of each test are plotted and compared. Data on bubble nucleation and motion, heat transfer effects and the observed dramatic thermal gradient in the vapor space are discussed. Finally, a computer model of the blowdown (simple, but incorporating the major relevant aspects of the process) is developed and compared to exprerimental results.

Table 1. List of Tests Conducted

ORIFICE DIAMETER	INITIAL % FILL OF LIQUID	INITIAL MASS OF FREON-12	WALL MATERIAL
1.59 mm	100 %	1530 g	aluminum, plexiglas
1.59	97	1480	aluminum only
1.59	93	1430	aluminum only
1.59	87	1335	aluminum only
1.59	75	1140	aluminum (2 dup. tests)
1.59	75	1140	plexiglas
1.59	50	750	aluminum, plexiglas
1.59	25	370	plexiglas only
3.18 mm	100 %	1530 g	aluminum, plexiglas
3.18	93	1430	aluminum only
3.18	87	1335	aluminum (2 dup. tests)
3.18	75	1140	aluminum, plexiglas
3.18	50	750	aluminum, plexiglas
3.18	25	370	aluminum, plexiglas
4.76 mm	100 %	1530 g	aluminum, plexiglas
4.76	93	1430	aluminum only
4.76	87	1335	aluminum (2 dup. tests)
4.76	75	1140	aluminum, plexiglas
4.76	50	750	aluminum, plexiglas
4.76	25	370	aluminum, plexiglas

II. EXPERIMENTAL APPARATUS AND PROCEDURE

Experimental Apparatus

The main components of the test assembly are depicted photographically in Figures 1. and 4. and schematically in Figures 2., 3. and 5. The test chamber consists of an instrumented section sandwiched between two clear windows. Two instrumented sections were made, one of aluminum and one of plexiglas (see Figure 1.), to investigate the effect of their greatly different thermal conductivities on the blowdown of a flashing liquid. The configurations of these sections are nearly identical; both have inner dimentions of 40.00 cm x 7.94 cm (wide) x 3.49 cm (deep) and a wall thickness of 2.54 cm all around. Several holes are drilled through the walls to accommodate various probes. The locations of corresponding probes are the same for both sections, except that the void fraction indicator and the bottom pressure probe are deleted from the plexiglas section. The machined exit sections of both frames are identical (see Figure 2.). It is necessary to recess the orifice as shown in order to achieve a thin, square-edged orifice while ensuring adequate structural strength under high pressure, particularly for the plexiglas device. Finally, shallow recesses are cut into the front and rear surfaces of the aluminum section to hold gaskets.

The instrumented section is placed between two 2.54 cm-thick plexiglas windows, making a 1.1 liter (0.039 ft^3) chamber. For the aluminum insert a pressure seal is used to make the chamber leak-tight. Two rubber gaskets are placed between the aluminum section and the windows and the entire assembly is tightly clamped. The plexiglas section, however, is bonded permanently to the windows with acrylic

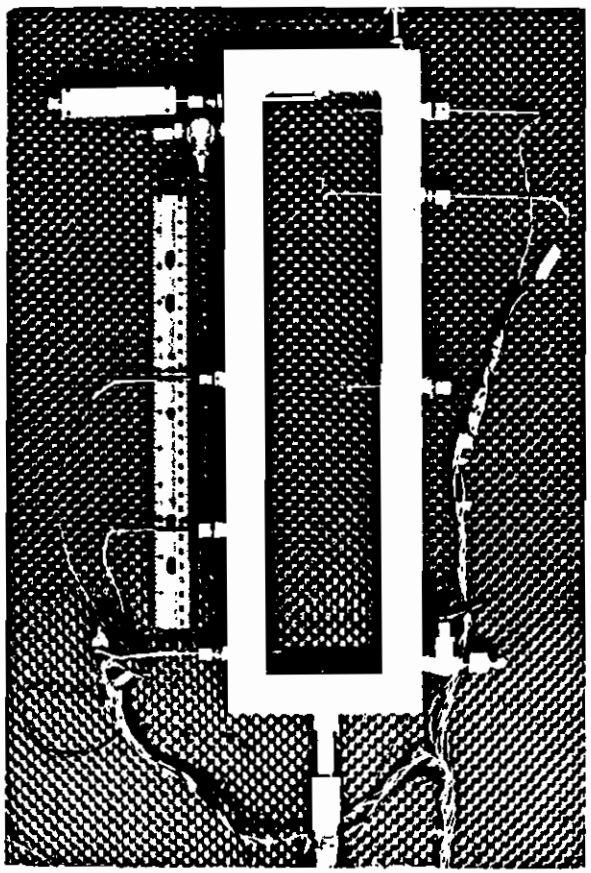

(a) The aluminum section, showing thermocouple probes, pressure tap at bottom and orifice at top.

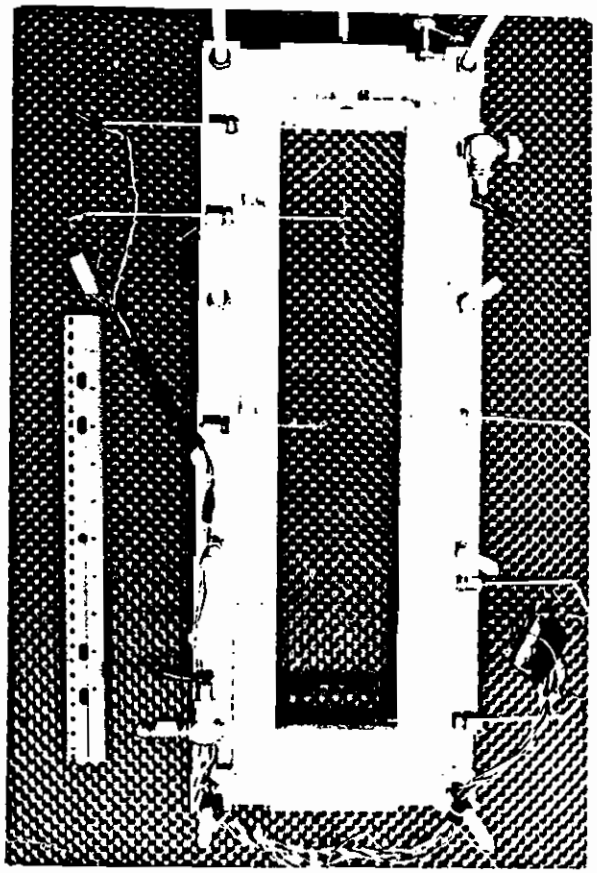

(b) Plexiglas section installed in outer aluminum support frame.

Figure 1. The Instrumented Sections.

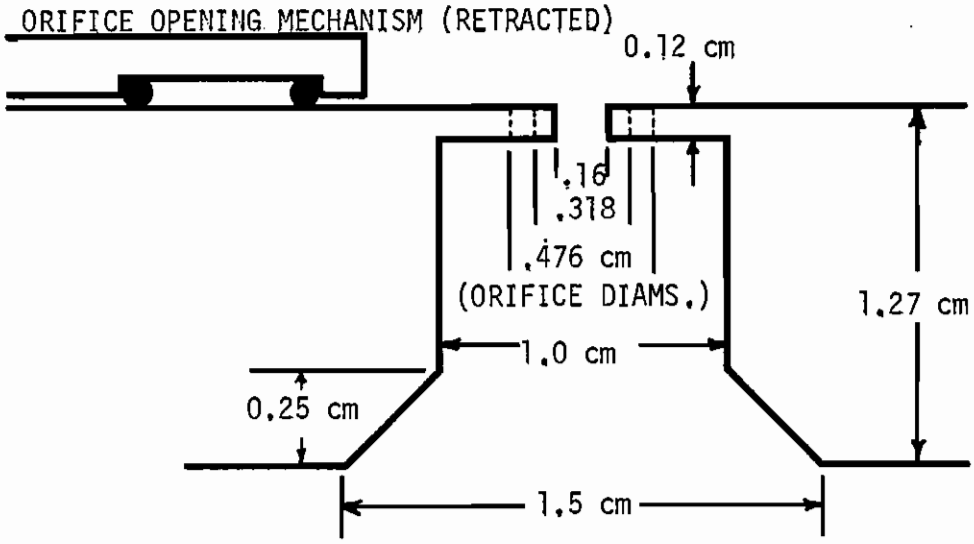

Figure 2. The Orifice and Exit Section.

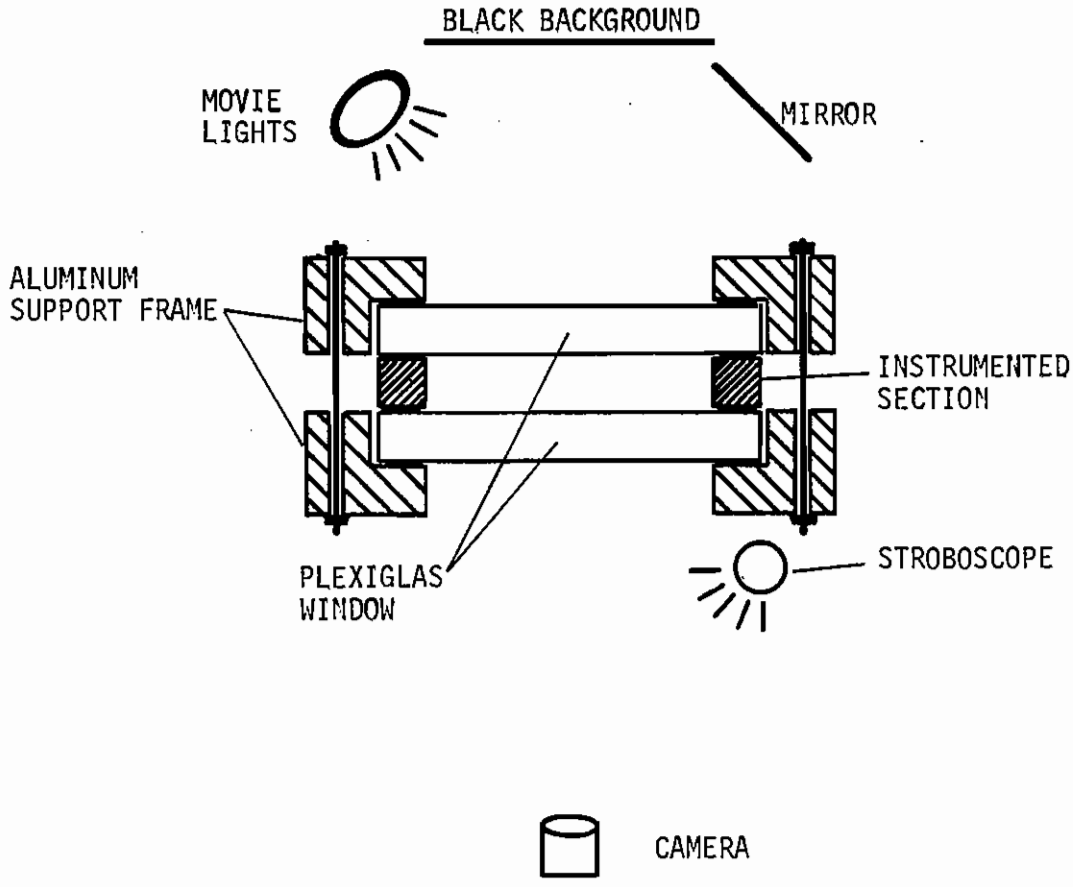

Figure 3. Cross Section of Experimental Chamber.

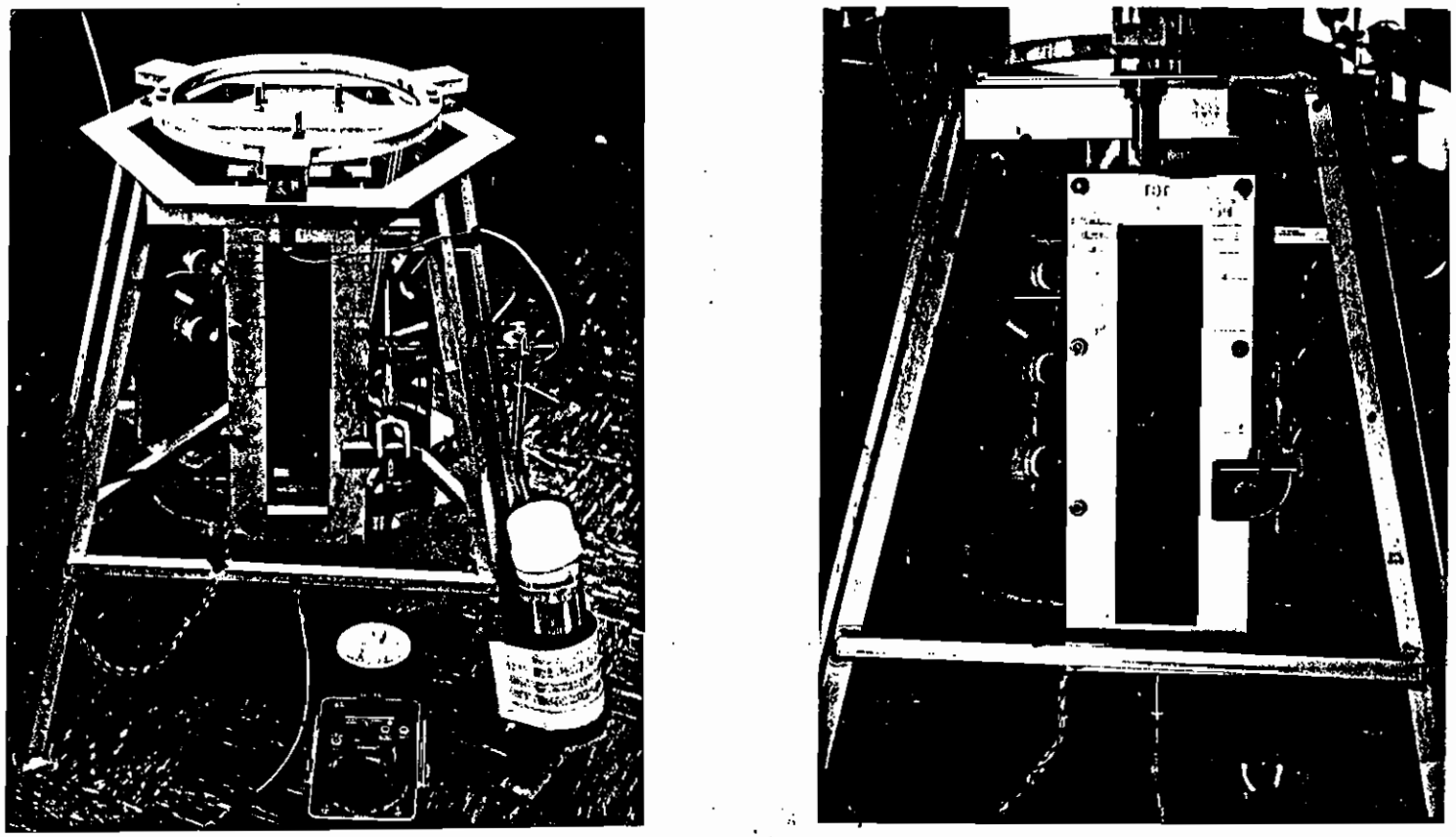

Figure 4. The Assembled Test Stand.

The pressure chamber is suspended from load cells on tripod stand, the stroboscopic timer is on the floor and the movie lights are behind the chamber.

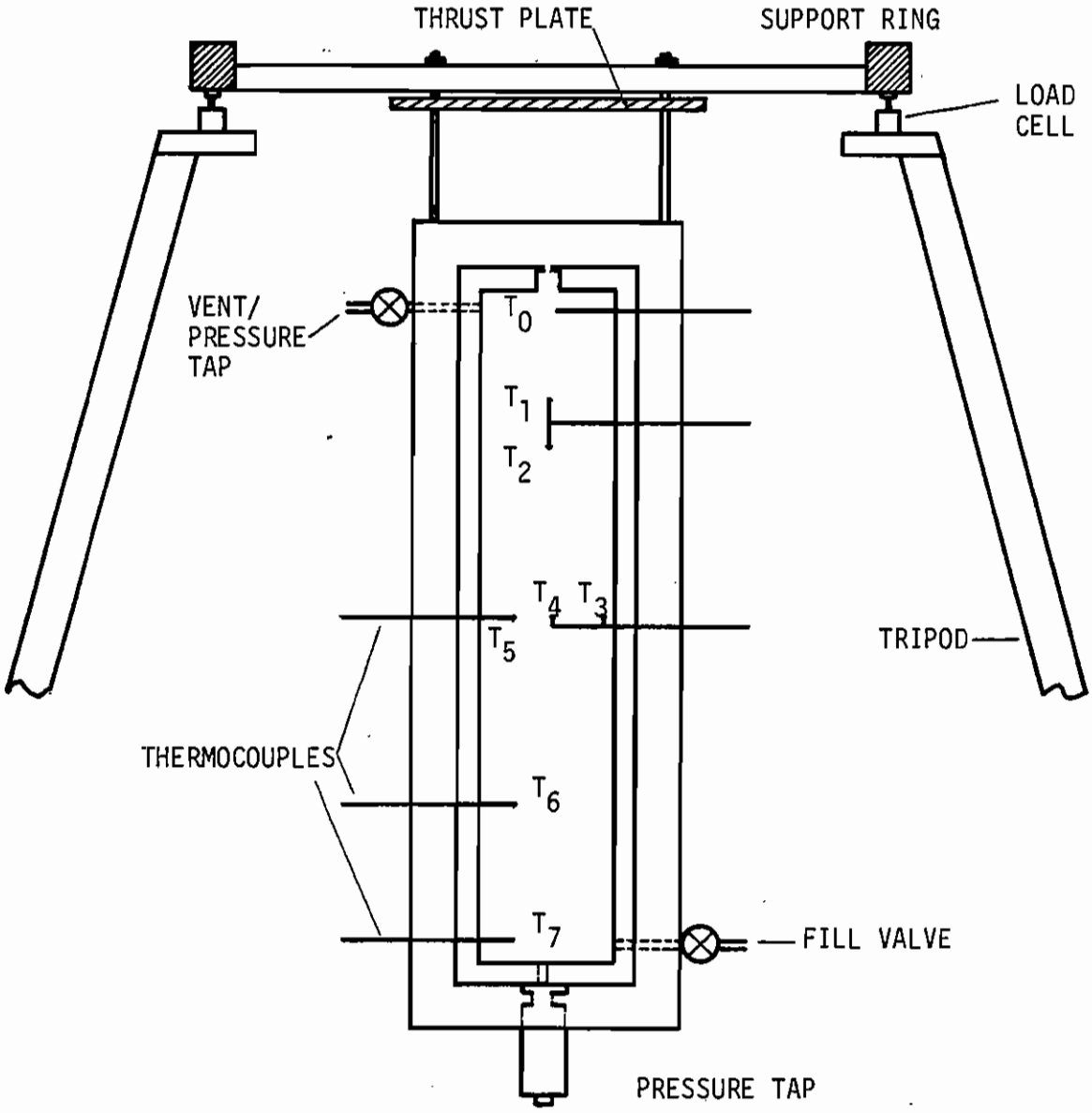

THERMOCOUPLE PROBE NO.	THERMOCOUPLE LOCATION	
	HEIGHT ABOVE VESSEL BOTTOM	HORIZONTAL DISTANCE FROM CENTERLINE
T_0	38.1 cm	0.64 cm
T_1	34.3	0.00
T_2	31.1	0.00
T_3	20.3	3.33
T_4	20.3	0.16
T_5	20.3	2.06
T_6	9.8	2.06
T_7	1.3	2.06

Figure 5. Schematic of Pressure Vessel with Locations of Thermocouples.

cement, making the assembly an integral sealed unit. The assembled test chamber is placed on cushioning gaskets between large aluminum frames as shown in Figure 3. The frames, with aperatures slightly larger than that of the instrumented section, are bolted tightly together to provide the main support to the test vessel against internal pressure. As shown in Figures 4. and 5., the entire assembly is centrally suspended below a support ring. This ring, in turn, rests on three equally spaced load cells installed in a tripod stand. A deflection plate is also secured to the ring, directly above the orifice, to negate the thrust of the exiting fluid. The tripod serves as a stable base for the experiments and supports the lighting system, thermocouple ice bath and stroboscopic timing system.

Instrumentation

The system mass is measured using three load cells (Statham, 22.7 kg maximum each) installed 120° apart in the same elevation plane on the tripod frame. The output of each load cell goes to an individual bridge amplifier (Vishay Instruments model BAM-1). The amplifier outputs are combined and the summed signal is recorded during tests on a strip chart recorder (Linear Instruments model 561 or Hewlett-Packard model 7702-B 2-channel recorder). As mentioned, the thrust of the exiting fluid is compensated for by a deflection plate above the orifice.

Pressure measurements are made with two diaphragm-type strain gauge transducers (CEC type 4-312-0001, 0-1.0 MPa [0-150 psi] and Bell & Howell type 4-326-0001, 0-1.7 MPa [0-250 psi]), one mounted near the top of the test vessel and one on the bottom. The bottom pressure gauge is installed in the probe assembly shown in Figure 6. The transducer is

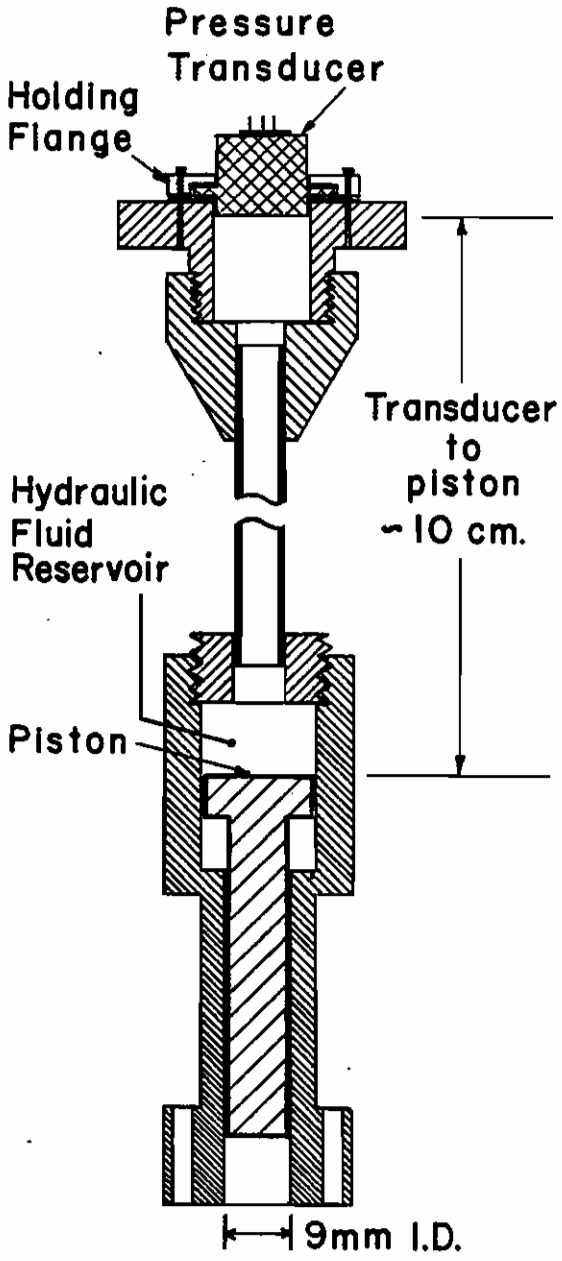

Figure 6. The Pressure Probe Piston Assembly.

mounted at the end of a fluid-filled piston chamber which isolates the the gauge from severe temperature gradients in the tests chamber. This is necessary on the bottom probe because the transducer, although well within its recommended temperature range, is very sensitive to the thermal gradients which inevitably occur during the rapid temperature drops in the blowdown process. While the temperature at the bottom of the vessel drops to -30°C (-21°F), the temperature near the top remains much closer to ambient, so the piston assembly was found to be unnecessary for the upper pressure transducer. Furthermore, it was verified during the series of tests conducted with the aluminum side walls that the pressures at the top and bottom of the vessel are equal (taking into account hydrostatic pressure differences) to within the accuracy of the measuring technique. Therefore, only the upper pressure probe is used in later tests with plexiglas side walls.

Local temperatures in the chamber are measured with eight ice-point-referenced thermocouples (ASTM type T: Copper-Constantan) whose locations are noted in Figure 5. A series of six thermocouples measures the vertical temperature distribution while a series of three thermocouples measures the horizontal temperature profile at mid-height in the test chamber. Thermocouple output goes to a multichannel digital printer (Fluke model 2240B) which samples the probes sequentially. The instrument used converts the thermocouple signal directly to a printed output in units of temperature (°C or °F) with a quoted accuracy of 0.06°C (0.1 °F).

In order to measure the quality of the exiting fluid a local void fraction probe is installed close to the orifice. The void fraction measuring system consists of three compatible units; the DISA model 55S52

optical probe, the DISA 55S02 phase indicator and the DISA 55S11 void fraction unit. The probe measures local void fraction integrated over a chosen time interval (for these tests, 1 second) and the resultant signal is converted internally to a digital output as percentage volume fraction of vapor. Although the probe tested satisfactorily in preliminary trials of bubbly flow of water, the system failed to respond during actual blowdown experiments with Freon, registering only 100% or 0%. The failure of the void fraction probe is probably due to the violence of the liquid frothing near the orifice. This condition is outside the operating limits of the device and because of this difficulty the data from the probe are not used. Instead, average void fractions and qualities for the entire two-phase column are estimated from the combination of temperature, mass and photographic data. Calculational methods are described in the section on data reduction.

A film of each test is made with a high speed 16 mm camera (Wollensak "Fastax" model W4F). The test vessel is back-lit by an indirect lighting system, as shown in Figure 3. Directly behind the vessel is a black backdrop to enhance contrast.

The film speed of the camera is not constant, but varies from about 270 to 300 frames per second. A stroboscope (General Radio model 1531A) calibrated to 60 flashes per second is therefore used as a timing device, making the actual film speed irrelevant to the determination of the time of any individual photograph. The quoted flash duration is no more than 1.2 microseconds, which implies an accuracy of within 0.01% using the strobe flash to determine time.

Experimental Procedure

The experimental procedure consists of the following activities. First, the pressure probe(s) is calibrated using a dead-weight tester. Linearity and reproducibility are checked and the reference point (ambient pressure) is established by sequentially adding, then removing weights from the tester. Considering temperature-induced errors, transducer nonlinearity and precision of reading the recorded output, the overall error in pressure measurements is determined to be less than $\pm 2\%$.

The pressure probe(s) is mounted on the test chamber and the entire empty chamber is set onto the load cells. A weight is suspended from a point directly above each load cell sequentially and the gain of each bridge amplifier is adjusted so that all three load cell outputs cause the same recorder deflection for the same load. The weight is then loaded centrally, above the orifice, to ensure that the resultant gain is the same as the gain for each eccentric loading.

It is recognized that a small error in apparent gain is incurred by calibrating individual load cells with the test assembly suspended from all three, but this is necessary because of the limitations of the instrumentation. The empty test assembly has a mass of about 20 kg, whereas the total mass of fluid in the vessel varies from 0.4 kg (25% fill) to 1.5 kg (100% fill) at the start of blowdown. Unfortunately, the response of the load cells is sensitive to large initial loads, so that the effective gain changes markedly from the unloaded to the loaded condition. Trying to re-equalize the three load cells in the loaded condition after balancing them unloaded proved to be a time-consuming and fruitless task. The modified balancing procedure is sufficient to

achieve adequate accuracy in the mass measurements.

With the test assembly in place and the load cells balanced, several equal weights are added to the vessel until their mass slightly exceeds the mass of fluid to be added for the blowdown. The recorder gain is then adjusted so that the planned charge of Freon will cause maximum deflection, thus assuring maximum sensitivity. Linearity is checked by comparing the recorder deflection per unit mass (mm/g) of each weight added. Since the system is calibrated before each test, errors are introduced only by small instrument nonlinearities and by the precision of the reading of recorded output. The total error in the mass determination is estimated to be no more than ±2% for any test, regardless of initial percentage fill.

The vessel is then filled with Freon-12 from a pressurized canister at ambient temperature. Controlled venting allows the vessel to be filled to any desired level. The resulting expansion of the fluid into the system causes slight subcooling. The chamber is left at rest for a time to allow vapor and liquid temperatures to come to equilibrium near the outside ambient temperature and to allow convection to cease. During the waiting period the stroboscope is calibrated and all other instruments are put on standby mode.

The final sequence proceeds as follows. First, the mass and pressure chart recorders are started. The movie lights are turned on as the camera is started to minimize the radiation heat input (thermocouples in the vapor space respond to radiant energy that they absorb with elevated temperature readings). With the stroboscope operating, the camera is allowed to come up to speed for approximately 4 seconds. Finally, the orifice is opened and the blowdown begins. On the pressure and mass

charts the onset of blowdown is marked by sudden distinct drops from initial readings. The time response of both measurement systems (on the order of 1 millisecond) is capable of following the very short transient associated with the initiation of blowdown. The temperature recorder initially samples a single thermocouple in the liquid at a rate of 2.7 times per second, limiting the response to rapid temperature transients.

As soon as the film in the camera is exhausted, the movie lights are turned off. The mass measurements are terminated when frost begins to form on exposed metal parts of the test vessel. Temperature and pressure readings continue until late in the blowdown when a quasi-steady state is achieved (system pressure comes within experimental error of ambient pressure).

At the conclusion of each experiment the mass, pressure and stroboscopic calibrations are rechecked. The accumulated data are reduced at a later convenient time.

Data Reduction

Temperature readings are made directly from the printed digital output of the recorder. The number of the thermocouple sampled and the time of the recording is also printed on the tape so no further processing of the temperature data is necessary. The quoted accuracy of $\pm$0.06°C (0.1°F) was verified by some preliminary tests.

The strip chart data of system pressure and mass are analyzed in a straightforward manner once linearity and calibration are verified. Cumulative error for both mass and pressure measurements was established in preliminary tests to be less than $\pm$2%.

The instantaneous mass flow rate $\dot{m}(t)$ is a derived quantity calculated by numerical differentiation of the system mass versus time curve, m(t). A series of exponential functions are fitted to small segments of the m(t) curve. The derivative of the function is calculated at the centerpoint of the chosen interval to give the mass flow rate at that point. The smoothed values of the system mass differed from experimental values typically by much less than the previously mentioned $\pm$2% maximum error, reflecting the fact that the major component of that error limit is load cell nonlinearity. Errors in the calculated mass flow rate result mainly from the accuracy of the actual reading of the m(t) strip chart. Depending on the gain, this reading error is from $\pm$2 to 3 grams but is constant for a given blowdown, no matter what the instantaneous mass in the chamber. The time intervals between mass data points are chosen as large as is practical to try to minimize the effect of reading errors, but the load cell nonlinearity cannot be cancelled out. The "worst-case" overall error in the mass flow rate is estimated to be $\pm$10% for small flow rates (below 4 g/s) and for the first two values (for which the computer program does not use the full bandwidth). Accuracy is better for larger flow rates during the major part of the blowdown, generally less than $\pm$4%.

The high speed motion pictures taken of each experiment are interpreted with the aid of a projecting "X-Y Analyzer" ordinarily used by the University of Maryland Physics Department to examine photographs of subatomic particle trajectories. The machine is loaded with the film reel and projects a still image onto a large screen one frame at a time. A movable cross hair sight (also projected) is manipulated by the viewer to locate points of interest in the frame. The sight is coupled to a

signal processor so that, as desired, the viewer can record the horizontal and vertical coordinates of any point. The digital output is in the form of punched and printed computer cards.

In the present application, the 16 mm film of a blowdown is analyzed as follows. First, the frame immediately preceding the first evidence of discharge is used to calibrate the distance scale and to establish time zero for the test. The resolution of the instrument is 50 microns (0.002 in) but the resolution of the film is limited to 0.25 mm (0.01 in), the diameter of the smallest discernable bubble. A point is chosen for the zero coordinate and is standardized for the rest of the frames of the film.

The extremely accurate stroboscopic flash is the time standard. Frames featuring the flash are counted and selected frames are analyzed. On each analyzed frame, the standard reference point is established. Then the two-phase column height and selected bubble locations and diameters are measured.

The column height and bubble dimensions are computed directly. Bubble rise velocities are calculated by tracking specific bubbles through many frames and dividing the change in vertical position between frames by the time elapsed between the frames. Bubble growth rate and column rise velocity are calculated similarly. Error limits in bubble locations and dimensions are $\pm$0.1 mm (.004 in) and for their time derivatives $\pm$0.2 mm/s (0.008 in/s). The violent activity of the two-phase column surface makes the accuracy of its measurement about $\pm$1 cm (0.4 in).

The void fraction and quality of the two-phase column are rather approximate derived quantities. The volume of the column, computed from

the measured column height and the known vessel cross section area, is divided by the measured instantaneous system mass to give an average specific volume for the column. Assumptions of homogeneity (valid for the 3.18 and 4.76 mm orifice tests but not for the 1.59 mm orifice tests) and of equilibrium of vapor and liquid at saturation are made. The tabular values for saturated vapor and liquid at the measured liquid temperature are then applied to the equation

$$\bar{v} = \frac{V}{m_{tot}} = (xv_g + [1-x]v_l)$$

to give the quality of the column. The void fraction is calculated from the quality and specific volume data. The accuracy of the void fraction estimate is about ±10% and accounts for all sources of error except the assumption of a homogeneous mixture.

III. INITIAL TRANSIENTS

General Description

The blowdown of pressurized Freon-12 from the test vessel in this series of experiments can be divided into three main regimes characterized by different parameters limiting the blowdown process. The first regime, to be discussed in this chapter, occurs for the first one to two seconds of the blowdown. This initial regime is characterized by violent boiling and the establishment of the two-phase column which will persist through the remainder of the blowdown. The second regime, during which either vapor flow or two-phase flow may exist in the orifice, is distinguished by choked flow (or its two-phase equivalent) which limits the mass discharge rate and therefore the depressurization rate. Finally, after the flow through the orifice becomes subsonic, the third regime gradually dominates. Here the mass discharge rate is governed by the heat transfer to the system from the environment.

A description of the events of the initial regime is as follows. Immediately upon the opening of the orifice, vapor escapes and the pressure of the entire system drops rapidly. The pressure in any part of the vessel at a given time is essentially the same, taking into account the hydrostatic pressure gradient (for a 100% fill of Freon the hydrostatic pressure difference between the top and bottom of the chamber is .004 MPa [0.57 psi]). No pressure gradient exists because pressure waves traverse the entire chamber in less than a millisecond. At the conditions of the tests sonic velocity in saturated Freon-12 vapor is 160 m/s (525 ft/s) and in liquid Freon is above 1200 m/s (4000 ft/s).

The liquid in the vessel is initially slightly subcooled (no more than 3°C (5°F) and so does not begin to boil until the pressure has dropped to a point where the bulk liquid becomes sufficiently superheated to allow bubble nucleation. This actually happens very quickly (within 0.02 seconds) since with no initial vapor generation replacing vented vapor, the rate of pressure drop is nominally 2.0 MPa/s (300 psi/s). Boiling begins with nucleation on the side walls of the test chamber and on the thermocouple probes. Even in the most extreme depressurizations no bulk boiling is observed. Once nucleation begins the bubbles grow explosively, fed by rapid vaporization of the surrounding superheated liquid as decompression continues.

The newly created two-phase column rises in response to bubble growth, but this has little immediate effect on the pressure drop. It causes the void fraction of the two-phase column to increase, but does not change the void fraction of the system as a whole. The pressure drop is arrested when the first burst of bubbles breaks into the vapor space. Numerous drops and filaments of liquid are thrown up and may be entrained in the flow out the orifice. System pressure rises once boiling has started in earnest, but more gradually than the sudden initial drop.

The rates of pressure drop and recovery are dependent on the venting rate and the liquid level at the start of the test, but they are not affected by wall composition. This suggests, and is supported by theoretical heat transfer calculations, that the initial transient is nearly adiabatic, occuring in a time too short to permit significant heat transfer from the walls. The main source of energy for boiling is the superheated liquid.

The characteristic pressure spike, present in every one of the present experiments, has been noted in previous publications on blowdown phenomena. It is documented in reports by Tanger, Vachon and Pollard [1], Ordin, Weiss and Chistenson [2] and Howell and Bell [7]. No explanations of the phenomenon are proposed, however.

During the time that the pressure drops at least 0.08 MPa (12 psi) and as much as 0.22 MPa (32 psi) the temperature in the chamber drops only about 1°C (2°F). The initial transient is therefore far from saturation. The system pressure does not return as high as the initial pressure, but rather drops again as the entire liquid volume becomes involved in boiling and turbulent mixing and the second blowdown regime begins. The liquid temperature remains uniform throughout the vessel during the initial transient, dropping slightly at the instant the orifice is opened but not recovering significantly as does the system pressure. For the duration of the initial transient the temperature remains essentially constant at the point to which it first dropped. As the second regime is entered the liquid temperature drops again.

Comparison of Individual Tests

Following the above generic description it should be noted that virtually all the tests differ from the "norm" in some respect. However, the differences reflect a well behaved dependence on the independent parameters of orifice size, liquid fill height and wall material (i.e. thermal conductivity). Figures 7. and 8. and Tables 2. and 3. summarize the phenomena of the initial transient.

Consider first the tests with 100% fills of liquid. Experiments are conducted with both plexiglas and aluminum walls (low and high heat

Table 2. Initial Mass Flow Rates.

INITIAL % LIQUID FILL	ORIFICE DIAMETER	INITIAL MASS FLOW RATE PLEXIGLAS WALLS	ALUMINUM WALLS
100 %	1.59 mm	18 g/s (2)	12 g/s (2)
	3.18	51 (2)	69 (2)
	4.76	174 (2)	196 (2)
75 %	1.59 mm	8 g/s (v)	7 g/s (v)
	3.18	31 (2)	25 (2)
	4.76	72 (2)	85 (2)
50 %	1.59 mm	7 g/s (v)	7 g/s (v)
	3.18	25 (v)	24 (v)
	4.76	29 (2)	51 (2)
25 %	1.59 mm	5 g/s (v)	7 g/s (v)
	3.18	22 (v)	21 (v)
	4.76	27 (v)	47 (?)

Notes: (2) indicates that exit flow is two-phase (i.e. there is liquid entrainment in the exit flow).

(v) indicates pure vapor flow in the exit section.

(?) indicates that there is insufficient data to tell the flow regime at the exit section.

Table 3. The Initial Decompression and Recovery.

ORIFICE DIAM.	INITIAL % LIQUID FILL	TIME TO MIN. PRESSURE, Pmin		RECOVERY TIME		MAXIMUM ΔP (P_o - Pmin)	
		PLEXI. WALLS	ALUM. WALLS	PLEXI. WALLS	ALUM. WALLS	PLEXI. WALLS	ALUM. WALLS
1.59 mm	100%	0.20s	<0.2 s	1.50s	1.40s	.11MPa	.11MPa
	97	-	0.1	-	1.30	-	.12
	93	-	0.20	-	1.00	-	.12
	87	-	0.25	-	1.20	-	.10
	75	0.45	0.5	1.00	1.30	.08	.10
	50	0.80	0.8	1.40	1.50	.09	.10
	25	1.00	-	∞	-	.09	-
3.18 mm	100%	0.05s	<0.1 s	1.00s	1.20s	.10MPa	.12MPa
	93	-	0.05	-	0.80	-	.18
	87	-	0.15	-	0.80	-	.19
	75	0.25	0.20	0.75	0.80	.17	.18
	50	0.35	0.35	0.70	0.75	.16	.14
	25	0.40	0.45	0.70	0.85	.13	.17
4.76 mm	100%	0.05s	0.05s	0.80s	0.90s	.13MPa	.12MPa
	93	-	0.06	-	0.80	-	.22
	87	-	0.08	-	0.70	-	.21
	75	0.20	0.15	0.65	0.70	.17	.22
	50	0.25	0.22	0.55	0.70	.14	.19
	25	0.45	0.30	0.75	0.60	.16	.21

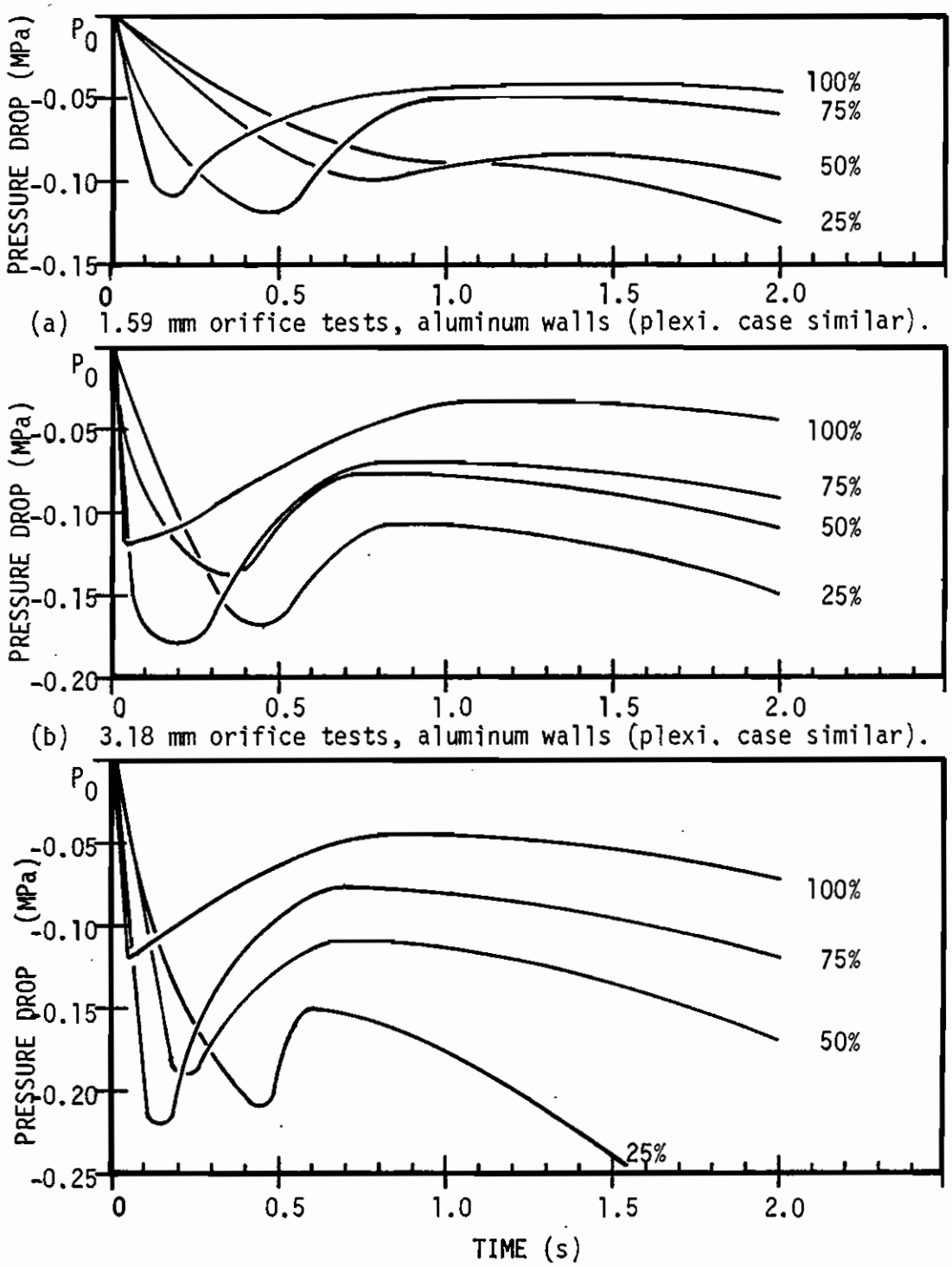

Figure 7. Initial Pressure Transients.
(vertical scale is MPa below initial pressure, P_0)

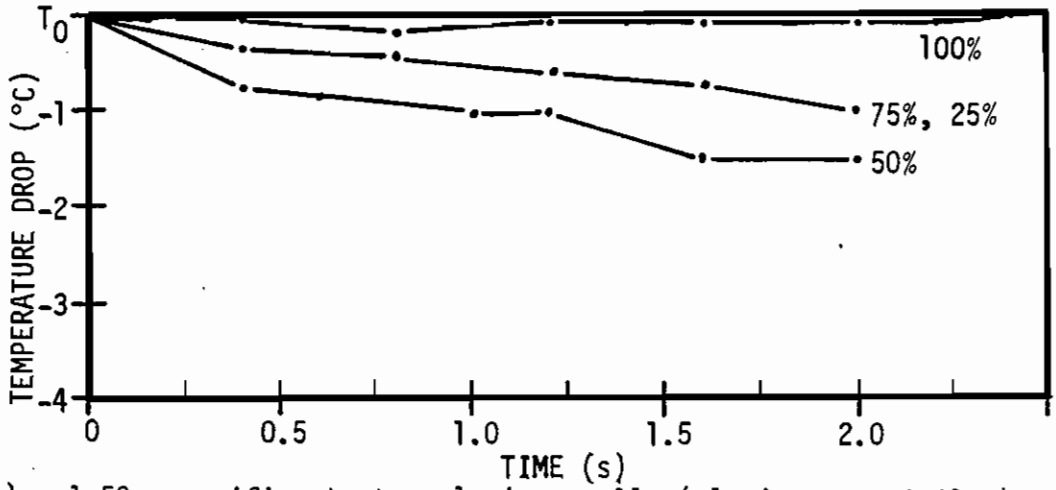

(a) 1.59 mm orifice tests, aluminum walls (plexi. case similar).

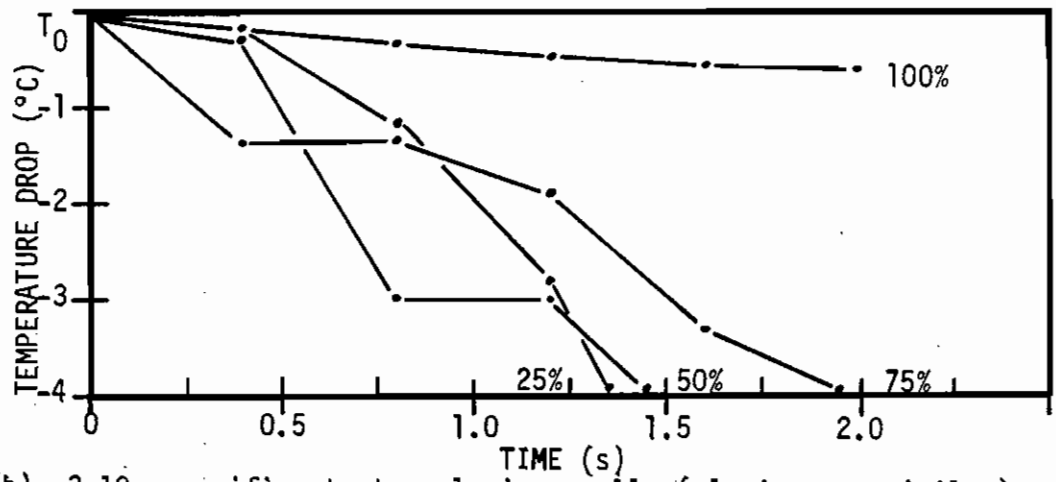

(b) 3.18 mm orifice tests, aluminum walls (plexi. case similar).

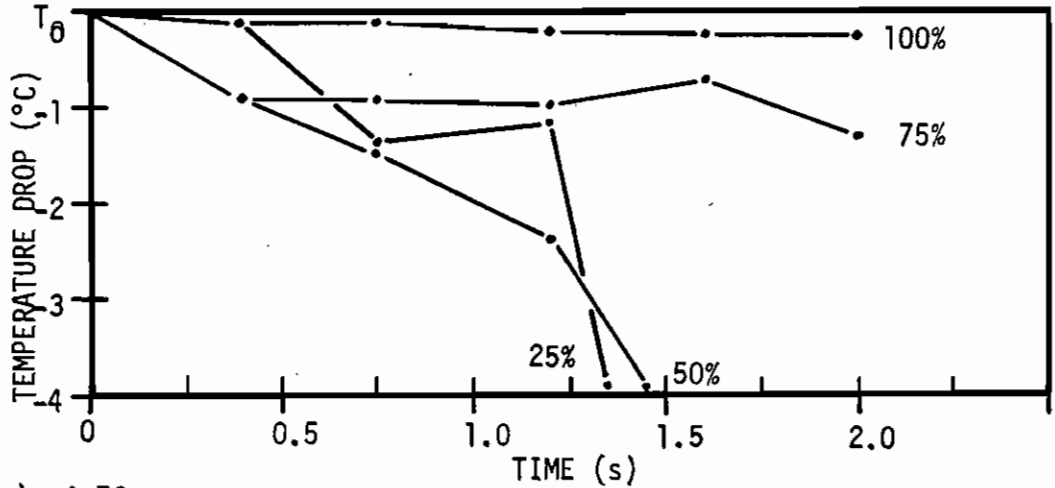

(c) 4.76 mm orifice tests, aluminum walls (plexi. case similar).

Figure 8. Initial Temperature Transients.
(vertical scale is °C below initial temperature, T_0)

transfer respectively) and with 1.59, 3.18 and 4.76 mm (1/16, 1/8 and 3/16 in) diameter orifices.

In the 1.59 mm orifice tests wall material makes no significant difference in the initial phenomena. The mass flow rates at the instant the orifice is opened are 12.5 and 18.5 g/s for plexiglas and aluminum walls respectively. This inital flow is very low quality for a moment, but the flow rate falls rapidly as boiling proceeds and less liquid is entrained in the exit stream.

Bubbles nucleate on the walls and on probe surfaces at any suitable nucleation site, the smallest discernable bubbles having diameters of about 0.25 mm (0.01 in). Applying the basic nucleation criterion,

$$\Delta T_{superheat} = 4 \cdot T_l \sigma v_{fg} / h_{fg} d \quad ,$$

the superheat required to allow nucleation of the 0.25 mm bubble at the initial system temperature of 24°C (70°F) is 0.05°C (0.09°F). This in turn requires a pressure drop of 1.5 kPa (0.02 psi) from saturation pressure. Larger bubbles, originating from surface depressions equal in width to the departing bubble's diameter, need less of a pressure drop to evolve. The low surface tension and the thermodynamic properties of Freon-12 permit nucleation essentially as soon as the small (0° to 3°C) initial liquid subcooling is overcome, within milliseconds of the start of decompression.

Once boiling commences, columns of bubbles rise up the walls with a mean velocity of 15 cm/s. Many small bubbles are generated, and they grow slowly, the largest reaching a diameter of about 5 mm (0.2 in). Growth of bubbles forces liquid into the orifice, causing the large

initial mass flow rate but slowing decompression. Continuing rapid vapor generation forces pressure back up until liquid superheat goes to zero and bubble nucleation actually ceases momentarily. Rising bubbles reach the top of the chamber, raising the exit void fraction. This allows the depressurization to again outpace vapor production as the initial regime gives way to the main blowdown segment. The entire opening transient is completed in 1.5 seconds.

The 3.18 mm orifice, 100% fill test with plexiglas walls begins similarly to the 1.59 mm orifice tests. Noticable differences in the initial transient behavior are as follows. The starting mass flow rate, including entrained liquid, is 51 g/s. Pressure drop and recovery are more rapid, as is the bubble growth rate. Bubble rise velocities average 17 cm/s. The motion of the bubbles is still mainly vertically up the walls, but in the 3.18 mm orifice tests a larger region near the top of the chamber is involved in turbulent mixing. A distinct downward current in the center of the vessel, not well developed in the 1.59 mm tests, reaches several centimeters down from the top of the vessel. The 3.18 mm orifice, 100% fill test with aluminum walls has an initial transient which nearly duplicates the corresponding test with plexiglas walls except that there is slightly more initial nucleation and more of the two-phase column becomes involved in downward eddy currents.

The 4.76 mm orifice, 100% fill tests show no distinction between plexiglas and aluminum walls. Bubbles first evolved rise with the same average velocity (17 cm/s) as in the 3.18 mm orifice tests, but bubble growth is explosive. Some bubbles coalesce into slugs over 3 cm across. The dramatic differences in the initial nucleation of bubbles can be seen in Figure 9., which compares the initial boiling event at the same

point in time (0.2 s) for all the orifice sizes. The violent bubble growth is due to the extremely large initial mass flow and decompression through the large orifice. The entire chamber is engulfed in turbulent mixing and the initial transient is over in 0.9 seconds.

Although the series of experiments begun with the vessel less than completely full are visually more dramatic than the 100% fill tests, the associated phenomena exhibit gradual progressive changes as the initial percentage fill is reduced. Referring back to Table 2., the low quality flow in the 100% fill tests causes the initial mass flow rate for those tests to be much higher than for corresponding tests with lesser percentage fills. Two-phase flow through the orifice does occur at the start of some incomplete fill tests, but in these cases the exit quality is still higher than in the 100% fill cases. The two-phase mass flow rates are consequently lower. The degree of liquid entrainment in the exit flow is a function of the initial liquid column height and the intensity of the boiling (i.e. the rate of decompression of the system).

As can be seen in Figure 7. and Table 3., the time required for pressure to drop to its minimum value in the initial transient is dependent upon the initial liquid fill height. For any test series with a particular orifice size, the greater the volume of vapor in the vessel the slower the pressure drop. Before the initially subcooled liquid reaches the bubble nucleation threshold the original mass of vapor decompresses as if it were in a constant volume vessel with a rigid wall where the liquid-vapor interface actually is. Even after boiling begins vapor production lags behind vapor venting until a substantial portion of the liquid volume is mixed with numerous growing bubbles. This may imply a dependence of the rate of pressure change on the interfacial

(a)
1.59 mm orifice,
aluminum walls,
87% initial fill
of liquid.

(b)
3.18 mm orifice,
aluminum walls,
87% initial fill
of liquid.

(c)
4.76 mm orifice,
aluminum walls,
87% initial fill
of liquid.

Figure 9. Boiling patterns at the beginning of the initial transient (approximately 0.2 seconds into the blowdown). These patterns are representative of the corresponding initial boiling event for any initial percentage fill of liquid.

area available for mass transfer via evaporation and calls for further study. The initial pressure drop ceases as vapor production through boiling overtakes vapor loss through venting.

The lengths of time for repressurization in the 3.18 and 4.76 mm orifice tests are noticably longer for the 100% fill cases but do not vary much between any of the lesser percentage fill tests. There is no significant variation in recovery time among any of the 1.59 mm orifice tests.

Visual differences in the initial regime among the lower percentage fill tests are summarized briefly, referring to Figures 10. through 13. These figures compare the appearances of the two-phase columns for 100%, 75%, 50% and 25% initial liquid fills and all three orifice sizes at the end of the initial regime (about 1.0 s). Bubbles appear as dark spots.

In the 1.59 mm orifice, 75% fill, plexiglas wall test a small leak in the chamber allows some bubble formation prior to the actual blowdown. When the orifice is opened these bubbles immediately grow while wall nucleation is less significant. The two-phase column rises less than 1 cm during the initial transient, increasing in volume and mean void fraction by 2%. As the boiling pattern stabilizes near the end of the initial regime there is turbulent motion near the top of the column, but very few drops are thrown up into the vapor space (see Figure 11a.). The corresponding test with aluminum walls does not have pre-existing bubbles at the start of blowdown. Consequently, wall nucleation (with probe surface nucleation) is seen exclusively. Otherwise the initial transient proceeds similarly to the plexiglas wall case (see Figure 11b.).

The 3.18 mm orifice, 75% fill tests with either plexiglas or aluminum walls begin more vigorously than the 1.59 mm orifice tests.

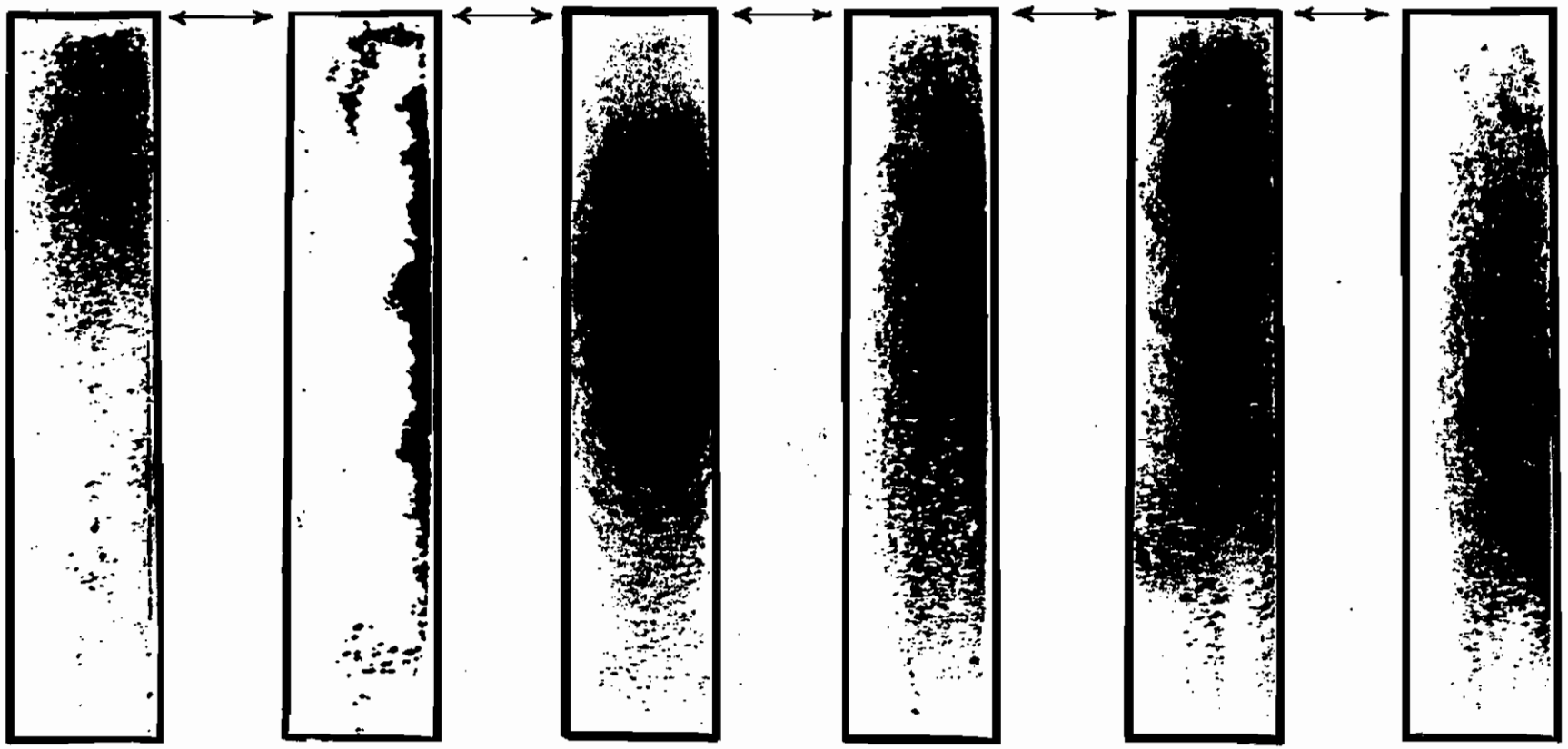

(a) 1.59 mm orifice, plexiglas walls.
(b) 1.59 mm orifice, aluminum walls.
(c) 3.18 mm orifice, plexiglas walls.
(d) 3.18 mm orifice, aluminum walls.
(e) 4.76 mm orifice. plexiglas walls.
(f) 4.76 mm orifice, aluminum walls.

Figure 10. Boiling patterns at the end of the initial transient; 100 % liquid fill tests. The drawn horizontal line indicates the height of the liquid prior to venting.

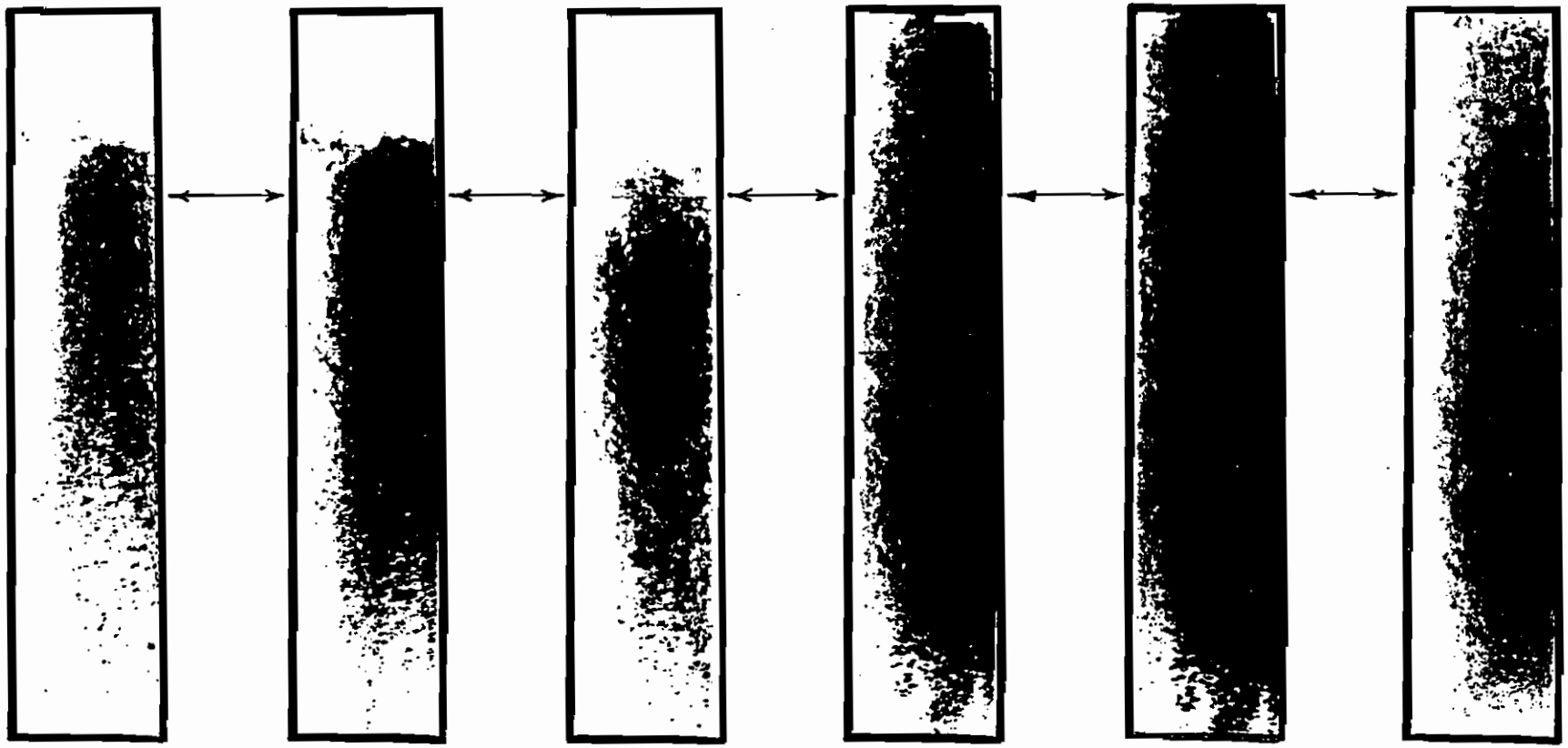

(a) 1.59 mm orifice, plexiglas walls.

(b) 1.59 mm orifice, aluminum walls.

(c) 3.18 mm orifice, plexiglas walls.

(d) 3.18 mm orifice, aluminum walls.

(e) 4.76 mm orifice, plexiglas walls.

(f) 4.76 mm orifice, aluminum walls.

Figure 11. Boiling patterns at the end of the initial transient; 75% liquid fill tests. The drawn horizontal line indicates the height of the liquid prior to venting.

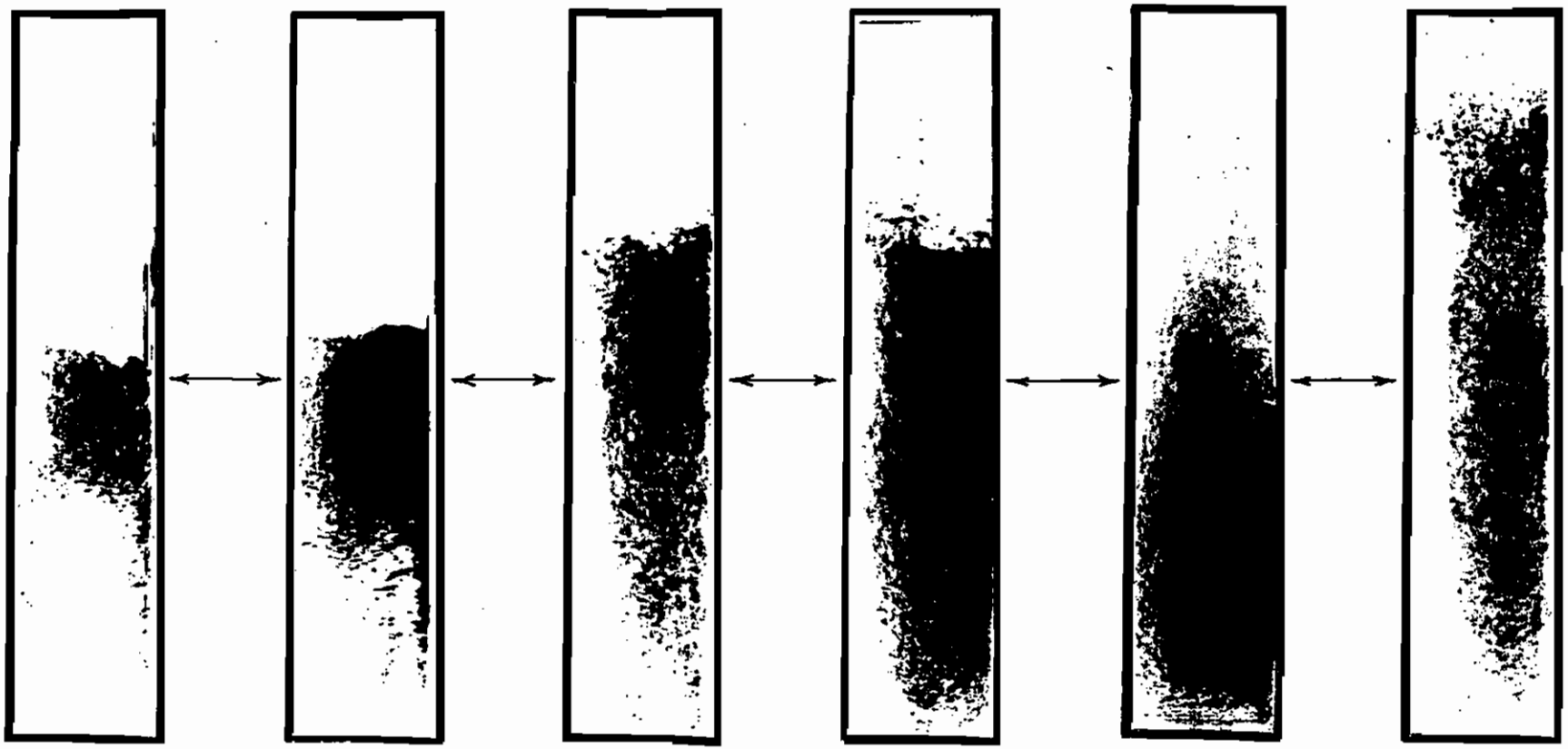

(a) 1.59 mm orifice, plexiglas walls.

(b) 1.59 mm orifice, aluminum walls.

(c) 3.18 mm orifice, plexiglas walls.

(d) 3.18 mm orifice, aluminum walls.

(e) 4.76 mm orifice, plexiglas walls.

(f) 4.76 mm orifice, aluminum walls.

Figure 12. Boiling patterns at the end of the initial transient; 50% liquid fill tests. The drawn horizontal line indicates the height of the liquid prior to venting.

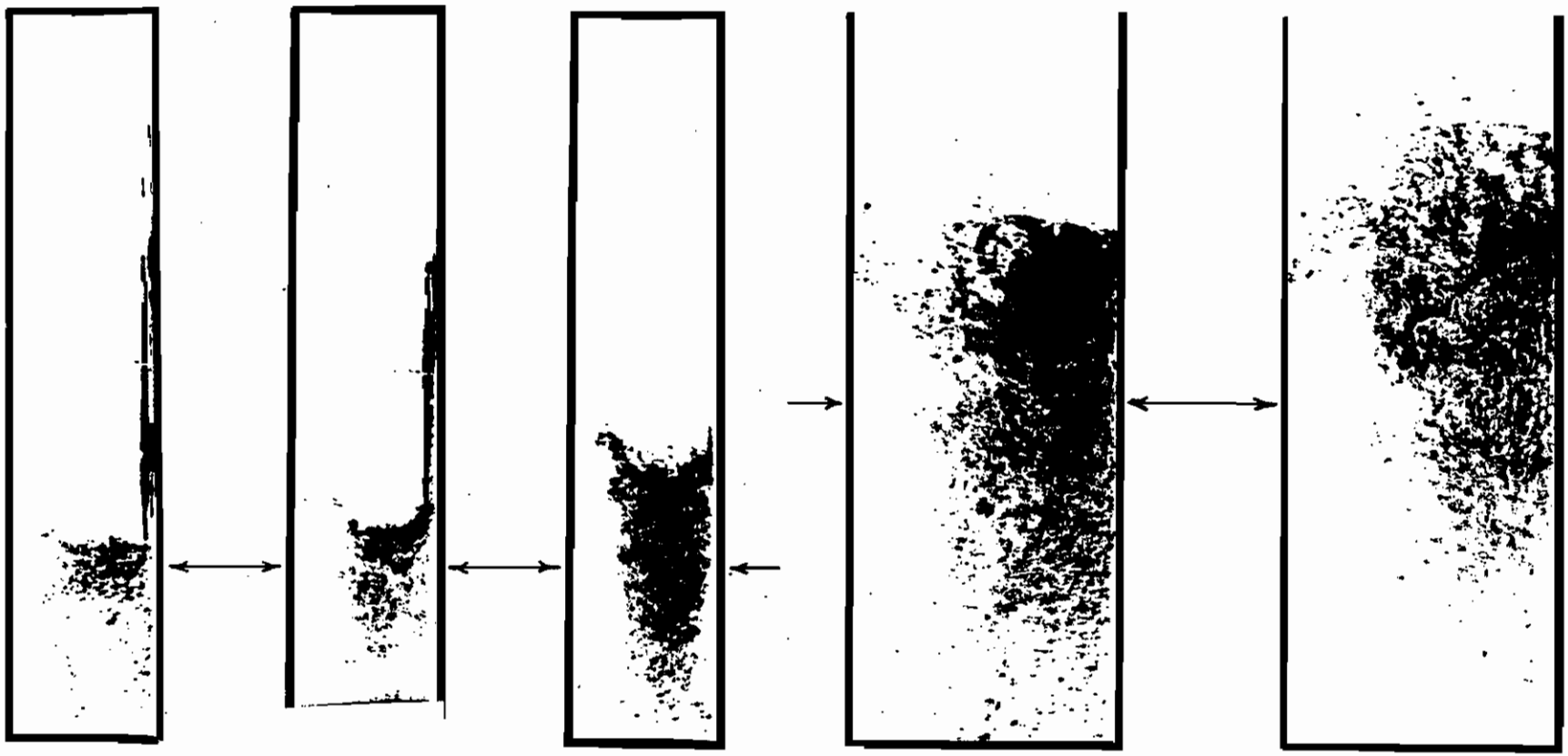

(a)
1.59 mm orifice,
plexiglas walls.

(b)
3.18 mm orifice,
plexiglas walls.

(c)
4.76 mm orifice,
plexiglas walls.

(d)
3.18 mm orifice,
aluminum walls
(enlarged view).

(e)
4.76 mm orifice,
aluminum walls
(enlarged view).

Figure 13. Boiling patterns at the end of the initial transient; 25% liquid fill tests. The drawn horizontal line indicates the height of the liquid prior to venting.

A cloud of evaporated Freon-12 appears immediately above the liquid-vapor interface when the orifice is opened and is drawn away by the vapor flow. More nucleation sites are active, including sites on the plexiglas windows (small cracks and surface imperfections) and at the liquid-vapor interface. The entire chamber is quickly involved in turbulent mixing and the two-phase column rises 8 to 10 cm, nearly filling the chamber. Drops and liquid filaments are thrown copiously into the exit section. The column's void fraction reaches about 0.28 by the end of the initial regime.

The 4.76 mm orifice, 75% fill tests with either plexiglas or aluminum walls (Figures 11e. and 11 f.) follow the same patterns as the 3.18 mm orifice tests, but are even more vigorous. Bubble nucleation again occurs initially at the liquid-vapor interface as well as at wall nucleation sites. Bubble growth is so rapid that bubbles are forced horizontally into the center of the chamber after forming on the side walls (see Figure 9c.), displaced by bubbles evolving behind them. The two-phase column, quickly and thoroughly mixed, vaults to the top of the vessel. Before the initial transient ends the column is apparently homogeneous and reaches a void fraction of about 0.40, filling the entire vessel.

The 50% and 25% fill tests exhibit no phenomena different from those already described. Figures 12. and 13. show that, visually, these low percentage fill tests are very similar to the 75% fill blowdowns during the initial regime. The progressive changes recorded in the beginning pressure drop have already been discussed.

The interface boiling event mentioned earlier is a phenomenon not reported in other investigations of the unsteady discharge of fluids

from pressurized containers. In the present study sudden ebullition at the liquid-vapor interface occurs in all 3.18 and 4.76 mm orifice tests with less than 100% inital liquid fills, but it does not occur in any of the 1.59 mm orifice tests. The effervescence appears to originate around the perimeter of the interface where it contacts the vessel walls and begins 0.05 to 0.1 seconds after wall nucleation starts.

Documentation of an interfacial boiling phenomenon extremely similar in detail to that observed in this study is presented in a report by Grolmes and Fauske [8]. In their investigation water, methanol and Freon-11 (trichlorofluoromethane) at saturation were subjected to sudden depressurization to an evacuated vessel. In a carefully prepared system that suppressed nucleate and bulk boiling, surface boiling was observed for all three liquids. Most relevant to this report is the discovery of a threshold liquid superheat required for interface boiling. Below the threshold only evaporation occured at the liquid surface.

The threshold superheat was dependent on system geometry, being lower for free surfaces of greater diameter. For a free surface of similar area to the interface in the present study (but notably of much smaller radius of curvature) the required superheat for surface boiling of Freon-11 was about 25°C (45°F).

In the present series of tests the initial depressurizations cause sudden liquid superheats which are consistently about 7°C (12°F), 11°C (20°F) and 14°C (25°F) for 1.59, 3.18 and 4.76 mm orifice tests, respectively. This implies that the threshold for interface boiling of Freon-12 in a 3.49 cm x 7.94 cm rectangular chamber is between 7°C and 11°C of liquid superheat. This threshold is much greater than the threshold for

nucleate boiling.

The mechanism inducing interfacial boiling is not fully explained. The concurrent free surface boiling and nucleate boiling observed in this study without the bulk boiling noted in other studies suggests that the phenomenon of free surface boiling should be investigated further.

The initial regime gives way to the main part of the blowdown as the system pressure peaks at a level somewhat lower than the initial pressure and boiling stabilizes to a quasi-steady pattern.

IV. THE BLOWDOWN FOLLOWING INITIAL TRANSIENTS

General Description

Once the initial stage of the blowdown is complete the pressure of the system begins a continuous decay towards atmospheric pressure. The liquid temperature decays similarly, always staying within a few degrees of the saturation point at the system pressure of the moment. The temperature in the vapor space above the boiling column rises above the saturation temperature as the liquid column subsides. The thermal gradient mentioned in the introduction develops in every test conducted and is duplicable.

Early in the blowdown the exit flow is choked and may include entrained liquid. At this point the pressure and related properties fall at rates governed by the mass discharge rate. As system pressure drops the two-phase column subsides to a height that will not provide liquid entrainment to the exit flow, which therefore becomes choked vapor flow. At a lower pressure a threshold is reached where the vapor flow becomes subsonic.

The system pressure eventually drops to within experimental error of atmospheric pressure. The liquid temperature levels off at -29.2°C (-20.5°F), which corresponds to a saturation pressure of 0.104 MPa (15.1 psia). The mass discharge rate here is controlled by the vapor generation rate through boiling, which in turn is controlled by the rate of heat transfer to the liquid from the environment.

The character of the boiling process changes near the end of the pressure decay. Earlier, nucleation was copious and bubble growth was rapid, with energy for evaporation supplied by the superheated liquid

(maintained superheated by continuous depressurization). When the system nears atmospheric pressure little energy is available from the liquid and boiling appears much more subdued. Bubbles nucleate from fewer sites per unit area on the walls and rise in vertical columns causing little disturbance of the surrounding liquid.

All the elements of the blowdown; pressure and temperature decay, mass discharge, exit quality, vapor production and heat transfer; are interrelated and difficult to describe individually without repeated references to the other phenomena. In the following sections each facet of the blowdown process is presented separately, but its intimate dependence upon the concurrent phenomena must be kept in mind. General remarks are made about the influence of other instantaneous system properties on the one under discussion, but detailed information on any related property is reserved for the section devoted to that property. It is hoped that this division will improve the clarity of the presentation concerning the complex two-phase blowdown process.

Pressure Decay

Comparative plots of the system pressure versus time are presented as Figures 14. through 19. These graphs are presented in a dimensional form (rather than a nondimensional form as instantaneous pressure divided by initial system pressure, $P(t)/P_0$) to provide easily interpretable quantitative pressure data. Comparisons to the accompanying temperature decays and to saturation conditions can be made directly. No loss of generality is incurred because initial pressures for all tests are within 0.035 MPa (5 psi) of each other. This variation has very little effect on the blowdown process.

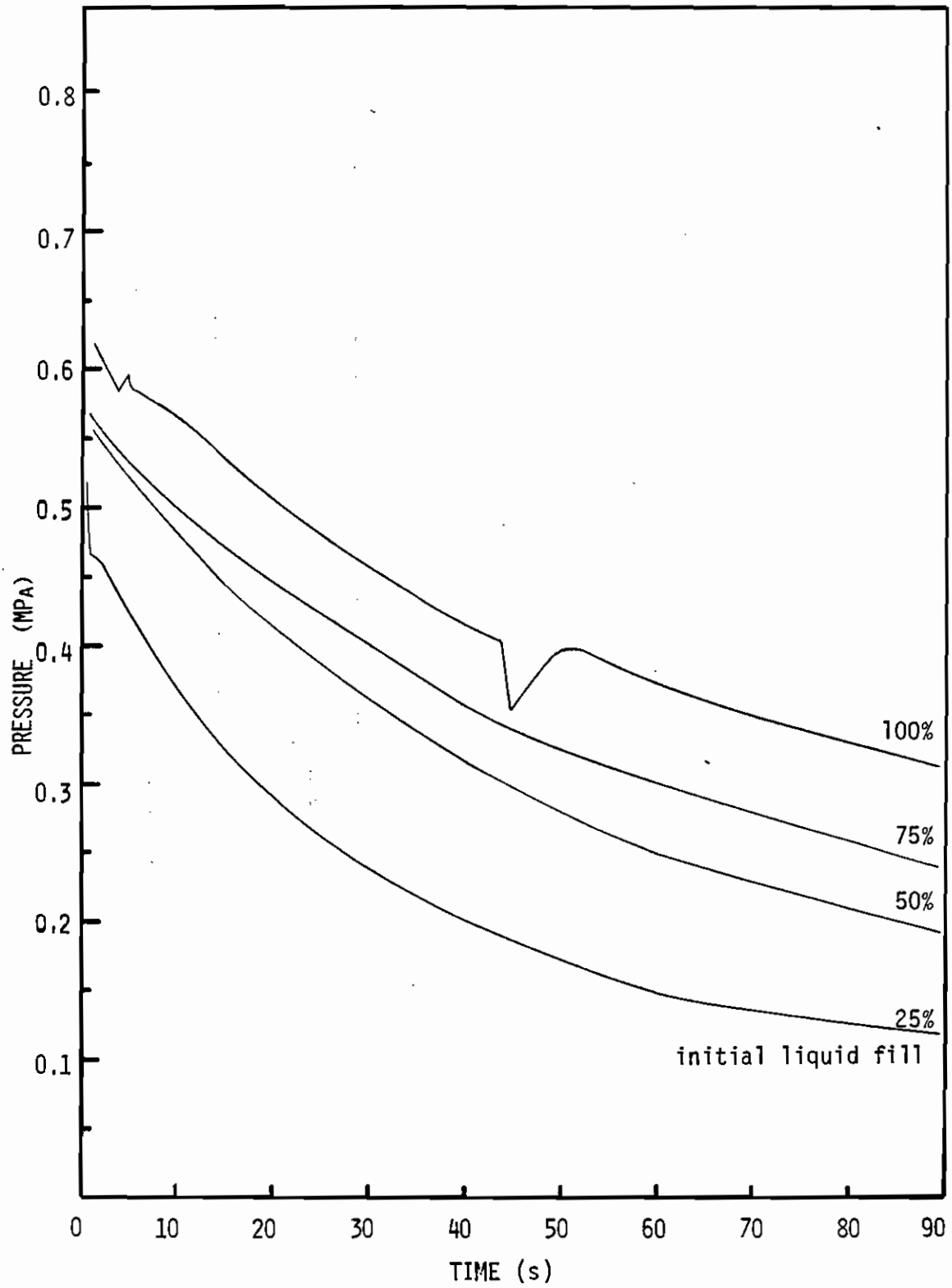

Figure 14. Pressure Decay Curve: 1.59 mm orifice, plexiglas wall tests. (for pressure in psia, multiply plotted value by 145)

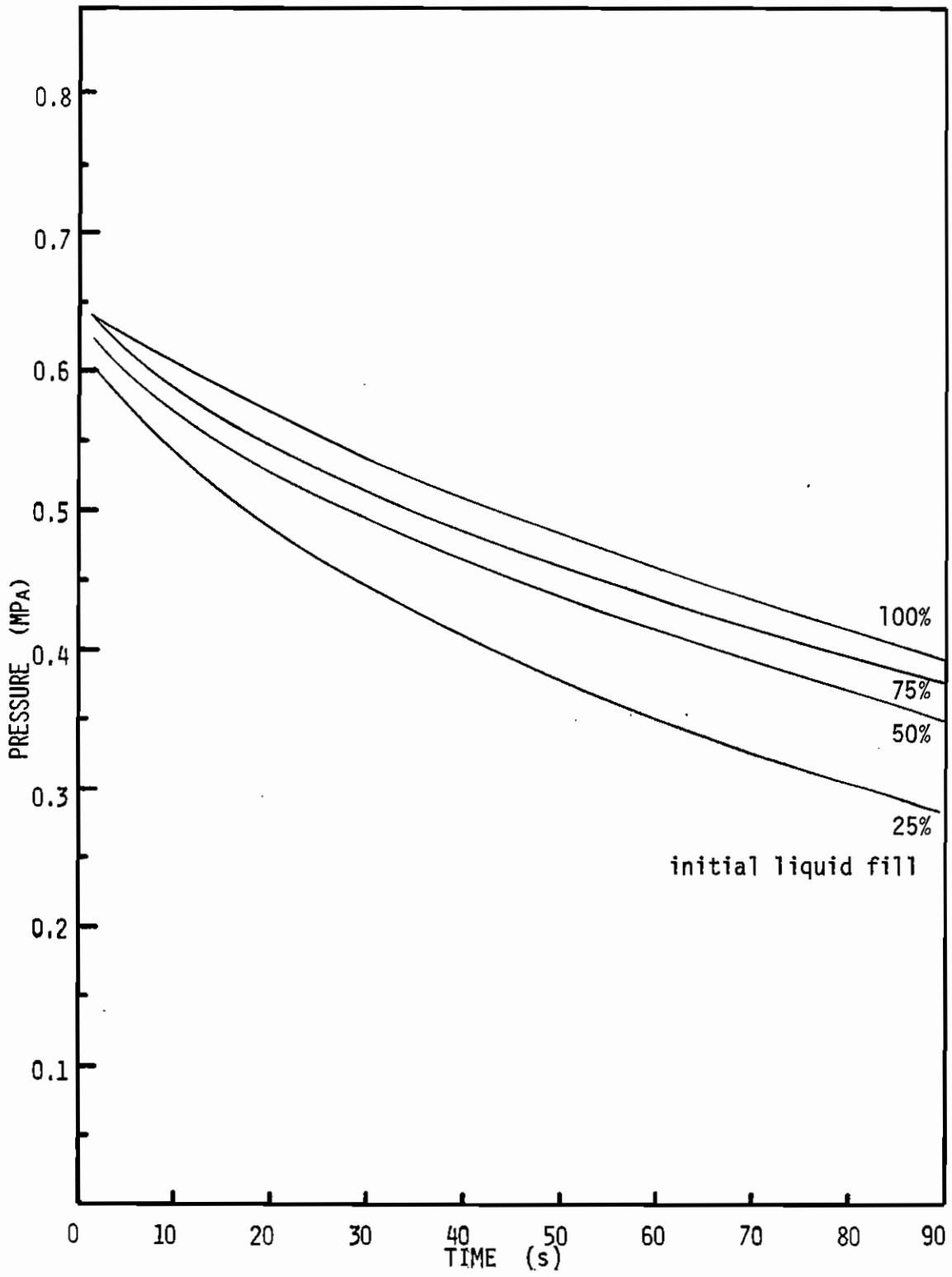

Figure 15. Pressure Decay Curve: 1.59 mm orifice, aluminum wall tests. (for pressure in psia, multiply plotted value by 145)

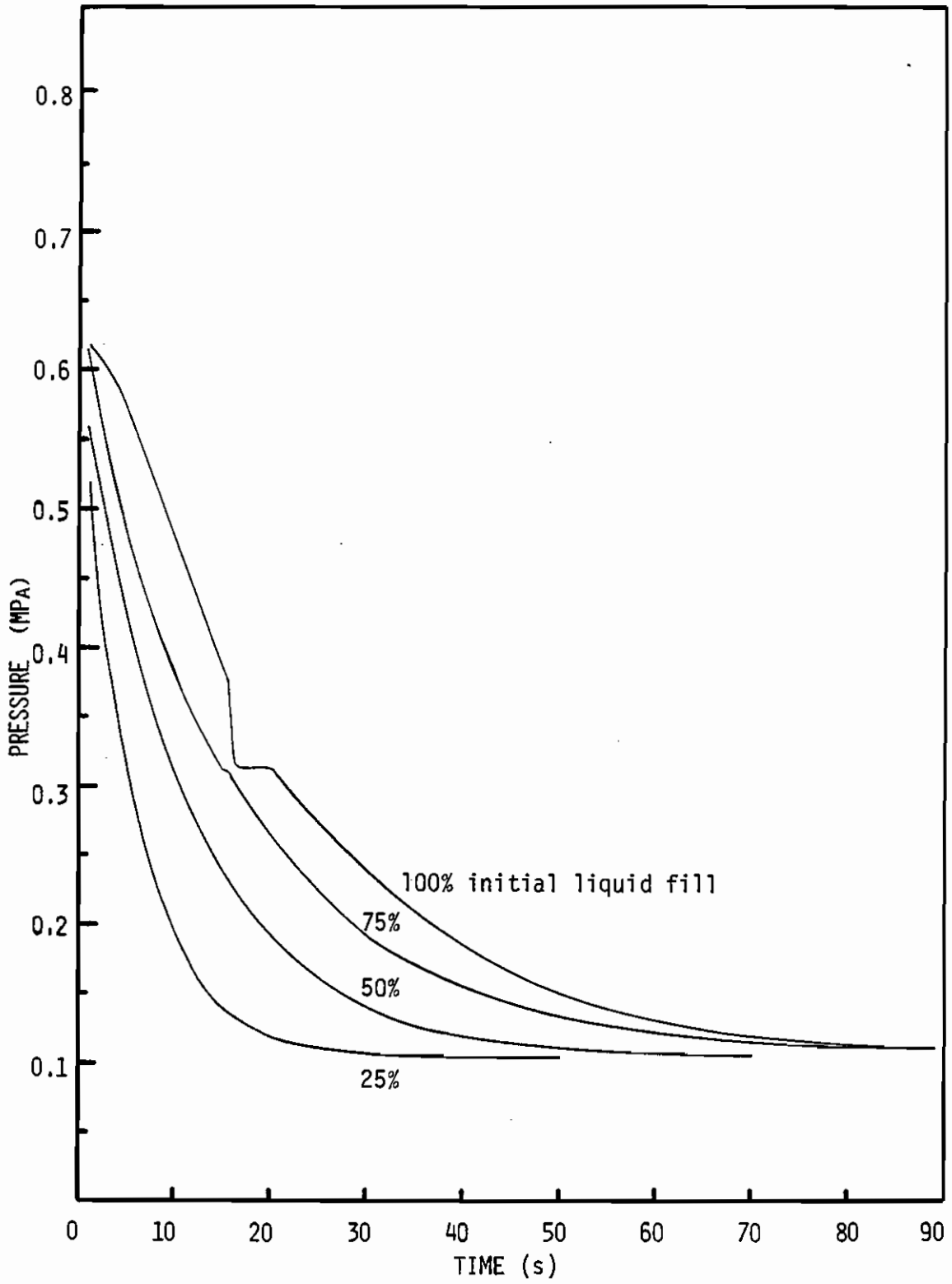

Figure 16. Pressure Decay Curve: 3.18 mm orifice, plexiglas wall tests. (for pressure in psia, multiply plotted value by 145)

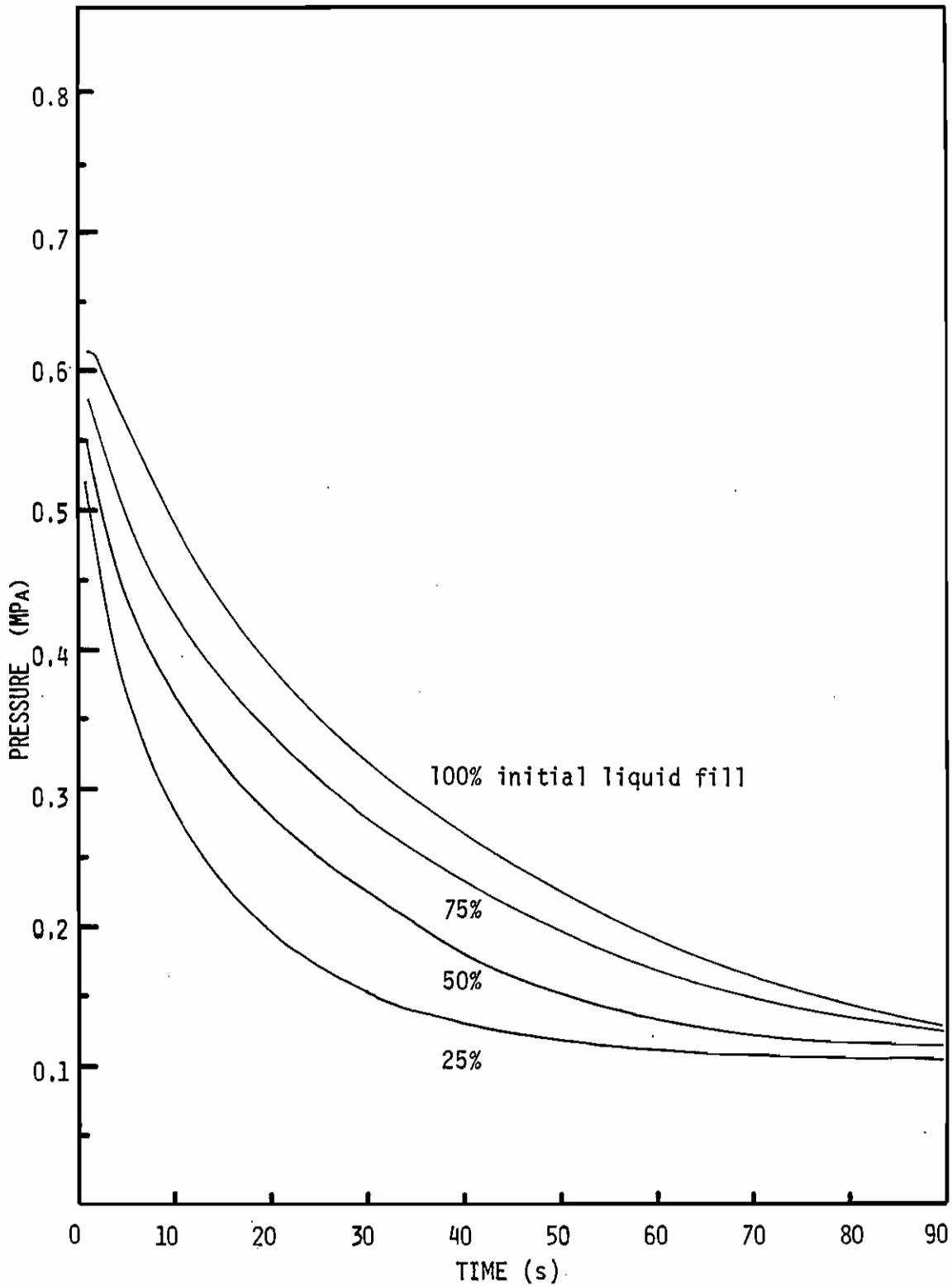

Figure 17. Pressure Decay Curve: 3.18 mm orifice, aluminum wall tests. (for pressure in psia, multiply plotted value by 145)

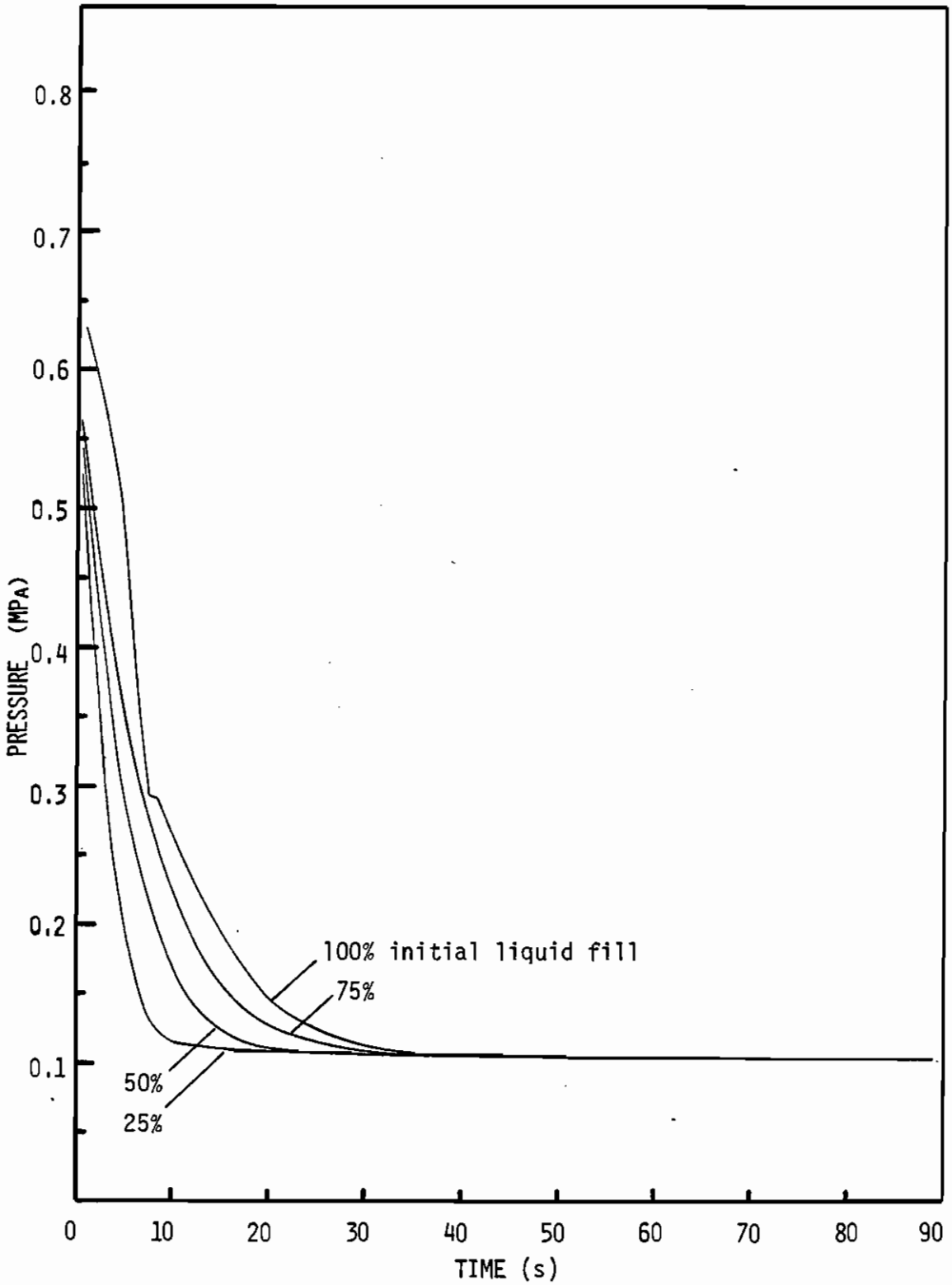

Figure 18. Pressure Decay Curve: 4.76 mm orifice, plexiglas wall tests. (for pressure in psia, multiply plotted value by 145)

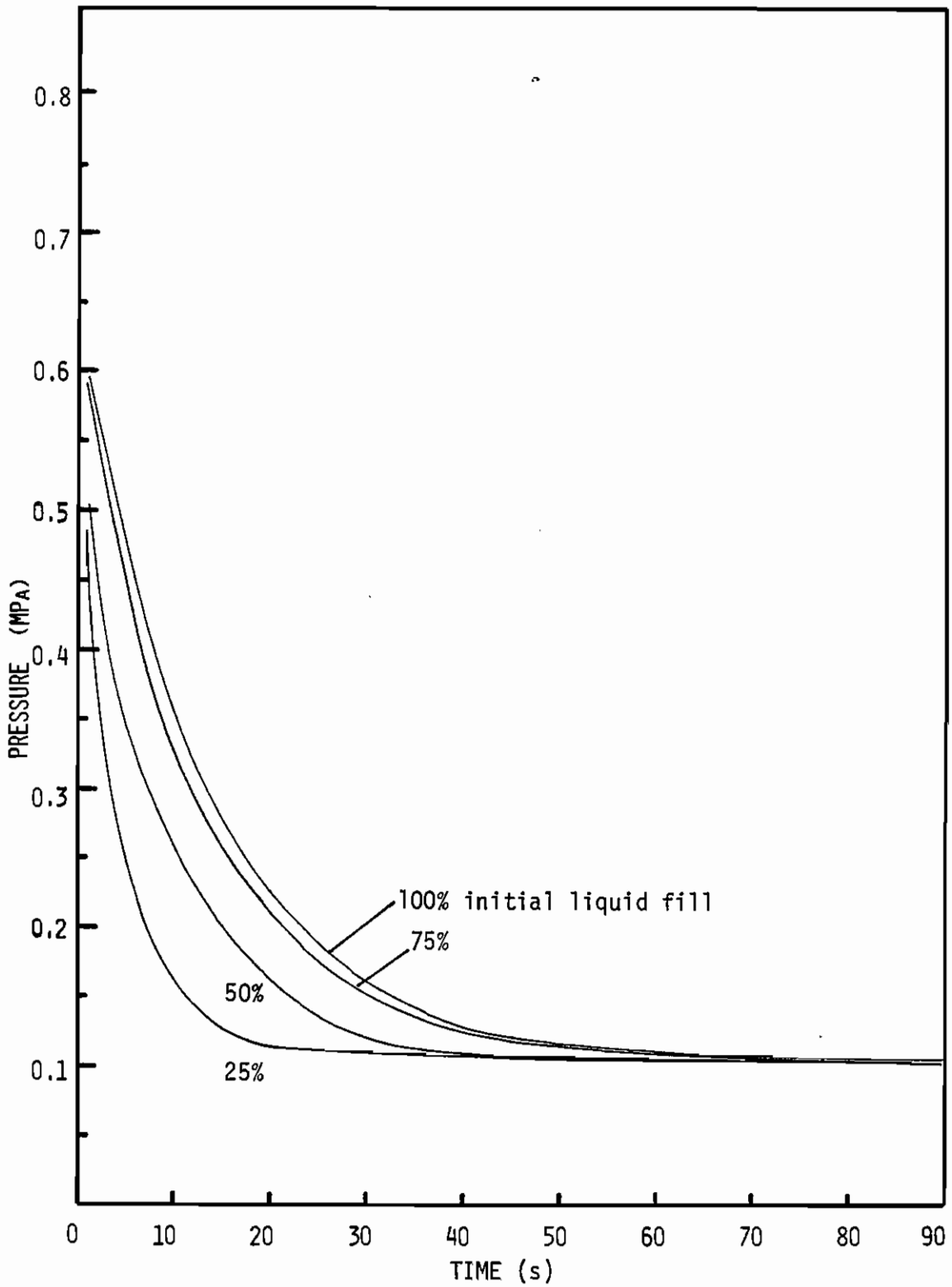

Figure 19. Pressure Decay Curve: 4.76 mm orifice, aluminum wall tests. (for pressure in psia, multiply plotted value by 145)

As would be expected, the pressure decay is more rapid the larger the orifice used (i.e. the larger the mass discharge rate). Gühler, Hanneman and Sallet [4] and Howell and Bell [7] observed the same behavior in earlier studies. In tests using the same orifice the pressure drop is more rapid the smaller the initial fill of liquid. Finally, it is observed that for otherwise duplicate tests the pressure drop in the vessel with plexiglas walls is more rapid than in the vessel with aluminum walls.

All the above observation can be explained by an energy balance equation for the venting system,

$$\dot{E} = \dot{Q} - \dot{W} - \dot{m}_e(h_e + V_e^2/2 + gZ_e)$$

Pressure (and temperature) in the saturated fluid is a function of the system's internal energy. System pressure decreases as the total energy of the system decreases during blowdown. In the present experimental setup no work is done by or on the system and changes in height are negligible. Also, the expression

$$h_{oe} = h_e + V_e^2/2 ,$$

where h_{oe} is the exit "stagnation enthalpy", can be used in the preceding equation, which then becomes

$$\dot{E} = \dot{Q} - \dot{m}_e h_{oe}$$

Increasing the mass discharge rate, $\dot{m}_e$, hastens the decrease of

system energy and therefore the drop in pressure. Similarly, plexiglas walls transfer energy to the liquid more slowly than do aluminum walls, resulting in a smaller $\dot{Q}$ term and thus a more rapid drop in system energy and pressure.

Freon-12 liquid contains roughly ten times the energy of Freon-12 vapor at ambient temperature on a volumetric basis. Therefore, a higher percentage fill of liquid provides the system with a larger initial store of energy, E_o. The energy balance equation in terms of ratios to the initial system energy becomes

$$\frac{d(E/E_o)}{dt} = \frac{d(Q/E_o)}{dt} - \frac{d(m_e h_{oe}/E_o)}{dt}$$

On this fractional basis the same instantaneous mass discharge rate or heat input rate causes a greater percentage change in system energy the smaller the initial fill of liquid (i.e. the smaller the initial system energy). The fractional drop in system pressure will be correspondingly greater for lesser initial fills of liquid.

One other difference between plexiglas and aluminum wall tests was detected. A sudden small pressure drop breaks the continuity of the pressure decay in the plexiglas wall tests at the moment when the two-phase column separates from the orifice. This does not occur in the corresponding aluminum wall tests. It is suspected that the transition from two-phase flow to vapor flow through the orifice is smoother in the aluminum wall case because greater heat transfer from the wall near the exit section enhances liquid flashing there.

Liquid Temperature Profiles

The behavior of the liquid temperature as the blowdown progresses is very similar to the system pressure behavior for the same reasons as discussed in the preceding section. The temperature of saturated Freon-12 varies with its internal energy, decreasing as internal energy decreases. Liquid temperature drops faster the larger the orifice and the smaller the initial fill of liquid. It also drops faster in the plexiglas wall tests than in the aluminum wall tests. Figures 20. through 25. are graphs of liquid temperature versus time for the various blowdowns conducted.

Throughout a blowdown the liquid temperature is essentially uniform in the well mixed two-phase column. No significant horizontal thermal gradient exists in the liquid. The only persisting vertical effect observed is that the bottom thermocouple, T_7, 1.3 cm above the vessel bottom, consistently records temperatures about 0.3°C (0.5°F) above those recorded by thermocouple T_6, 8.5 cm above T_7. Otherwise, local liquid temperatures vary randomly, but by no more than ±0.3°C from the instantaneous saturation temperature after the two-phase column has subsided from the exit section.

For experiments in which the boiling column fills the vessel at the beginning of the blowdown the Freon remains superheated as long as there is low quality flow through the orifice. Figure 26. depicts this situation for the 100% fill tests. From being initially subcooled the liquid quickly becomes superheated up to 2°C (4°F) during the initial regime. The superheated condition persists until the two-phase column no longer fills the chamber. Once the exit flow becomes high quality (virtually pure vapor flow) the liquid temperature rapidly drops to

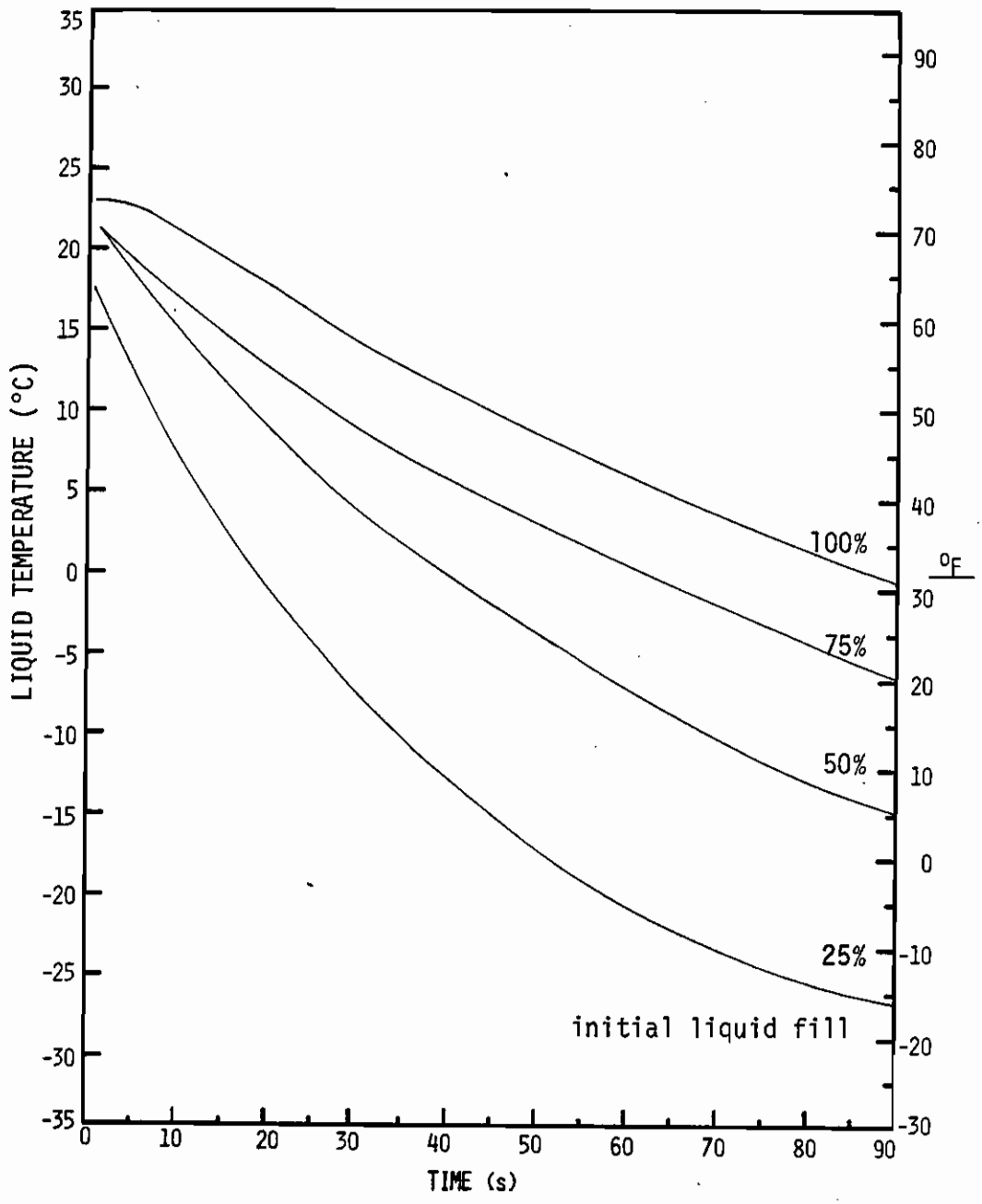

Figure 20.

Temperature Decay Curve: 1.59 mm orifice, plexiglas wall tests.

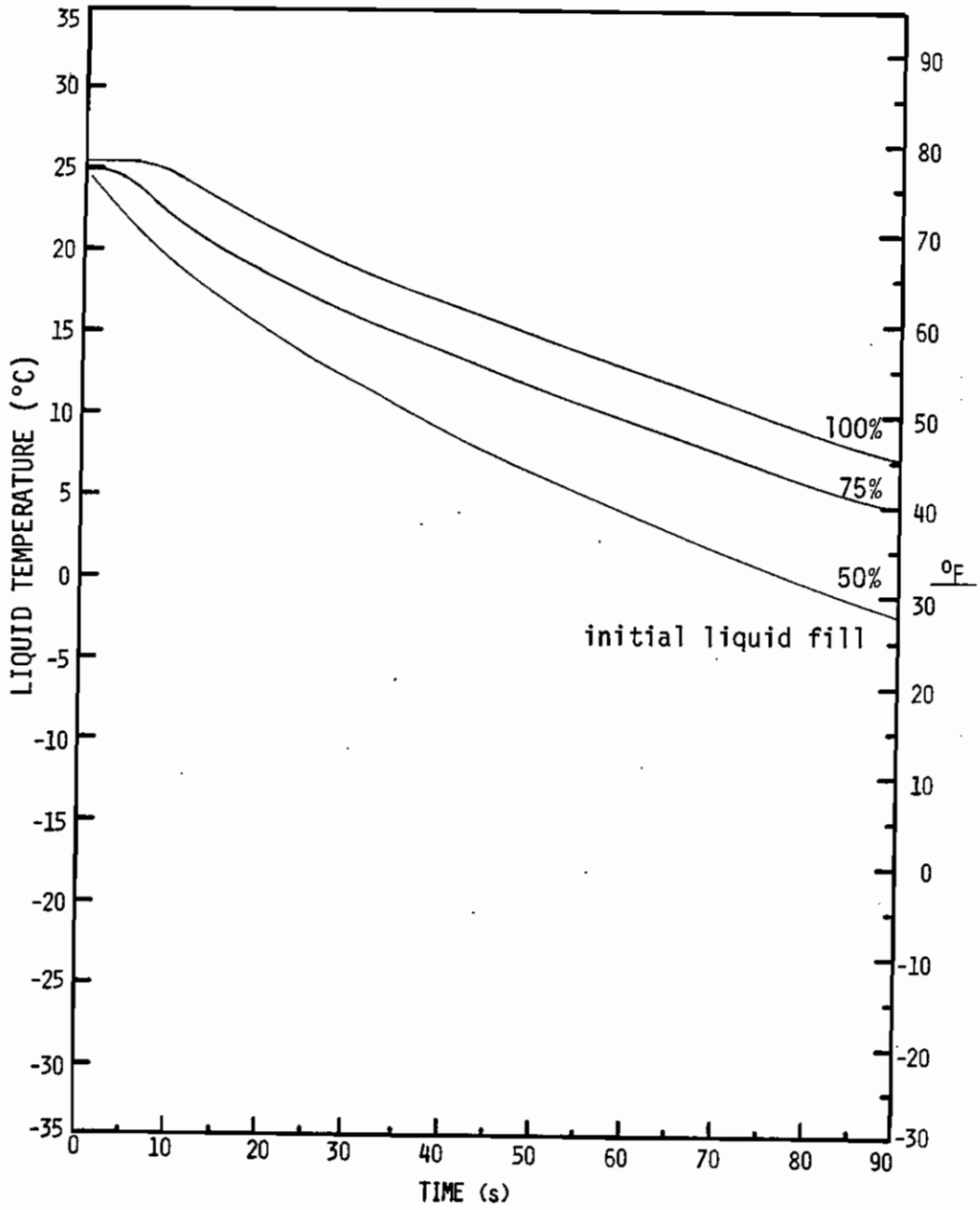

Figure 21.

Temperature Decay Curve: 1.59 mm orifice, aluminum wall tests.

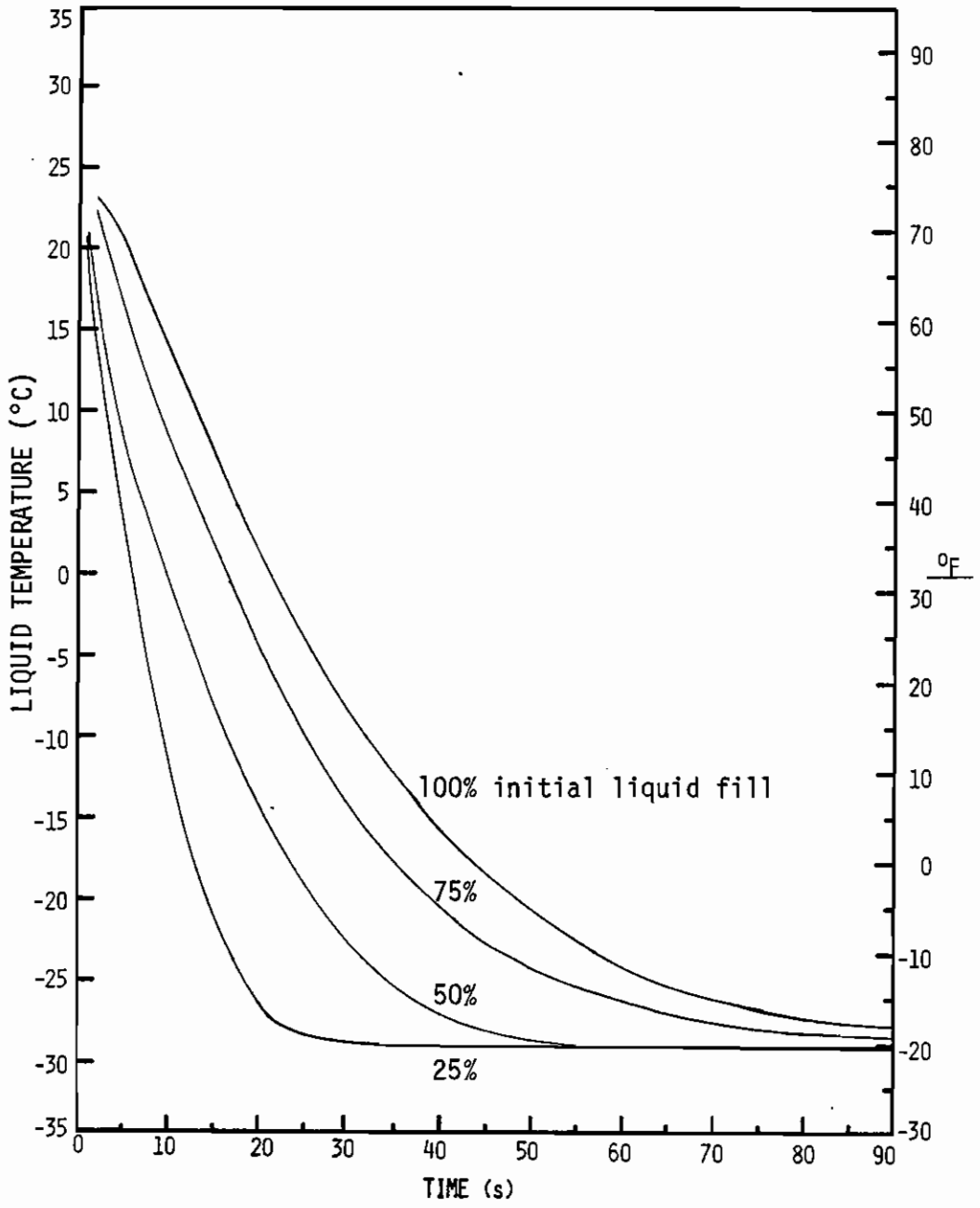

Figure 22.

Temperature Decay Curve: 3.18 mm orifice, plexiglas wall tests.

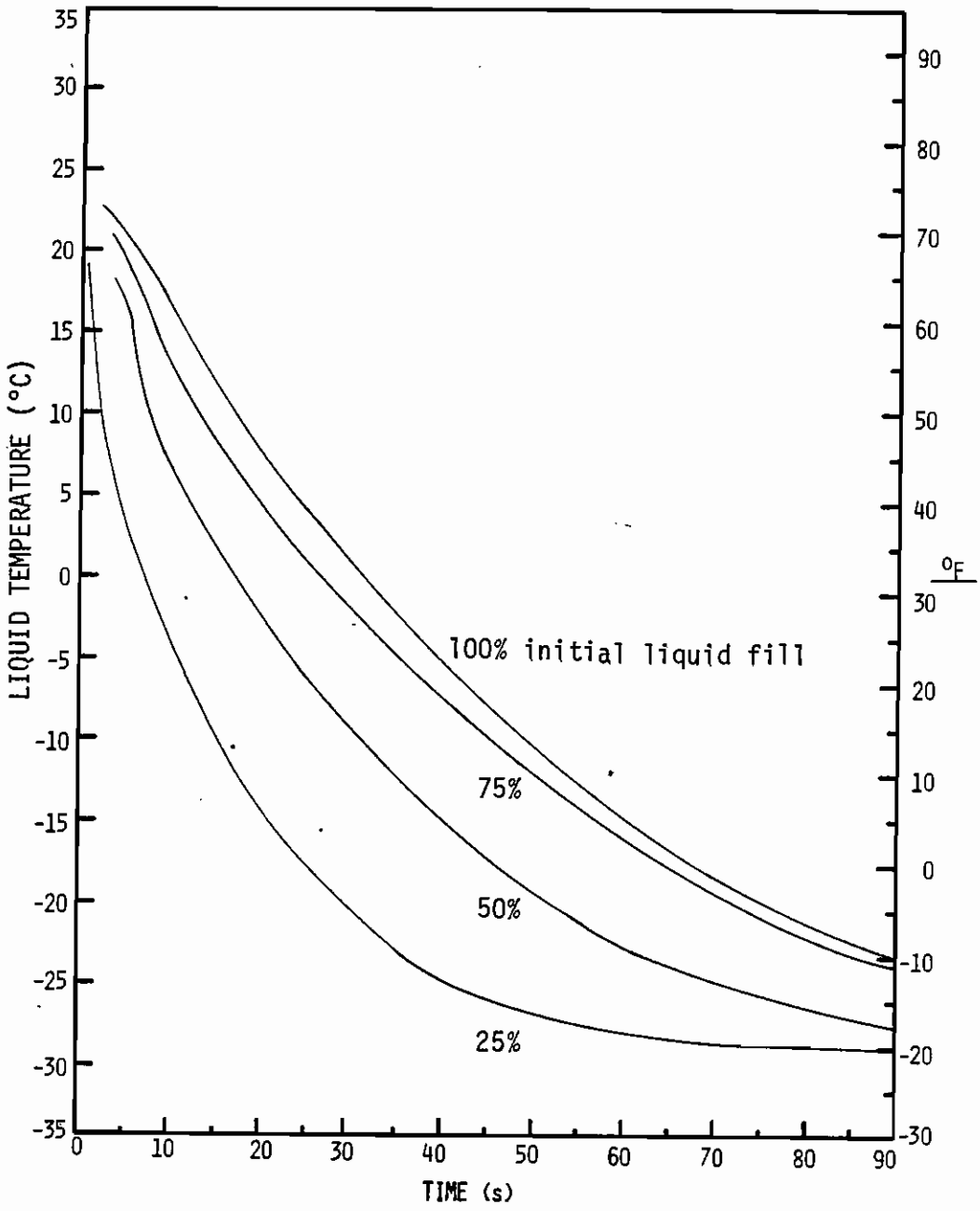

Figure 23.

Temperature Decay Curve: 3.18 mm orifice, aluminum wall tests.

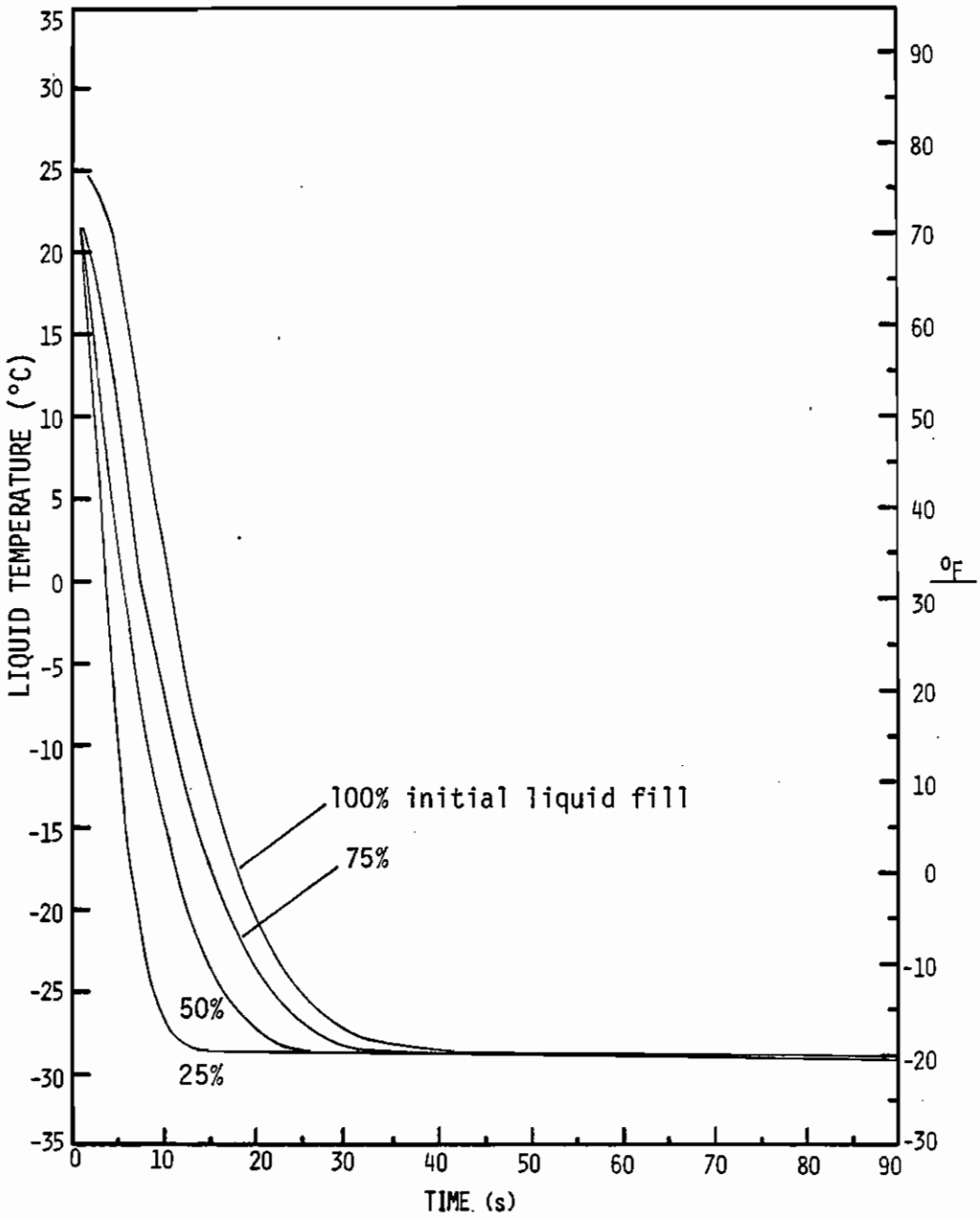

Figure 24.

Temperature Decay Curve: 4.76 mm orifice, plexiglas wall tests.

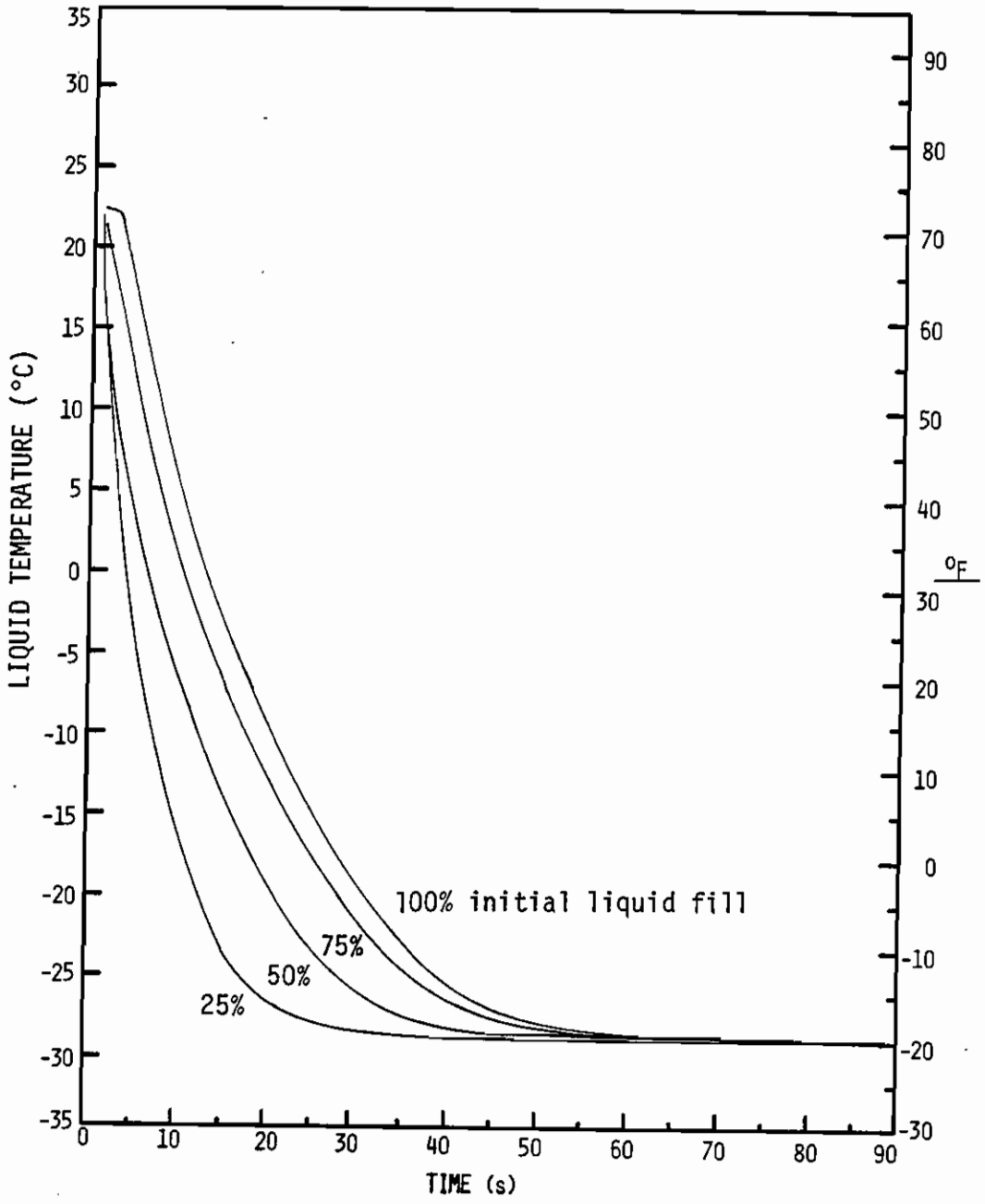

Figure 25.

Temperature Decay Curve: 4.76 mm orifice, aluminum wall tests.

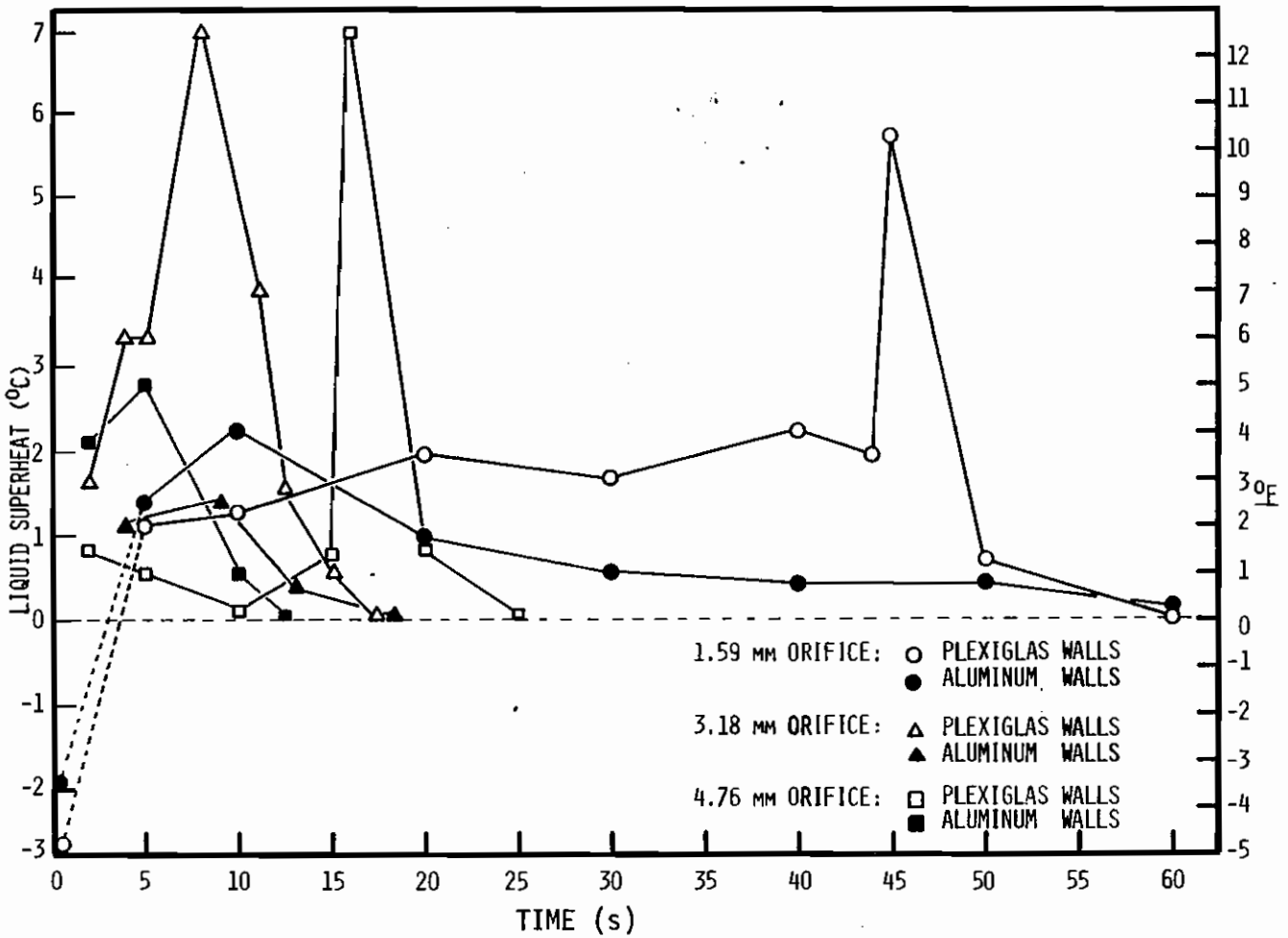

Figure 26. Liquid Superheat at the Beginning of the 100% Liquid Fill Tests.
(Spikes in the plexiglas wall tests correspond to sudden pressure drops associated with the separation of the 2-phase column from the orifice)

within experimental error of the saturation temperature at the measured instantaneous system pressure.

The prominent liquid superheat spikes occuring in the plexiglas wall tests correspond to the brief dips in pressure (also observed only in the plexiglas wall tests) at the moment the boiling column drops below the exit section. No effect on the actual liquid temperature profiles results from the dips in pressure, so the deviations manifest themselves as sudden jumps in liquid superheat.

Some previous studies, for example Tanger, Vachon and Pollard [1], report subcooling of the liquid at late times in blowdown processes. In this investigation, however, no evidence of significant liquid subcooling is detected. Near the end of the blowdowns the liquid temperatures remain within experimental error of saturation temperature.

Vapor Superheat

One distinctive feature of every blowdown conducted is the development of a thermal gradient in the vapor space above the boiling liquid. This phenomenon was first reported by Gühler, Hanneman and Sallet [4], who observed it in the blowdown of Freon-12 from a 1.2 liter vessel through 1.59 and 4.76 mm orifices. No satisfactory explanation of the phenomenon has yet been proposed.

Figures 27. through 31. present the thermal gradient in the vapor region as a function of time for some of the 1.59 mm orifice tests. It is apparent that the 87% fill test temperature profile nearly duplicates that of the 100% fill test with aluminum walls. The 97% and 93% fill tests with aluminum walls are not included because they do duplicate the thermal gradient development in the 100% fill, 1.59 mm, aluminum wall

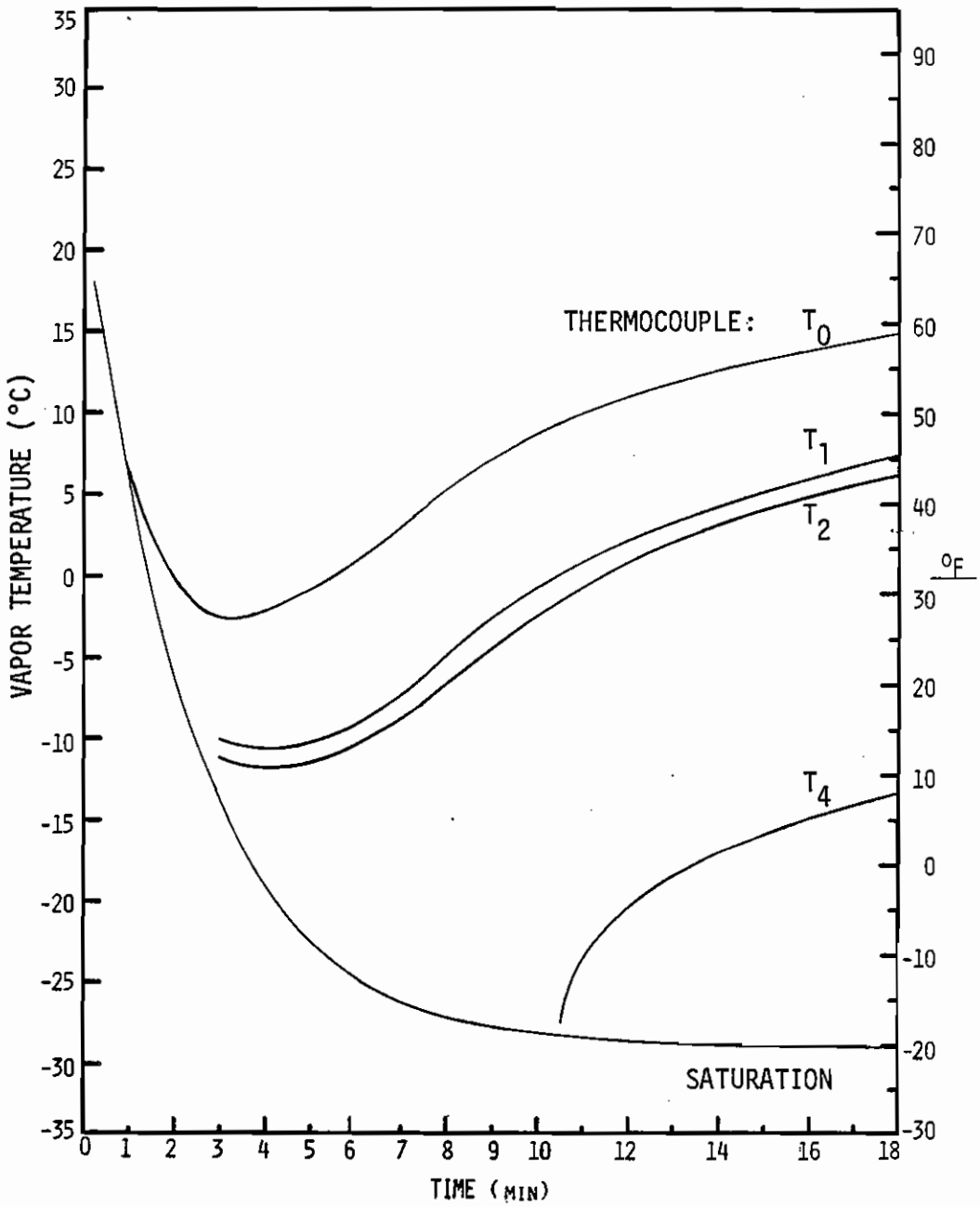

Figure 27. The Thermal Gradient in the Superheated Vapor Region: 1.59 mm orifice, 100% liquid fill, plexiglas wall test.

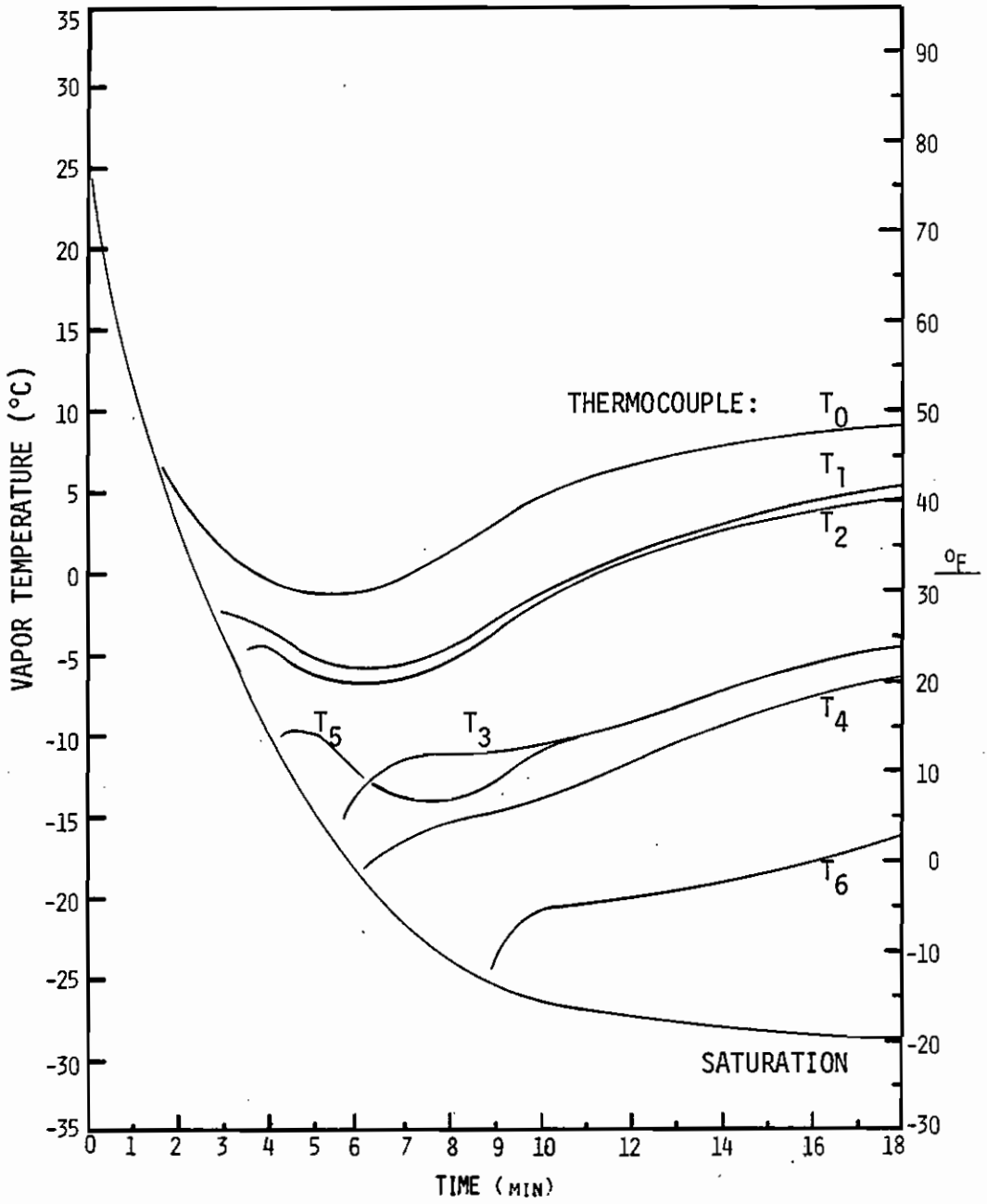

Figure 28. The Thermal Gradient in the Superheated Vapor Region: 1.59 mm orifice, 100% liquid fill, aluminum wall test.

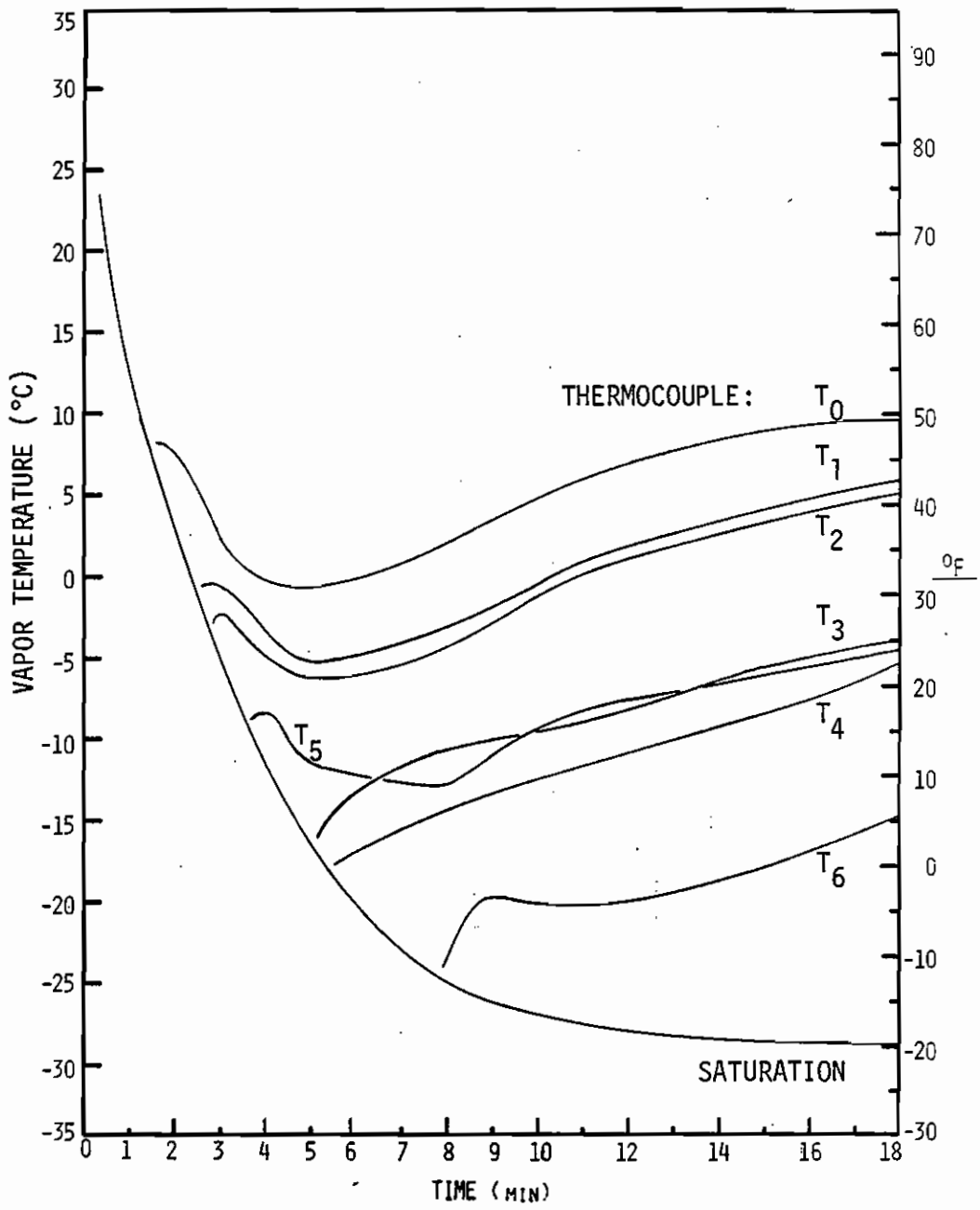

Figure 29. The Thermal Gradient in the Superheated Vapor Region: 1.59 mm orifice, 87% liquid fill, aluminum wall test.

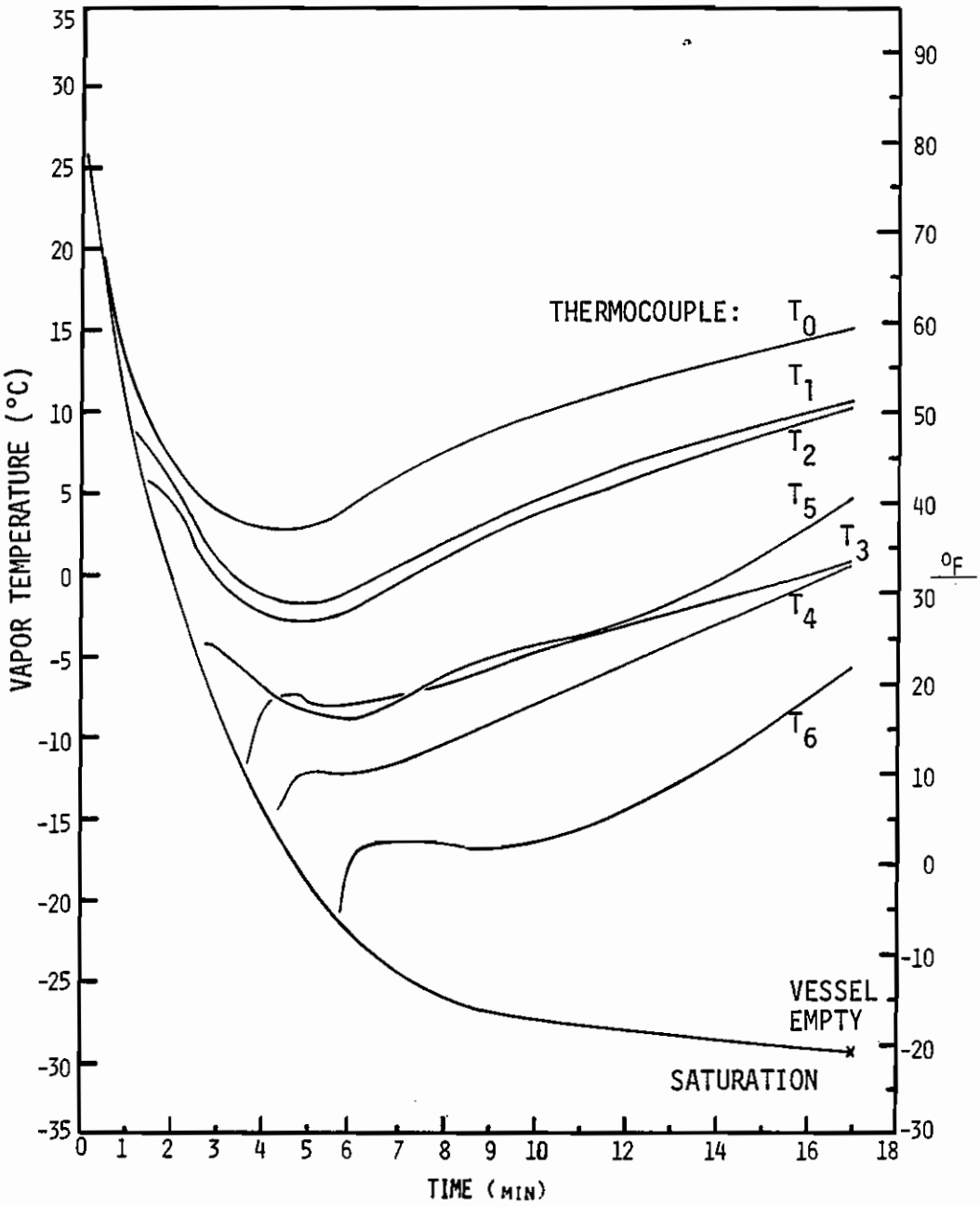

Figure 30. The Thermal Gradient in the Superheated Vapor Region: 1.59 mm orifice, 75% liquid fill, aluminum wall test.

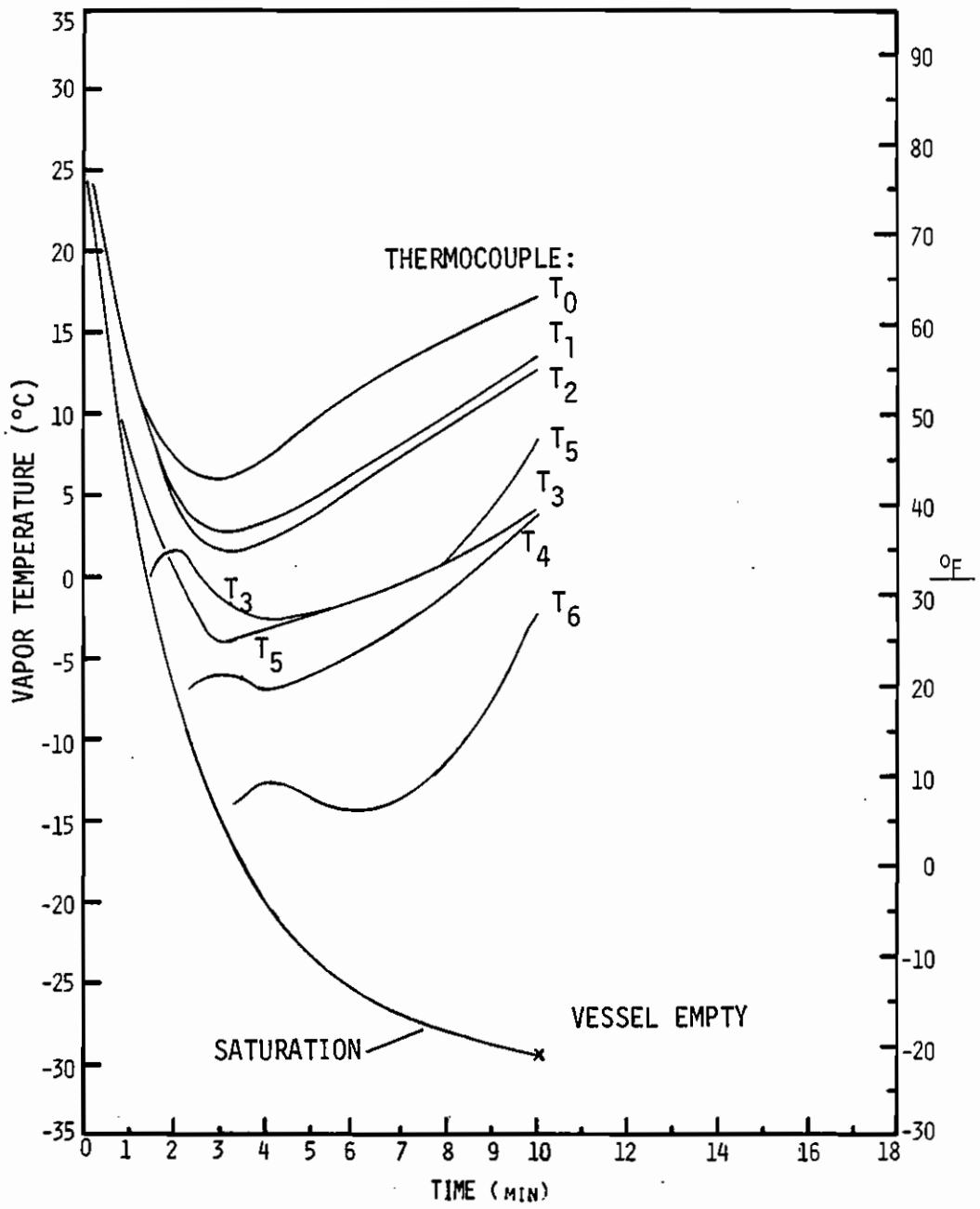

Figure 31. The Thermal Gradient in the Superheated Vapor Region: 1.59 mm orifice, 50% liquid fill, aluminum wall test.

test. The growth of the thermal gradient in the 3.18 and 4.76 mm orifice tests follow the same pattern as the 1.59 mm orifice tests, but on a shorter time scale.

As the thermal gradient develops it shows a nearly linear vertical temperature profile. The local superheat above the instantaneous saturation temperature varies directly with vertical distance, as can be seen in Figure 32. The local spatial derivative of the temperature profile (°C/cm) is therefore roughly constant spatially, but it does tend to increase with time by about 10 to 20% as the vessel closely approaches final emptying. Table 4. summarizes the values of the vapor region temperature gradient for all tests.

Except for the 25% fill tests, which have consistently milder gradients, the steepness of the gradients appears independent of orifice size (mass discharge rate) and initial percentage fill of liquid (that is, at least for fills of no less than 50%). Significantly, the gradients in the plexiglas wall tests are invariably steeper and achieve consistently higher absolute temperatures and superheats than in the aluminum wall tests. This implies that the primary cause of the gradient is not simple heat transfer from the walls of the chamber, which would lead to steeper gradients for aluminum wall tests (due to greater conductivity of the wall material).

Paradoxically, in the plexiglas wall tests thermocouples tend to remain at saturation temperature after the liquid column has subsided well below them. Vapor at mid-height in the chamber is still at the instantaneous saturation temperature when the liquid-vapor interface is as much as 4 cm below it. This is in contrast to the aluminum wall tests, in which the vapor is recorded as being superheated by the time

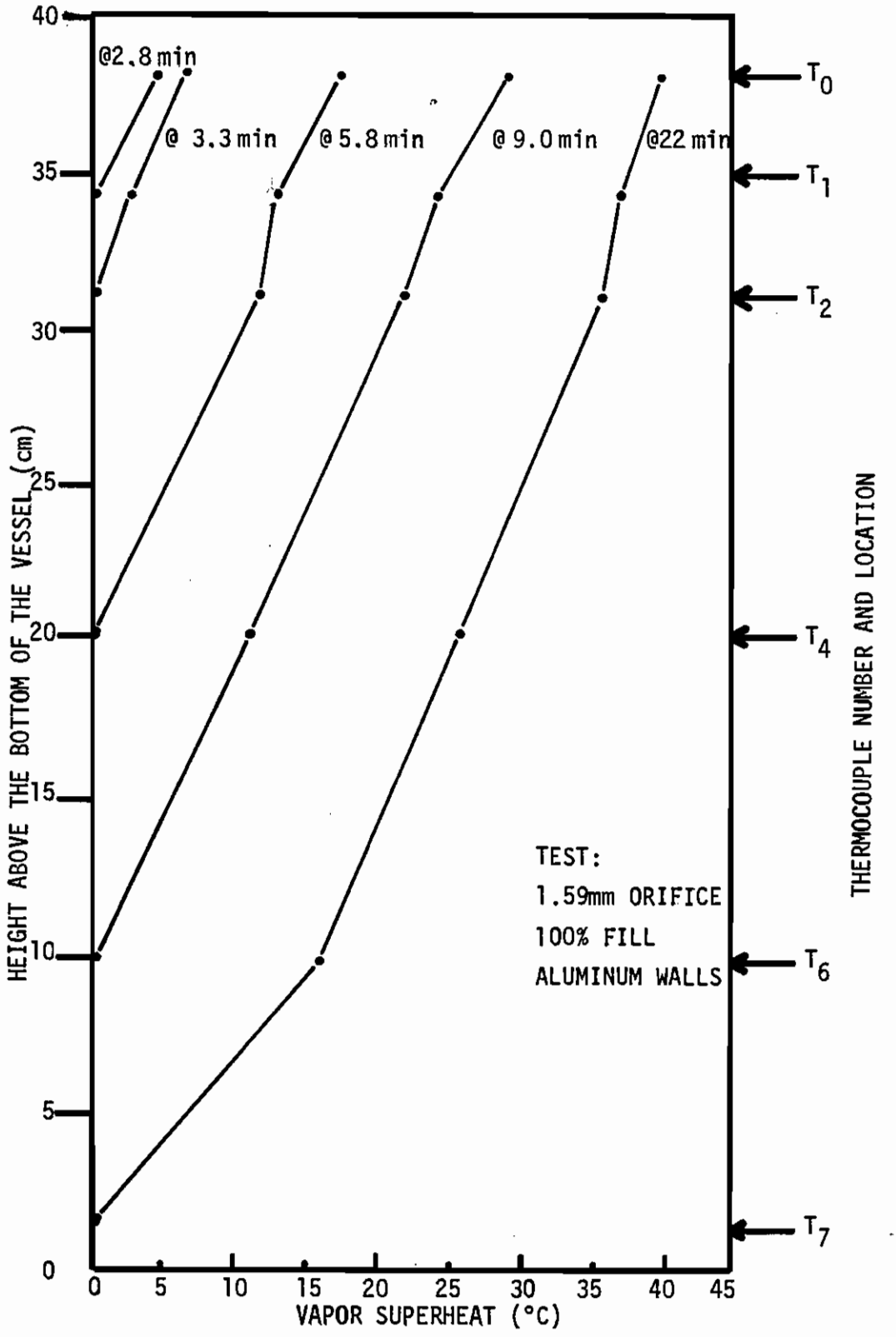

Figure 32. Vapor Superheat Profile in the Pressure Vessel. (profiles are plotted at the times when each thermocouple emerges from the boiling liquid column into the vapor space)

Table 4. Vapor Region Temperatures and Thermal Gradients.

ORIFICE DIAMETER	INITIAL % LIQUID FILL	TEMPERATURE @ T_0[1] PLEXI. WALL	TEMPERATURE @ T_0[1] ALUM. WALL	THERMAL GRADIENT PLEXI. WALL	THERMAL GRADIENT ALUM. WALL
1.59 mm [2]	100%	9.8 °C	5.1 °C	1.7 °C/cm	0.9 °C/cm
	97	-	5.1	-	0.9
	93	-	4.4	-	0.9
	87	-	10.0	-	0.9
	75	18.2	10.2	1.8	1.0
	50	21.1	17.5	1.4	1.0
	25	23.5	-	0.9	-
3.18 mm [3]	100%	-11.2 °C	-13.2 °C	1.6 °C/cm	1.0 °C/cm
	93	-	-13.0	-	1.0
	87	-	-11.8	-	1.0
	75	-11.1	-11.4	1.8	1.0
	50	4.4	-10.9	1.7	1.0
	25	19.9	-0.1	[4]	0.7
4.76 mm [3]	100%	-5.0 °C	-12.5 °C	1.6 °C/cm	1.0 °C/cm
	93	-	-16.7	-	0.9
	87	-	-15.3	-	1.0
	75	1.7	-14.5	[4]	0.9
	50	7.3	-6.4	1.7	1.0
	25	21.7	9.7	0.8	0.6

Notes: [1] Thermocouple T_0 is nearest the exit section, 1.9 cm below the top of the test chamber.

[2] These values were recorded at 10.0 minutes into the blowdown (all 1.59 mm orifice tests).

[3] These values were recorded at 60 seconds into the blowdown (all 3.18 and 4.76 mm orifice tests).

[4] The thermal gradient was not fully developed at the time that temperature recordings were terminated.

'-' indicates that no test with these specifications was run.

it is visibly out of the two-phase column (no more than 1 cm above the liquid surface). This lag in the vapor temperature excursion in the plexiglas wall tests would seem to indicate that the larger heat transfer rates for aluminum walls enhance the thermal gradient in the region immediately above the liquid-vapor interface.

One thermodynamic result of the thermal gradient would be a concurrent density gradient in the superheated vapor. For Freon-12 at 0.103 MPa (15 psia) saturation temperature is -29.3°C (-20.8°F). A rise in temperature to 15.5°C (60°F) at constant pressure induces a decrease in density from 0.0064 g/cm^3 (0.40 lb/ft^3) to 0.0053 g/cm^3 (0.33 lb/ft^3), a drop of 17%. An experimental search for such a density gradient would be important in the determination of the mechanism governing development of the thermal gradient in the vapor space.

The three thermocouples in a horizontal array indicate that there is also a horizontal temperature gradient in the vapor region. During the main part of the blowdown the temperature at the center of the vessel is typically 3 to 8°C (5 to 15°F) cooler than the temperature near the walls at mid-height in the chamber. This is observed in all tests, with the steeper horizontal gradients occuring for the more rapid decompressions. At late times in the blowdowns with aluminum walls, when the vessel is very near to final emptying and the mass discharge rate is low (less than 1 g/s), the highest temperature recorded in the horizontal profile is often at thermocouple T_5, midway between the wall and the vessel's centerline (see Figure 30.). Both the center and the wall thermocouples record temperatures several degrees cooler. This phenomenon appears repeatedly in the aluminum wall tests and implies a complicated flow pattern in the vapor space at low mass flow rates. The

average vapor velocity in the chamber for a discharge rate of 1 g/s is about 3 cm/s.

In the plexiglas wall tests data on the vapor temperature near the wall could not be obtained because the thermocouple nearest the wall was affected by heat conducted through its metal probe barrel, which has a thermal conductivity about 1000 times greater than that of the plexiglas wall surrounding it. More centrally located thermocouples were not noticably affected in this manner, and the horizontal as well as the vertical temperature gradient could be demonstrated reliably for the plexiglas wall tests.

System Mass and Mass Discharge Rate

The entire blowdown process is essentially a mass and energy balance problem. Any model of the process must include accurate predictions of both the instantaneous system mass and the mass discharge rate. Specific enthalpy, internal energy and mean density in the system depend on the instantaneous system mass. As demonstrated earlier, the mass discharge rate is an important factor in the energy balance as wall as in the mass balance.

Figures 33. through 38. present the total mass of Freon-12 discharged as a function of time. This format was chosen, rather than the mass remaining in the system versus time, in order to readily compare the effects of different initial masses of liquid. Values of the initial system mass for all tests conducted are given in Table 1. (page 5). The rapid venting of mass in the higher percentage fill tests results mainly from liquid entrainment in the exit flow at the beginning of the blowdowns. At later times all the mass curves level off to about

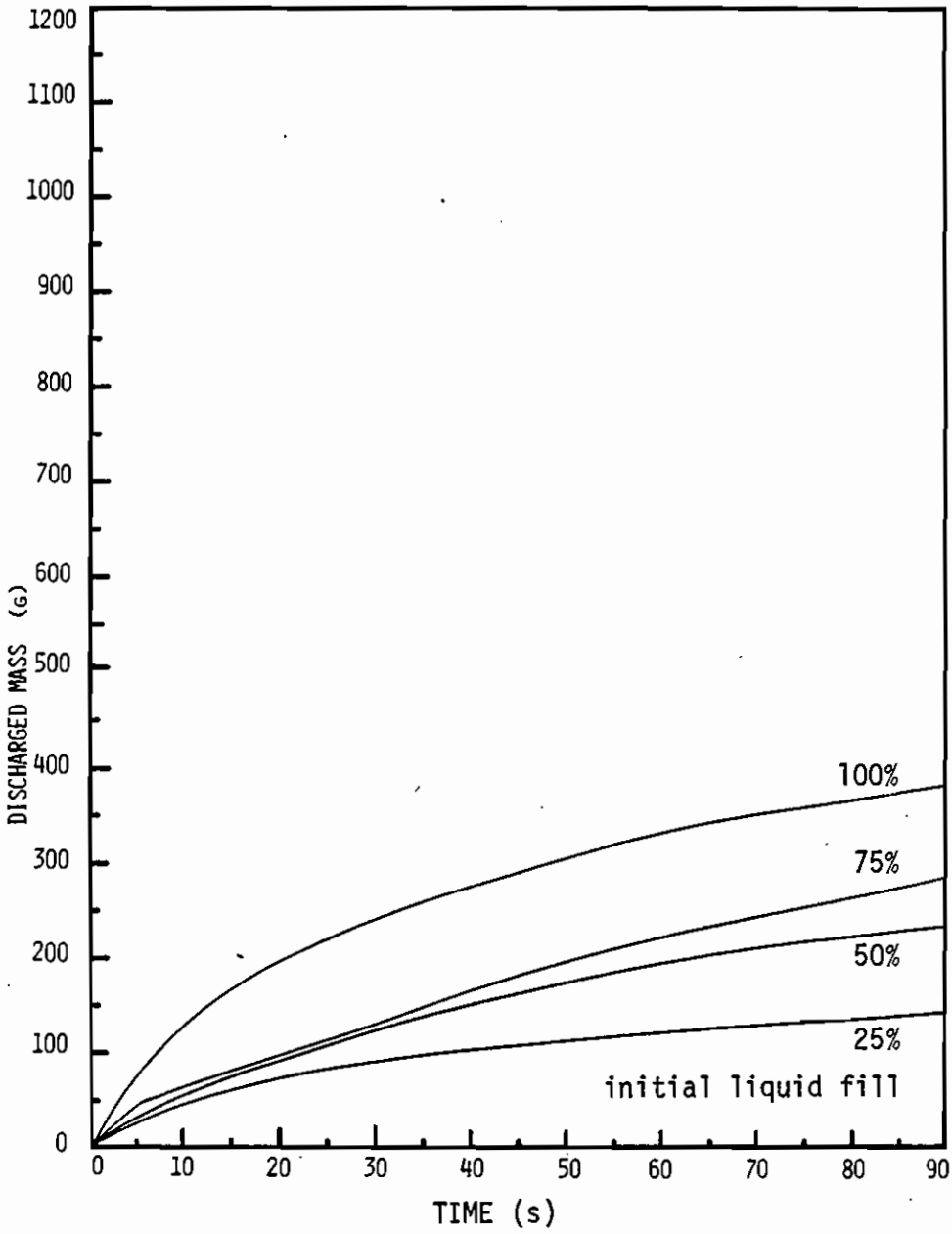

Figure 33. Discharged Mass: 1.59 mm orifice, plexiglas wall tests.

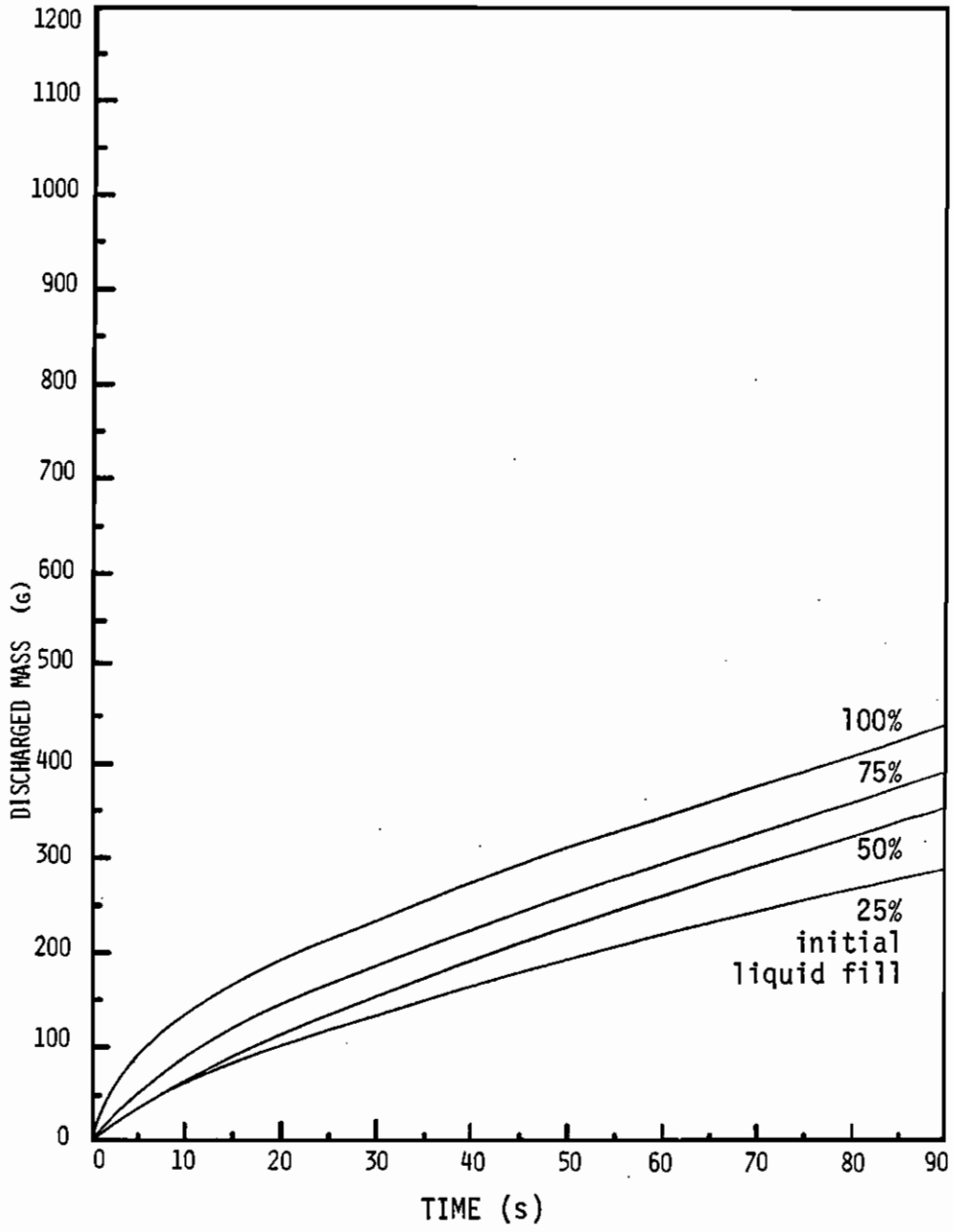

Figure 34. Discharged Mass: 1.59 mm orifice, aluminum wall tests.

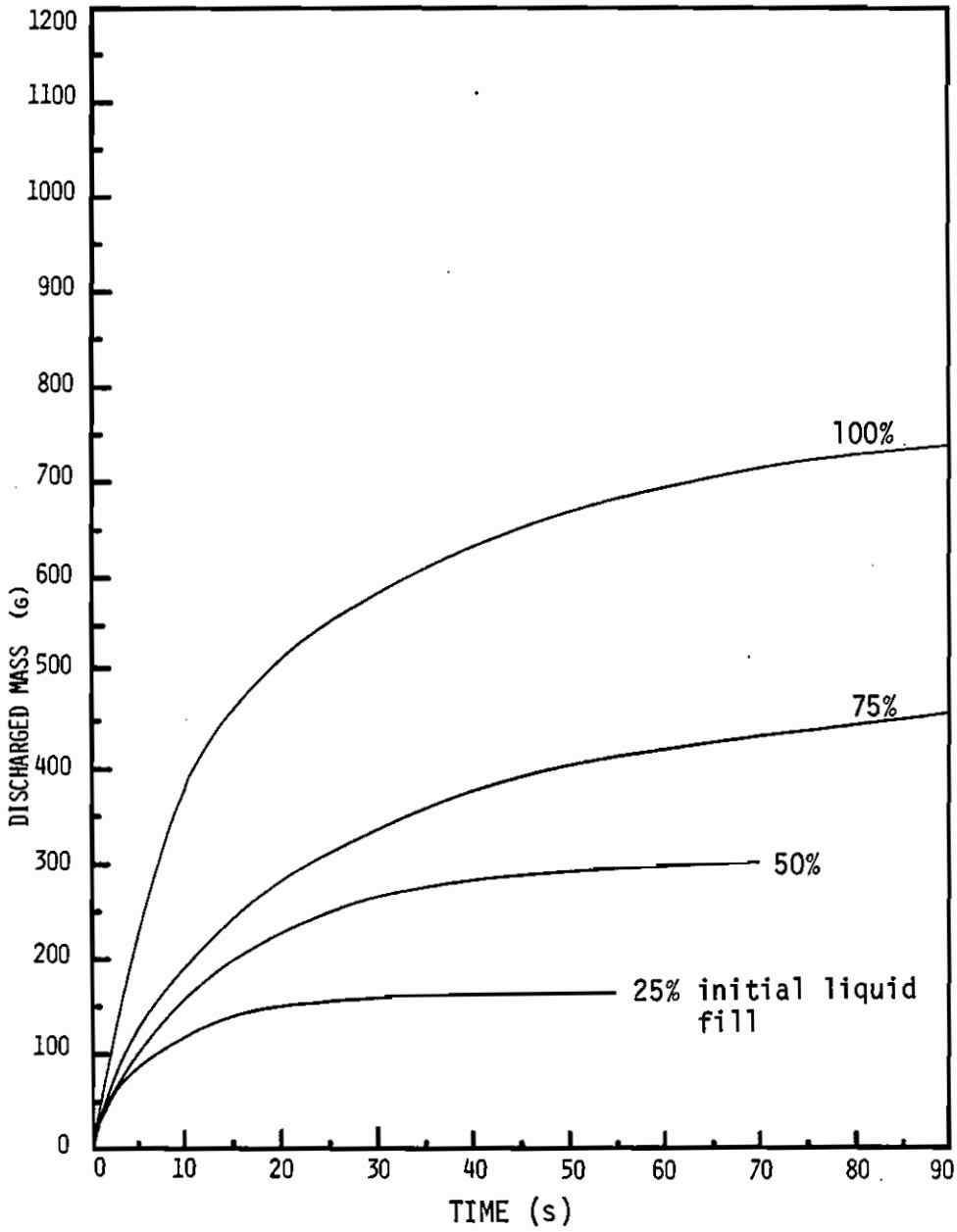

Figure 35. Discharged Mass: 3.18 mm orifice, plexiglas wall tests.

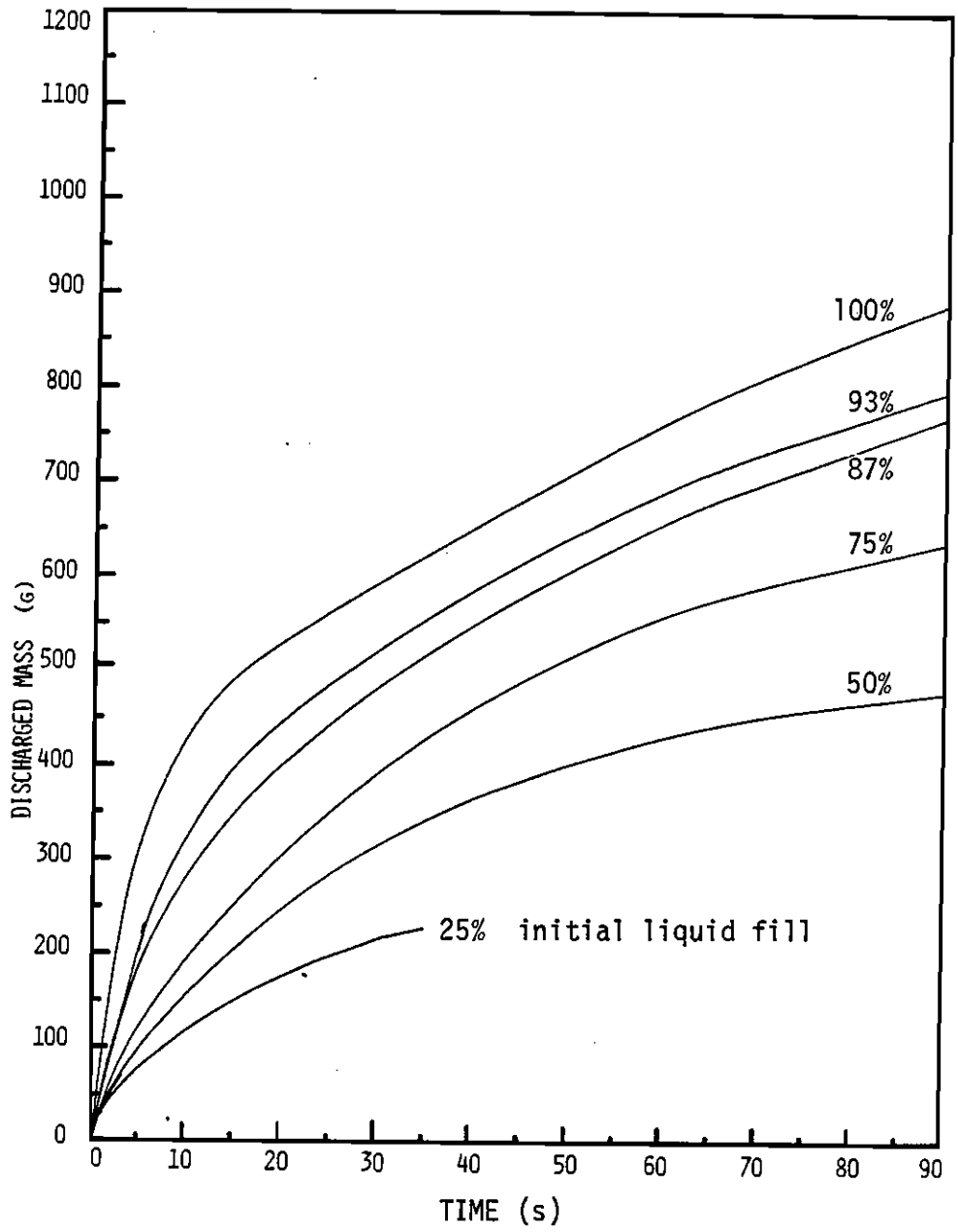

Figure 36. Discharged Mass: 3.18 mm orifice, aluminum wall tests.

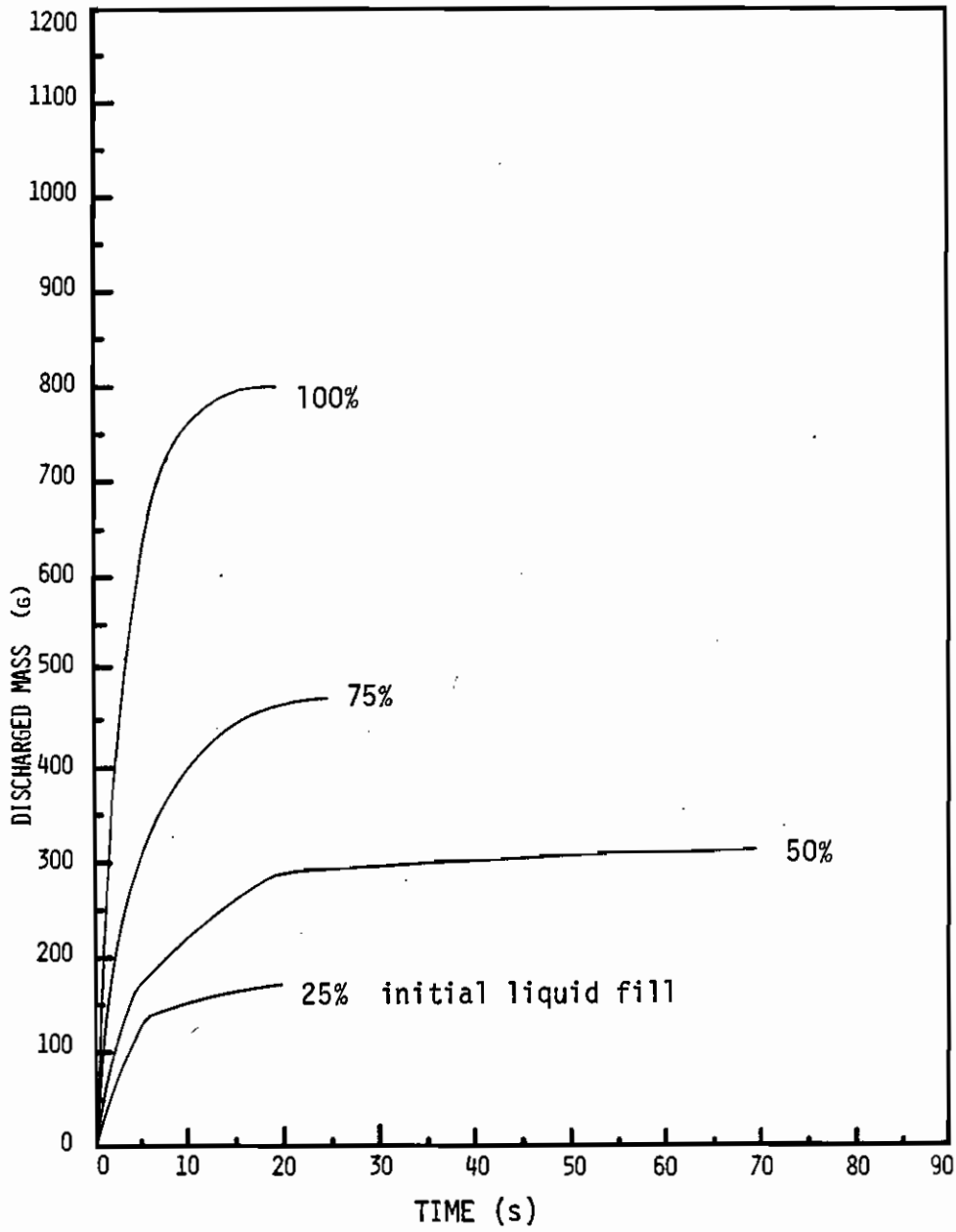

Figure 37. Discharged Mass: 4.76 mm orifice, plexiglas wall tests.

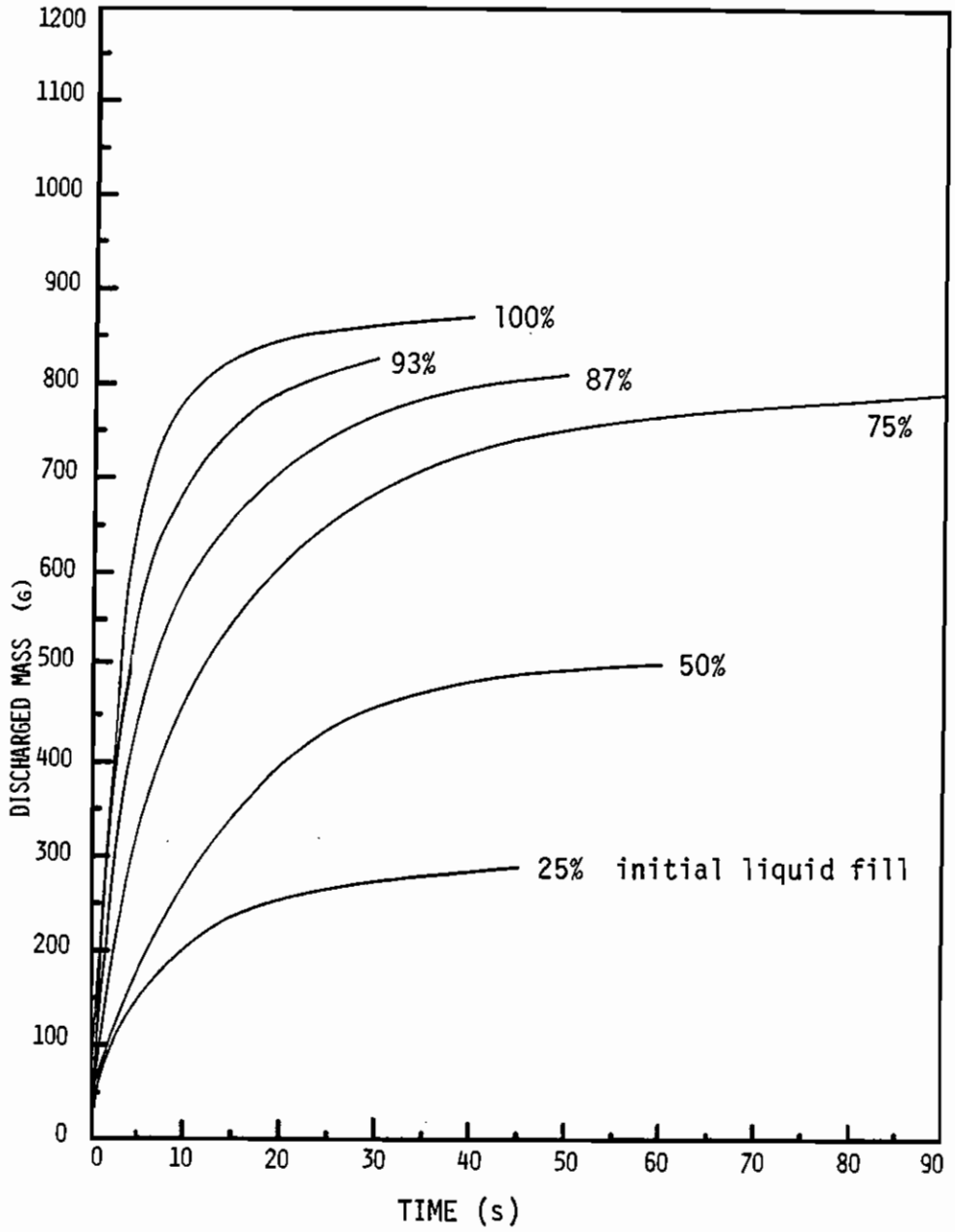

Figure 38. Discharged Mass: 4.76 mm orifice, aluminum wall tests.

the same slope. These observations are reflected in the mass flow rate curves also, since the instantaneous mass discharge rate is actually a more fundamental parameter than the instantaneous system mass in these blowdown experiments. Comparisons of the mass flow rates of the 100%, 75%, 50% and 25% liquid fill tests are presented in Figures 39. through 44.

As would be expected, the mass discharge rate is larger the larger the orifice during the major part of the blowdown. At the beginning of the blowdowns two-phase discharges greatly increase the mass flow rates for tests in which the boiling column fills the chamber. During the second blowdown regime when only vapor flows through the orifice, the mass discharge rate is dependent only on the orifice size and the momentary system pressure and is independent of the instantaneous system mass. Thermodynamic properties of the fluid at saturation can be specified by pressure alone. When the system pressure closely approaches atmospheric pressure the mass discharge rate ceases to be a function of orifice size and becomes dependent solely on the rate of heat transfer to the fluid from the vessel walls. Here the mass discharge rate is effectively the rate of vapor production in the boiling liquid.

Boiling Characteristics

The boiling patterns for all tests continue throughout the second blowdown regime as they were established at the end of their respective initial regimes. Figures 10. through 13. (pages 33 through 36) characterize the boiling patterns in different tests at the transition from the initial regime to the main blowdown regime, about 1 second into the tests. The 1.59 mm orifice tests all exhibit the same pattern to the

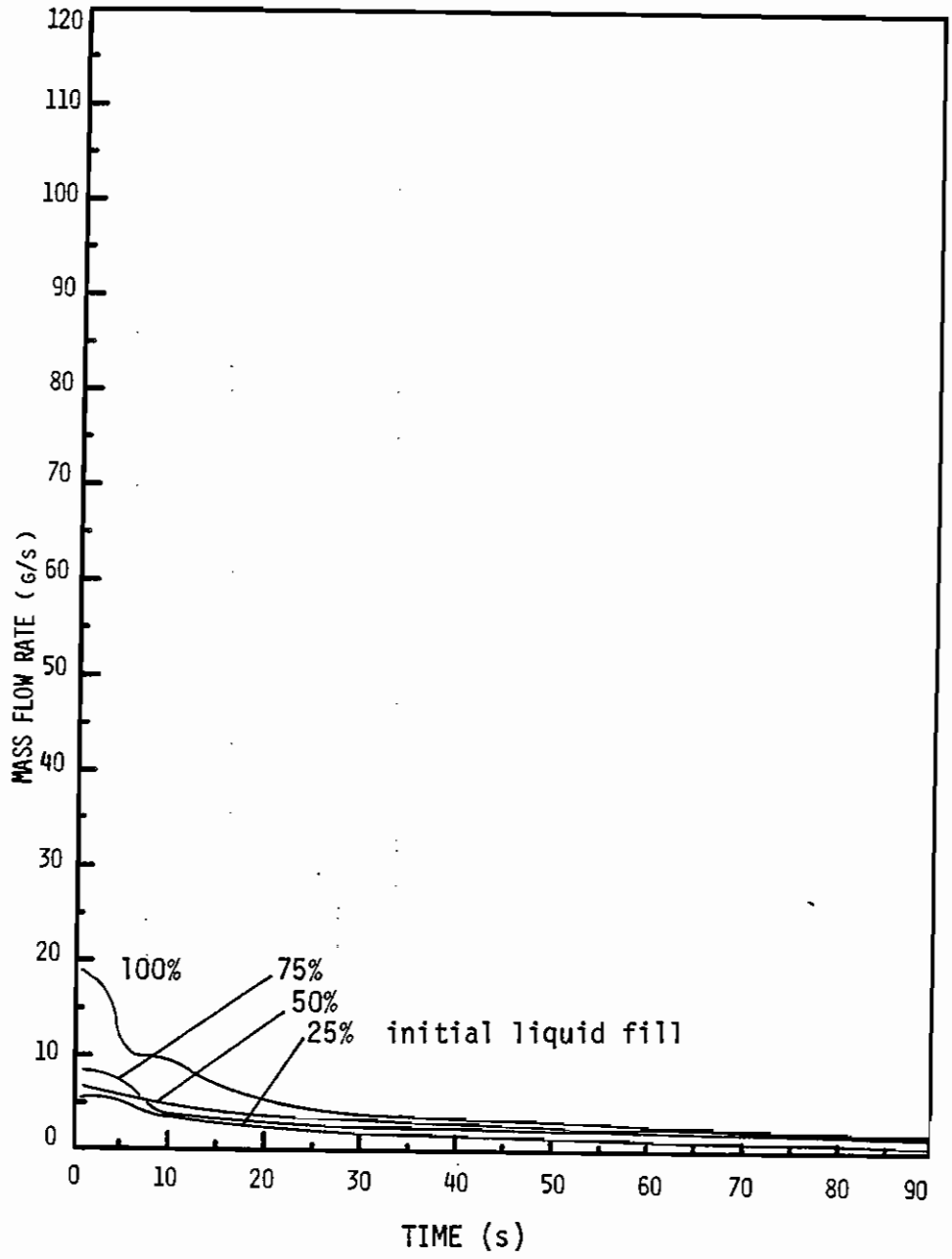

Figure 39. Instantaneous Mass Discharge Rate: 1.59 mm orifice, plexiglas wall tests.

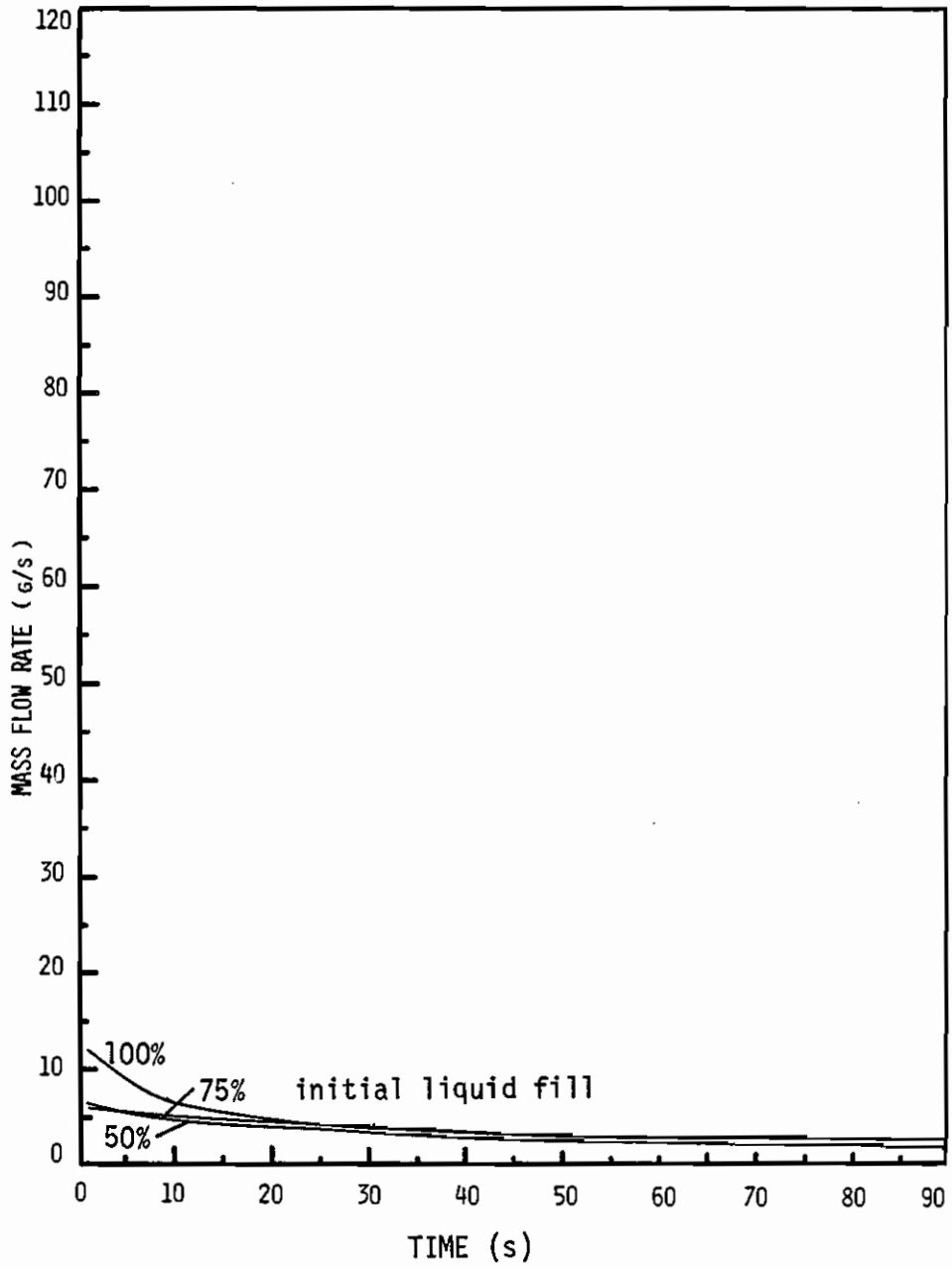

Figure 40. Instantaneous Mass Discharge Rate: 1.59 mm orifice, aluminum wall tests.

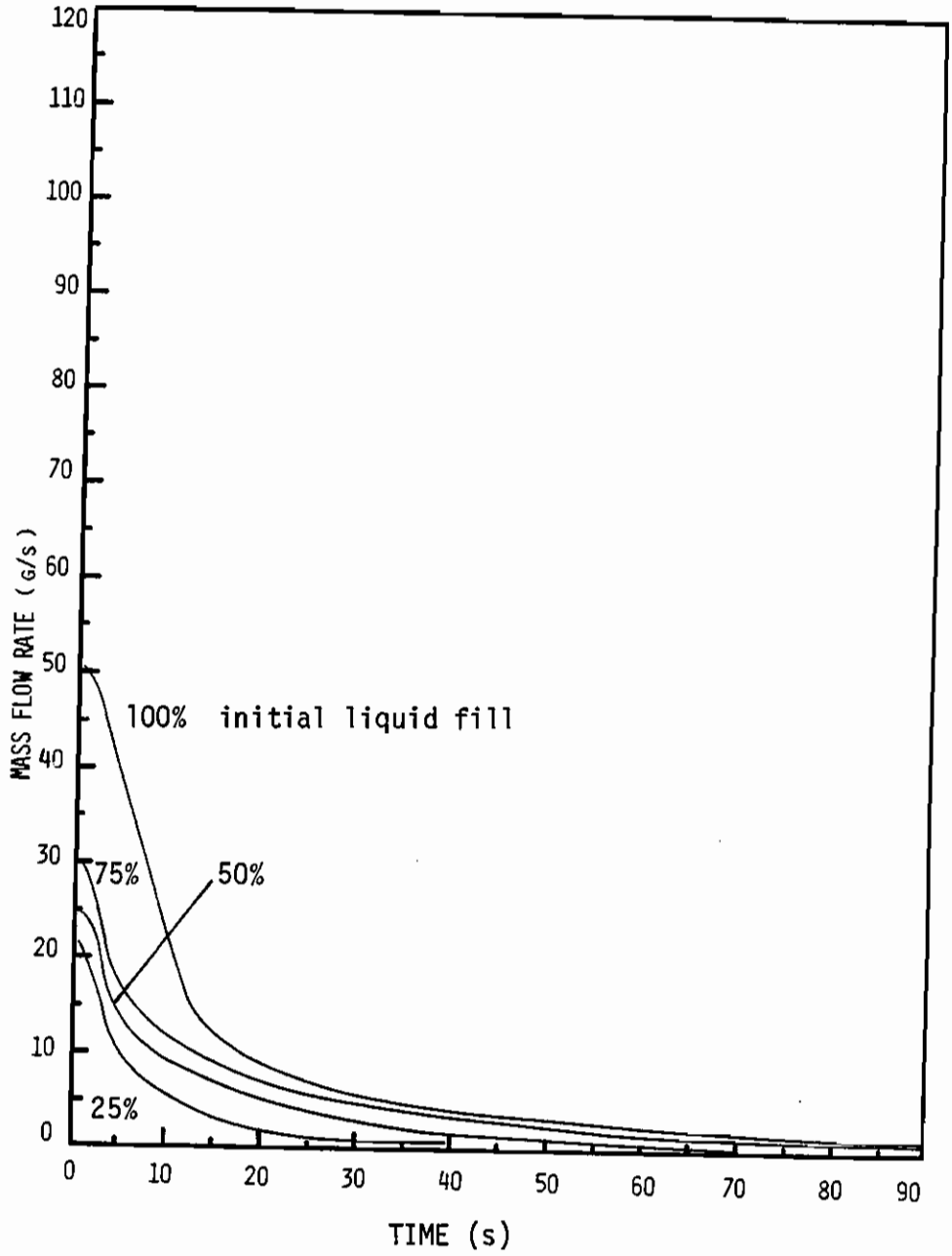

Figure 41. Instantaneous Mass Discharge Rate: 3.18 mm orifice, plexiglas wall tests.

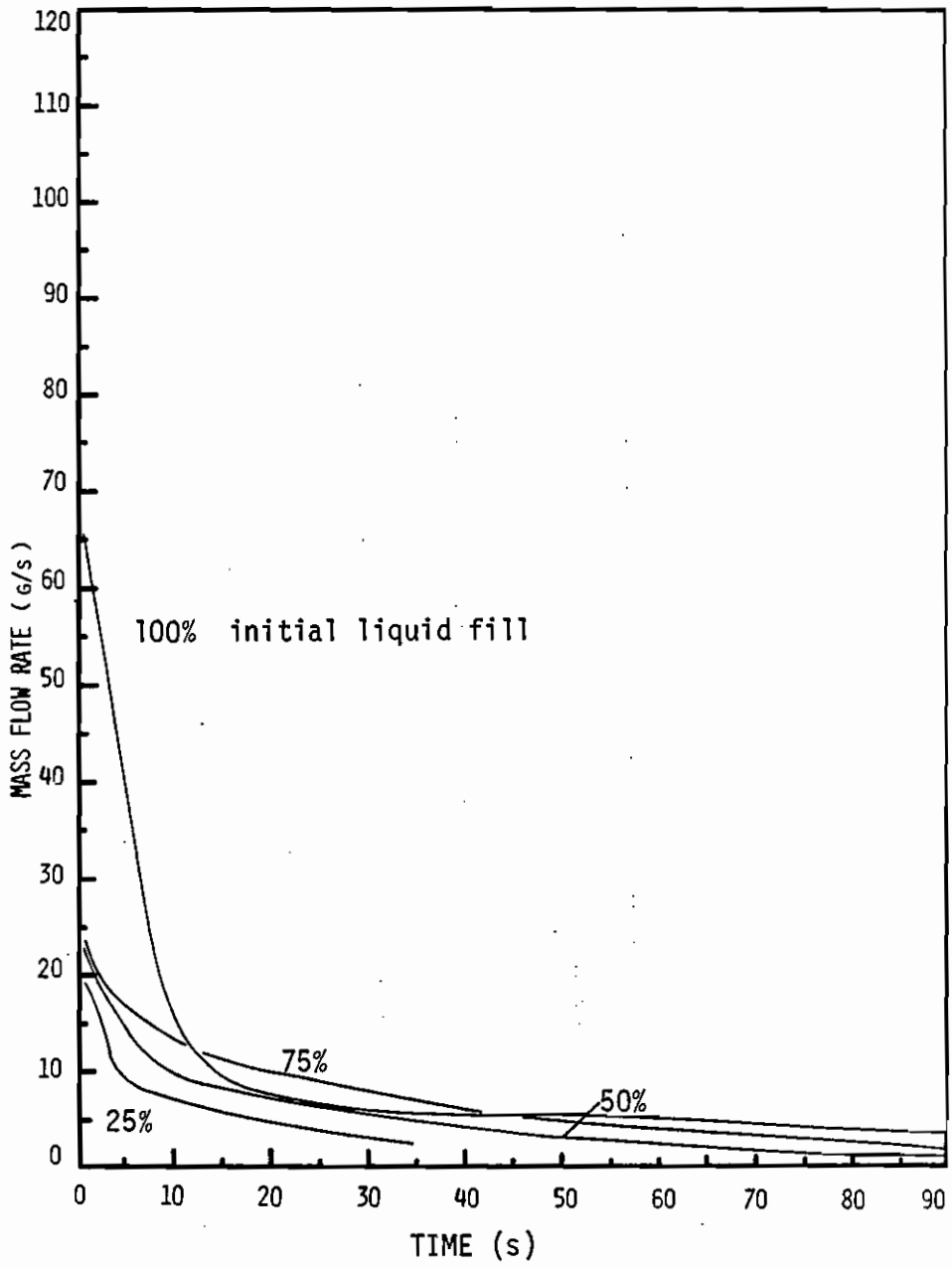

Figure 42. Instantaneous Mass Discharge Rate: 3.18 mm orifice, aluminum wall tests.

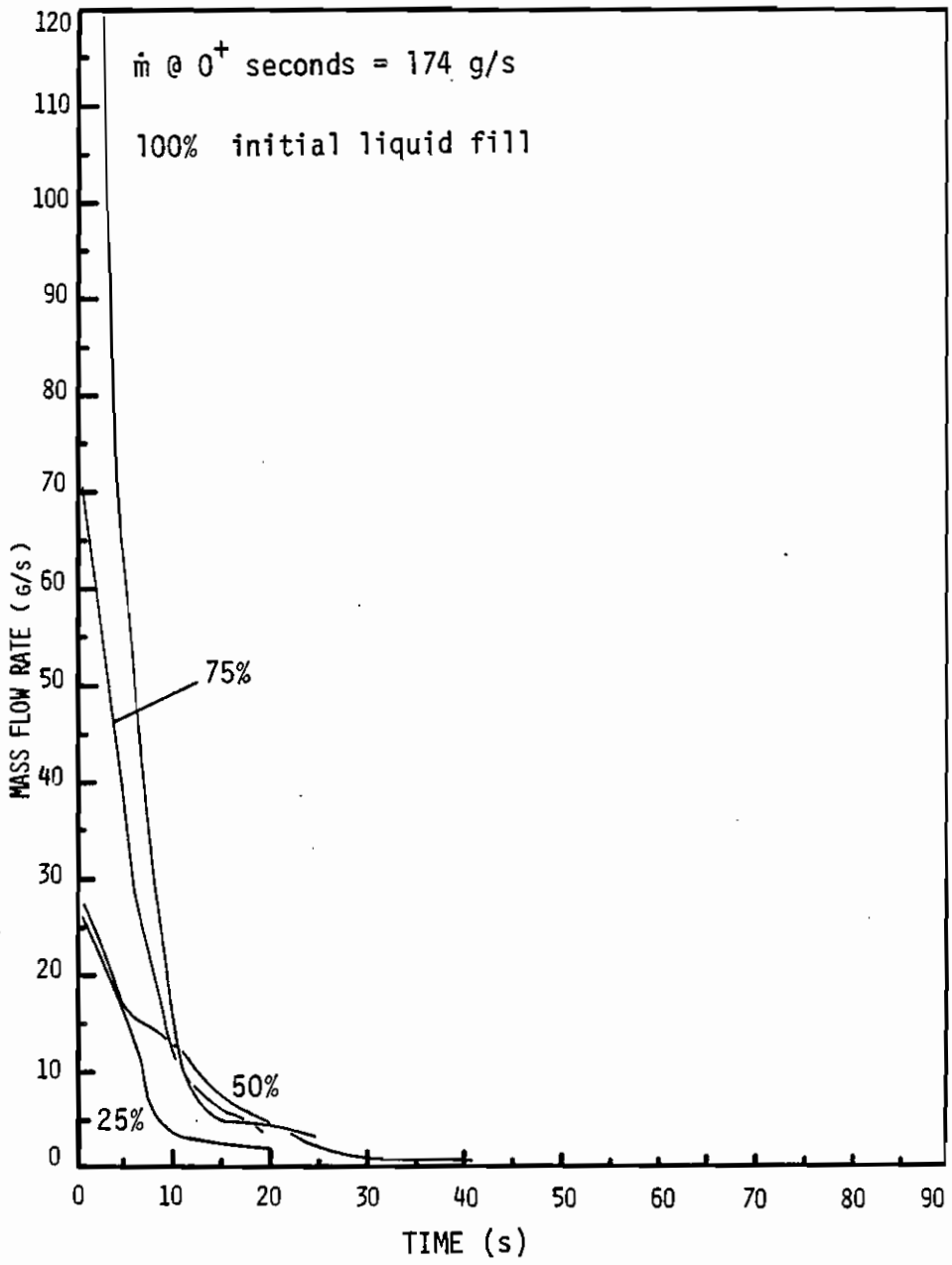

Figure 43. Instantaneous Mass Discharge Rate:
4.76 mm orifice, plexiglas wall tests.

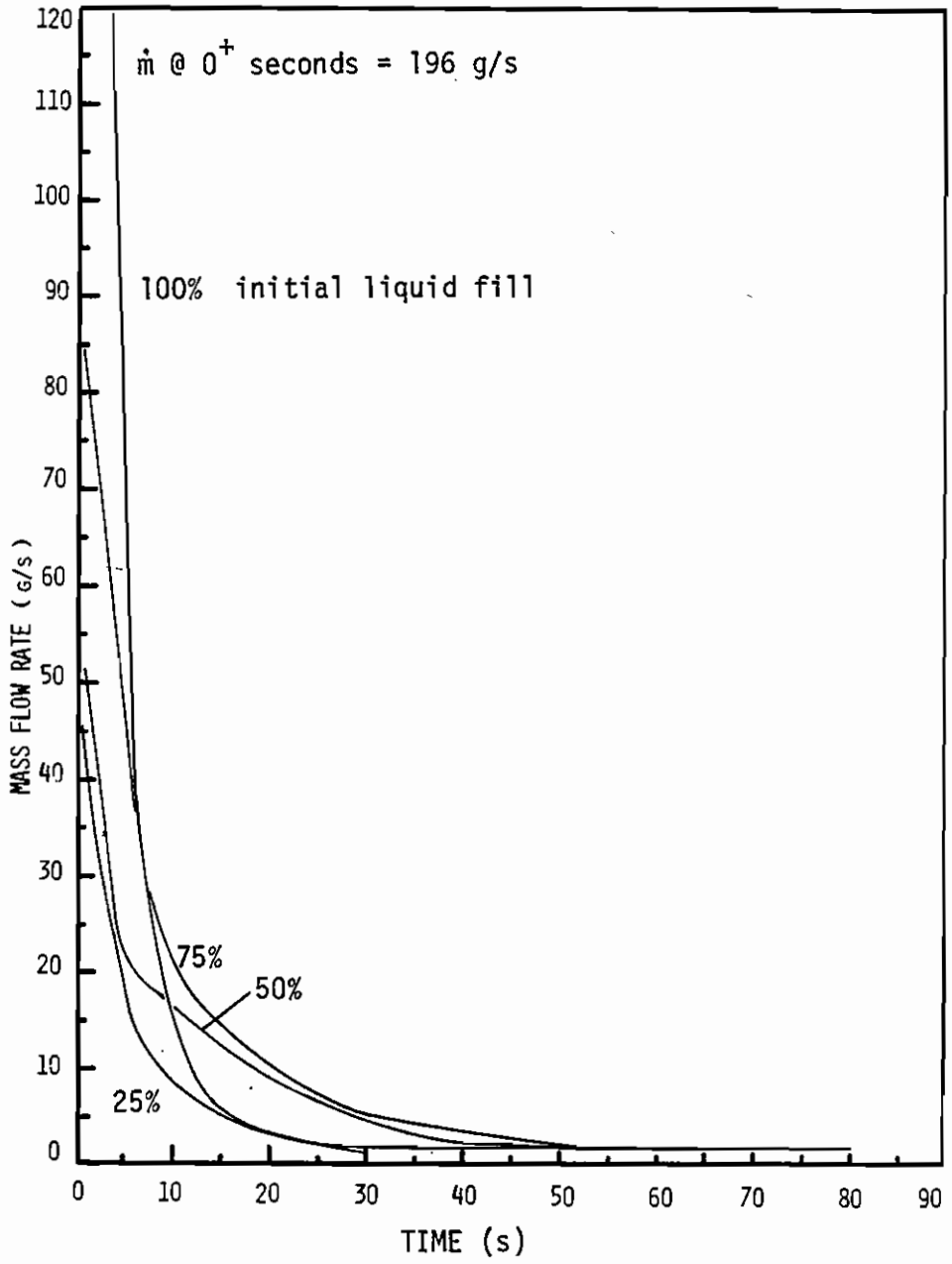

Figure 44. Instantaneous Mass Discharge Rate: 4.76 mm orifice, aluminum wall tests.

final emptying of the chamber. Some nucleation sites are active on the bottom of the vessel, but most nucleation occurs at sites along the side walls. The bubbles grow slowly as they rise up near the walls towards a thoroughly mixed region at the top of the two-phase column. This mixed region is sustained by a central downward current which draws bubbles from the liquid surface down into the two-phase column. Tatom, Brown, Knight and Coxe [9] and Bailey and Fearn [10] observed the same boiling pattern in depressurization experiments conducted in tanks of cryogenic liquids.

The 3.18 and 4.76 mm orifice tests exhibit the completely mixed, frothy two-phase column with few discernable bubbles until late times in the blowdowns. When system pressure reaches a steady value slightly above atmospheric pressure no more energy is available for bubble growth from the liquid. The boiling pattern then changes to appear more like nucleate boiling in a subcooled liquid, with bubbles rising vertically in columns through relatively undisturbed liquid. No significant liquid subcooling is actually found in any of the tests conducted, however.

After the point when system pressure becomes constant heat transfer from the walls provides the energy for vapor generation. All tests run exhibit the same boiling pattern at this point, regardless of orifice size.

Bubble growth rate varies among individual bubbles, but generally remains within certain bounds. Bubbles grow at rates from 1.2 to 1.6 cm^3/s in the 1.59 mm orifice tests and from 1.9 to 2.3 cm^3/s in the 3.18 and 4.76 mm orifice tests. It should be noted that individually recognizable bubbles are very short-lived in the larger orifice tests due to the rapid mixing and coalescence throughout the vessel. Bubble

growth rate data is therefore sparse for the two larger orifice test series.

In this investigation individual bubble growth rates are actually unimportant compared to the total vapor generation rate for the system. At any time the vapor generation rate is limited by the amount of energy available for vaporization in the superheated liquid and the vessel walls. The observation that when vapor flow exists during the main blowdown regime the liquid stays at saturation implies that the mass discharge rate governs the vapor generation rate; all energy in liquid superheat is transferred to the vapor as quickly as it becomes available. Thus the usual heat transfer limitation on bubble growth in open pool boiling is superceded in orifice-restricted venting of flashing liquids by the venting rate (depressurization rate) limitation.

Measurements of bubble rise velocities are presented as a histogram in Figure 45. Separate compilations are made for the 1.59, 3.18 and 4.76 mm orifice tests. The larger orifice tests show mean bubble rise velocities of about 17 cm/s, slightly higher than the mean of 15.3 cm/s for the 1.59 mm orifice tests. The spread of velocities for the 4.76 mm orifice tests is fairly wide because the turbulence in the tests superimposes random motion of the bulk fluid on the bubbles trapped in local currents. Also, relatively few bubbles could be tracked on film before they disappeared into the frothing two-phase mixture.

Diameters of bubbles recorded for velocity calculations typically range between 2.2 mm (0.087 in) and 3.9 mm (0.15 in) in the 1.59 mm orifice tests, between 1.5 mm (0.061 in) and 9.7 mm (0.38 in) in the 3.18 mm orifice tests and between 2.2 mm and 6.9 mm (0.27 in) in the 4.76 mm orifice tests. Both larger and smaller bubbles are frequently

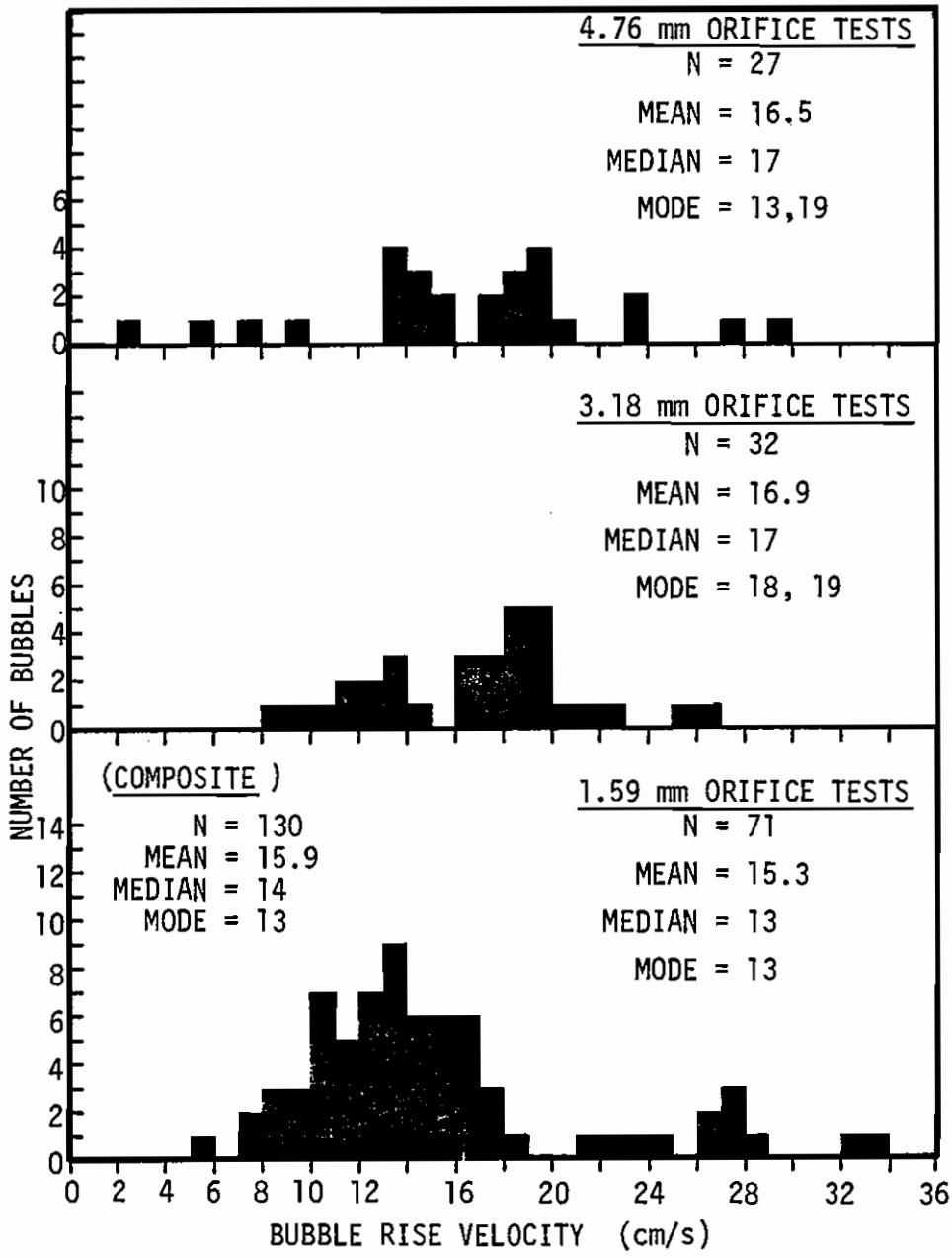

Figure 45. Histogram of Measured Bubble Rise Velocities.

seen, but bubbles larger than 10 mm (0.4 in) are too deformed for accurate measurement and bubbles smaller than 1.3 mm (0.05 in) are too near to their nucleation points to be useful in velocity calculations. Bubbles smaller than 0.25 mm (0.01 in) could not be resolved on film.

Theoretical development of bubble rise velocity is presented by Wallis [11]. Regimes are described in which bubble velocity varies as a function of bubble radius, and a brief synopsis is given here.

Bubble rise velocity is a function of bouyancy and inertial (ρg) effects, viscosity and surface tension (σ). For newly evolved bubbles (diameters less than 1.3 mm in this study) viscous effects dominate and bubble rise velocity (V_b) varies between

$$V_b \propto R_b^2 \quad \text{to} \quad V_b \propto R_b^{1.28} ,$$

where R_b is the "equivalent bubble radius" (the radius a bubble of equal volume would have if it were spherical). The actual theoretical rise velocities for small bubbles in a Freon-12 system range up to 10 cm/s. Bubbles between about 1.5 mm and 4.0 mm meet the criteria of Peebles and Garber [12],

$$5.75 < \frac{gR_b^4 V_b^4 \rho_f^3}{\sigma^3} \quad \text{and} \quad R_b < 2\left(\frac{\sigma}{g\rho_f}\right)^{0.5} .$$

Within this regime bubble velocity is essentially constant and given by

$$V_b = 1.18\left(\frac{g\sigma}{\rho_f}\right)^{0.25} ,$$

which for Freon-12 under present experimental conditions yields a bubble

rise velocity of 11.5 cm/s.

For bubbles with diameters larger than 4.0 mm the following equation is valid:

$$V_b = (gR_b)^{0.5} ,$$

which for some measured bubbles leads to the results listed in Table 5.

Table 5. Comparison of Some Measured Bubble Rise Velocities to Theory.

BUBBLE DIAMETER	THEORETICAL VELOCITY	MEASURED VELOCITY
5.0 mm	15.6 cm/s	13.2 cm/s
6.4	17.8	17.7
6.9	18.3	14.5
9.7	19.3	18.5

Notice also in Figure 45. (page 84) that the majority of bubbles in the 1.59 mm orifice tests rise more slowly than in the larger orifice tests. Neglecting the small group of velocities above 20 cm/s, the main part of the distribution has a mean velocity of 12.5 cm/s, corresponding to the theoretical intermediate-size bubble velocity of 11.5 cm/s. This is consistent with the observation that bubbles grow more slowly in the 1.59 mm orifice tests and the fact that the bubbles tracked in those tests are on the average smaller than bubbles tracked in the larger orifice tests.

Although there is some statistical spread in the plotted data, the measured bubble rise velocities generally conform to theory. No differences are found in nominal bubble rise velocities between aluminum and plexiglas wall tests or among different percentage fill tests. Therefore, bubble rise velocity in this series of experiments is shown to be a weak function of bubble size and can be theoretically predicted.

Caution should be used when applying the theoretical bubble rise velocity to processes with vapor generation rates which are large (on a volumetric basis) with respect to the vessel volume. In the present experiments, for example, although theory fairly accurately predicts rise velocities for isolated bubbles, the isolated bubble is a short-lived anomally in the system. The chamber is actually a well mixed turbulent system with very different (and complex) heat and mass transfer characteristics.

Two-Phase Column Characteristics

Boiling generates a two-phase mixture in the test vessel during blowdown. In the 3.18 and 4.76 mm orifice tests the entire system appears homogeneously mixed, but in the 1.59 mm orifice tests the homogeneous mixture is restricted to a small region at the top of the liquid coulumn and near the side walls where bubbles nucleate. However, for the purpose of comparison, an average quality and void fraction (the values of these properties if the two-phase mixture is assumed homogeneous) is computed for the two-phase column in each case.

Figures 46. and 47. are graphs of homogeneous quality versus time and void fraction versus time, respectively, for the 100% fill tests. The quality and void fraction histories of lesser percentage fill tests differ from the presented plots only in that the maximum values of the two properties are reached and their declines begin sooner. In all tests evaluated for void fraction where the two-phase column initially rises to hit the orifice the maximum void fraction occurs when the column ceases to fill the entire chamber. Maximum quality may occur slightly sooner due to the continuous drop in saturation vapor density as system

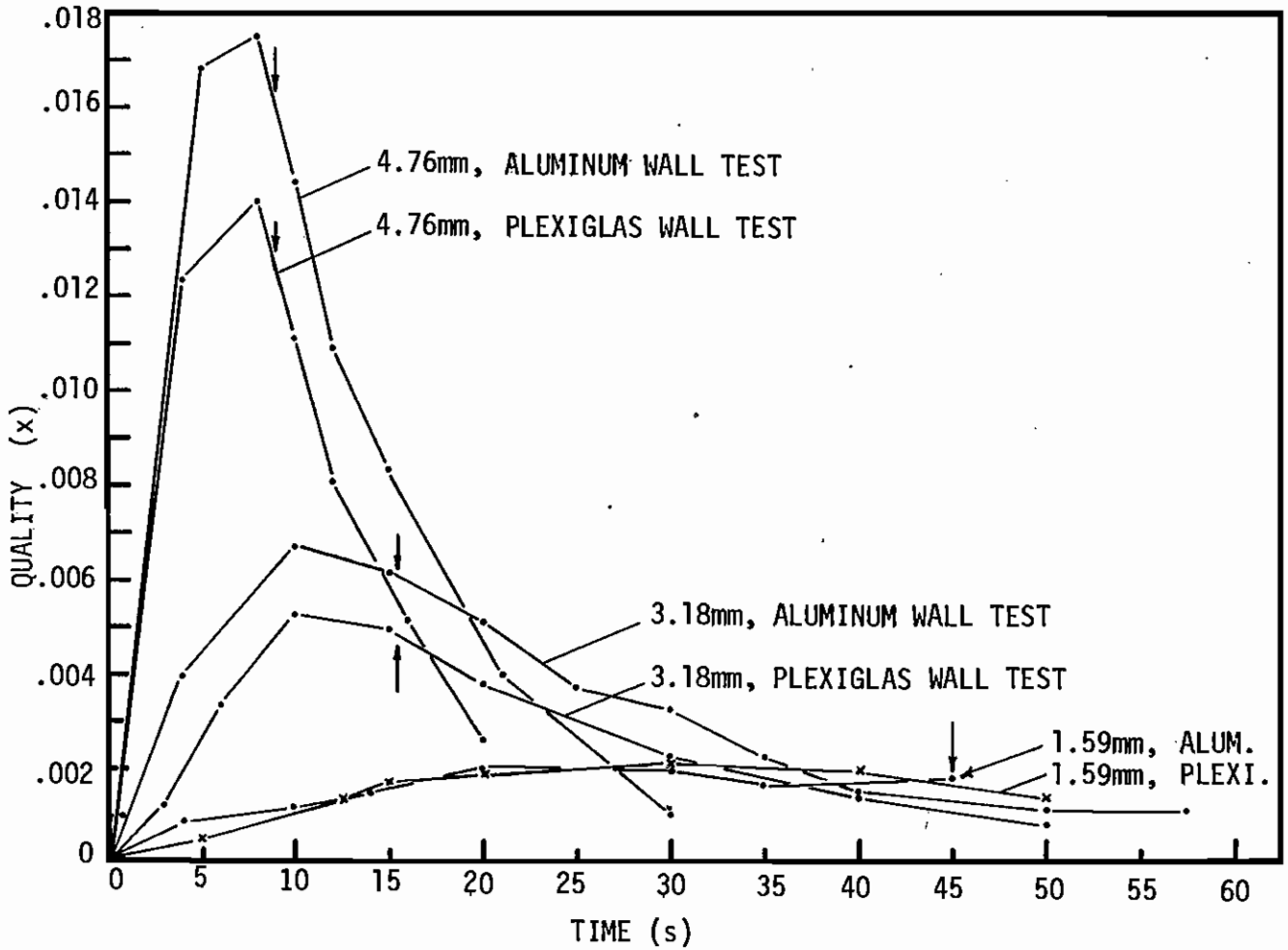

Figure 46. Average Quality of the Two-Phase Column Versus Time for the 100% Fill Tests. (The vertical arrows indicate the time at which the column no longer fills the vessel completely.)

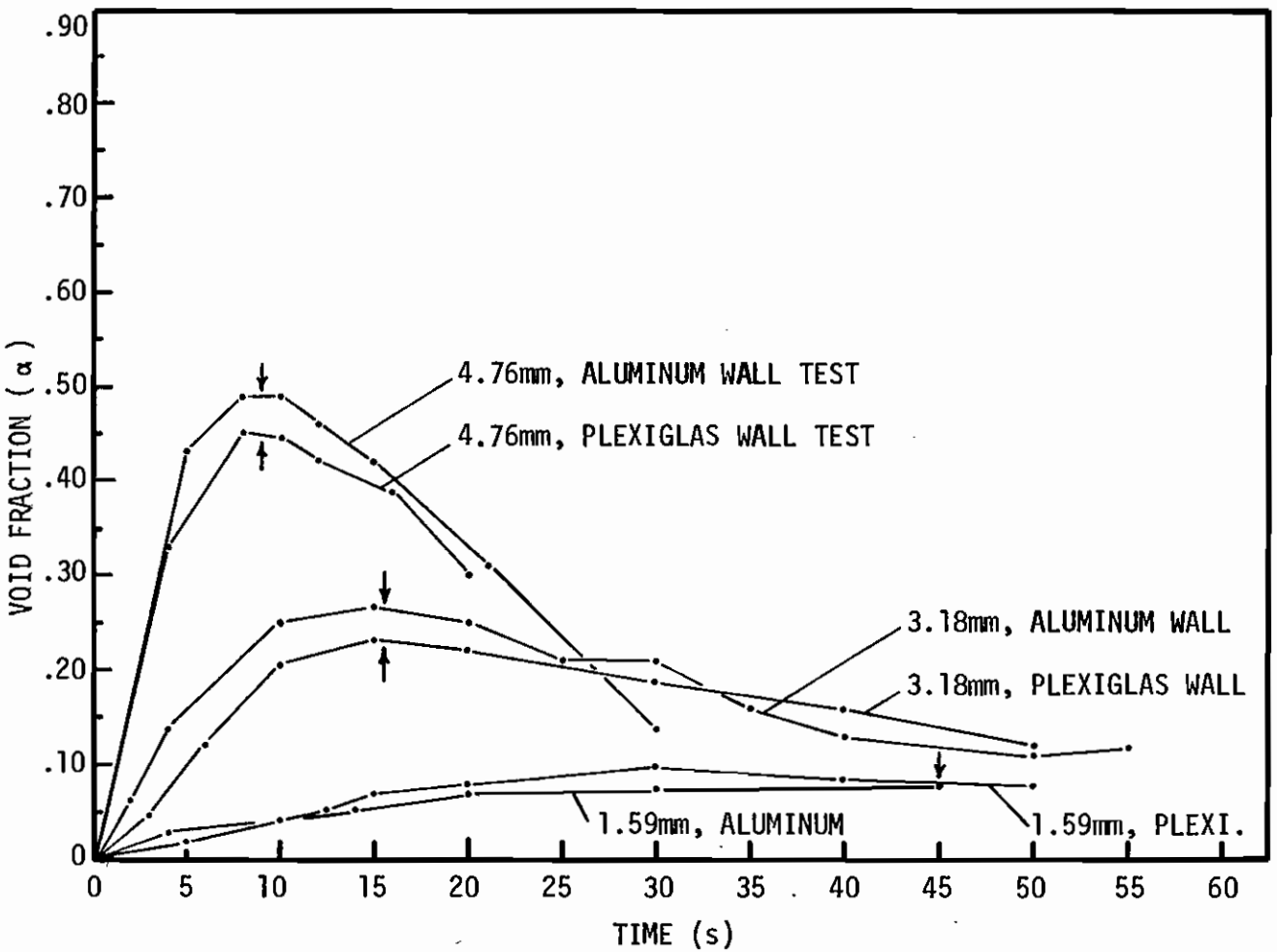

Figure 47. Average Void Fraction of the Two-Phase Column Versus Time for the 100% Fill Tests. (The vertical arrows indicate the time at which the column no longer fills the vessel completely.)

pressure and temperature fall. In all evaluated tests where the column never fills the chamber the maximum quality and void fraction occur by the end of the initial regime.

The actual values of the maximum quality and void fraction vary strongly with orifice size, vary weakly between plexiglas and aluminum tests, and are not appreciably affected by initial percentage fill. These observations are summarized in Table 6.

Table 6. Maximum Two-Phase Column Quality and Void Fraction

ORIFICE DIAMETER	100% LIQUID FILL TESTS PLEXIGLAS WALL	100% LIQUID FILL TESTS ALUMINUM WALL	LESSER % FILL TESTS (BOTH WALL MATERIALS)
		(MAXIMUM AVERAGE QUALITY)	
1.59 mm	0.0021	0.0020	approx. 0.002
3.18	0.0053	0.0067	approx. 0.006
4.76	0.0140	0.0175	approx. 0.015
		(MAXIMUM AVERAGE VOID FRACTION)	
1.59 mm	0.08	0.10	approx. 0.10
3.18	0.23	0.27	approx. 0.25
4.76	0.45	0.49	approx. 0.50

The measured parameter that the two-phase column quality and void fraction correlate most closely with is the instantaneous mass discharge rate. From their maximum values, quality and void fraction fall along with the mass flow rate in the two larger orifice tests. For the 1.59mm orifice tests the film ran out just after the liquid column subsided from the orifice. Both quality and void fraction level off to steady values at the same time the mass flow rate does in all 100% fill tests (films of lesser percentage fill tests were not taken long enough to reach that stage of the blowdown). The values of both two-phase

properties are consistently lower at corresponding points in the blowdown for the plexiglas wall tests than for the aluminum wall tests in the 3.18 and 4.76 mm orifice test series. However, quality and void fraction are essentially unaffected by wall composition in the 1.59 mm orifice tests. These observations also parallel the mass flow rate behavior in each case.

The observed correlation between quality and void fraction and the mass discharge rate during the main part of the blowdown is reasonable. Replacement of vented vapor comes solely from vapor generation in the liquid. This implies that the faster the mass is vented the faster the vapor generation in the liquid and therefore the higher the quality of the two-phase column.

In addition to the mass discharge rate, the instantaneous thermodynamic state of the system affects the quality and void fraction at any given point in the blowdown.

V. THE BLOWDOWN PROCESS MODEL

A computer model was developed for the blowdown process in this investigation to roughly check the observations and assumptions made in the study. Of particular interest is the effect on the blowdown of heat transfer to the fluid from the environment, which has been described only qualitatively so far in this report. The model is admittedly simple, neglecting any nonequilibrium phenomena such as the observed initial regime, a possibly non-unity slip ratio in the two-phase discharge and the thermal gradient in the vapor region. However, the model does include basic thermodynamic, fluid mechanic and heat transfer relationships which are adequate to follow the blowdown process and to reproduce with fair accuracy the trends seen in the various experiments.

Heat Transfer Effects

The plexiglas and aluminum walls are used in this study to assess the influence that different rates of energy input to the system have on the blowdown process. Comparisons of the pressure, temperature, mass flow rate and quality histories amply demonstrate that heat transfer does have a significant effect on the blowdown. However, only qualitative descriptions of heat transfer effects have been made because quantitative analysis of the heat transfer process during this nonsteady event is exceedingly complex.

On the outside surface of the vessel's walls free convection of air governs heat transfer from the atmosphere to the vessel. The 2.54 cm thick walls conduct heat to the inner surface and to the Freon in the chamber. At the wall's inner surface two distinct regions exist, the

two-phase column and the vapor space, whose wall contact areas both change continuously as the liquid level falls. The heat transfer to the vapor region is by forced convection, while the heat flux to the two-phase region is due mainly to nucleate boiling on the walls. Finally, the liquid and vapor temperatures change continuously, making the wall boundary conditions in both regions transient.

An analytical solution for this complicated nonsteady problem is unmanagable. Futhermore, no data were collected on temperature distributions in the vessel walls. However, estimates of relative heat transfer rates can be made following some simplifying assumptions. To begin the heat transfer model the thermophysical properties of the wall materials and some system-specific properties are presented in Tables 7. and 8.

The vessel walls are modeled as a lumped system with an assumed uniform wall temperature. Although this assumption is not actually valid for this system, it provides a rough approximation of the relative magnitudes of the heat input from plexiglas and aluminum walls. The heat flux ($\dot{q}$) into the fluid from the walls is given by

$$\dot{q} = k_{wall}(T_{wall} - T_{liquid})/L_c \qquad (W/cm^2) \quad ,$$

where T_{wall} is the mean wall temperature, T_{liquid} is the temperature of the liquid Freon and L_c is a "characteristic length" equal to the wall volume divided by its surface area exposed to the boiling liquid.

The area exposed to vapor is neglected because heat transfer to the vapor is calculated to be only a small fraction of that to the boiling liquid. The heat flux to the vapor region under experimental conditions is calculated from two different correlations from Ozisik (14)

Table 7. Thermophysical Properties of Plexiglas and Aluminum.

PROPERTY	PLEXIGLAS [13]		ALUMINUM [14]	
DENSITY (ρ @ 0°C)	1.19	g/cm^3	2.71	g/cm^3
SPECIFIC HEAT (c @ 25°C)	1.47	J/g°C	0.871	J/g°C
THERMAL CONDUCTIVITY (k @ 0°C)	0.0019	W/cm°C	2.024	W/cm°C
THERMAL DIFFUSIVITY (α @ 0°C)	0.0011	cm^2/s	0.859	cm^2/s

Table 8. Properties of the Experimental Vessel.

PROPERTY	PLEXIGLAS WINDOWS	INSTRUMENTED SECTIONS	
		PLEXIGLAS	ALUMINUM
WALL THICKNESS	2.54 cm (each)	2.54 cm	2.54 cm
TOTAL VOLUME	2980 cm^3	930 cm^3	930 cm^3
TOTAL HEAT CAPACITY	5.21 kJ/°C	1.63 kJ/°C	2.20 kJ/°C
INSIDE SURFACE AREA	635 cm^2	335 cm^2	335 cm^2
OUTSIDE SURFACE AREA	660 cm^2	405 cm^2	405 cm^2

and is found to range between

$$\dot{q}_{(\text{F-12 vapor})} = 0.001(\Delta T) \quad \text{to} \quad 0.002(\Delta T) \quad W/cm^2 \quad .$$

Clark, Van Wylen and Fenster [3] found values of the vapor region heat flux in experimental decompression of liquid nitrogen to be between

$$\dot{q}_{(\text{vapor})} = 0.002(\Delta T) \quad \text{to} \quad 0.004(\Delta T) \quad W/cm^2 \quad .$$

However, for the present experiments the heat flux due to boiling at the walls in the liquid region, as estimated with Rohsenow's correlation [15],

$$\frac{c_{p(1)}\Delta T}{h_{fg}\left[\frac{c_{p(1)}\mu_1}{k_1}\right]^{1.7}} = 0.01\left[\frac{q}{\mu_1 h_{fg}}\left(\frac{g_c\sigma}{g\rho_{fg}}\right)^{0.5}\right]^{0.33}$$

(all terms are defined in the nomenclature section),

is between

$$\dot{q}_{(\text{F-12 boiling})} = 0.003(\Delta T)^3 \text{ to } 0.028(\Delta T)^3 \quad W/cm^2 \quad ,$$

depending on the condition of the boiling surface. For modest ΔT's the boiling heat transfer exceeds the vapor heat transfer by orders of magnitude.

Referring back to Table 7. (page 94) it can be seen that the surface boiling heat flux will always be much larger than the conduction rate in the plexiglas walls. In the aluminum wall case, however, it is

not clear which term will dominate the heat transfer process.

On the vessel's outer surfaces free convection transfers energy to the walls from the atmosphere. McAdams [16] developed the following correlations for free convection of air at atmospheric pressure and moderate temperatures.

For vertical plates: (laminar flow) $h_{mean} = 1.42 \times 10^{-4}(\Delta T_a/H)^{0.25}$ W/cm^2°C ,

For cooled horizontal lower surfaces: $h_{mean} = 1.32 \times 10^{-4}(\Delta T_a/W)^{0.25}$ W/cm^2°C ,

For cooled horizontal upper surfaces: $h_{mean} = 0.59 \times 10^{-4}(\Delta T_a/W)^{0.25}$ W/cm^2°C ,

where $\Delta T_a = T_{atm} - T_{wall}$, H = wall height and W = surface width. Applying these equations to the apparatus, the system is found to absorb heat according to the relationship

$$\dot{q} = 1.7 \times 10^{-4}(\Delta T_a)^{1.25} \quad W/cm^2 .$$

For the vessel's 1065 cm^2 outside surface the total heat transfer rate from free convection is

$$\dot{Q} = 0.18(\Delta T_a)^{1.25} \quad W \quad (\Delta T_a \text{ in } °C)$$

This factor is not included in the heat input calculations because it is insignificant for most of the blowdown. ΔT_a never exceeds 22°C (40°F) in the plexiglas wall tests, so the heat input from the atmosphere never exceeds 9 watts. Whereas, a 1°C/s (1.8°F/s) drop in wall temperature

(a modest rate relative to the typical temperature decay rate in the liquid) provides 1,630 watts to the fluid in the system from stored heat in the plexiglas walls. Similar conditions hold for most of the aluminum wall tests, where frost forms on the outer wall surface (i.e. outer surface temperature drops slightly below 0°C) only after the liquid Freon temperature has dropped to about -26°C (-15°F). Neglecting atmospheric heat transfer therefore leads to an error of not more than 0.6%, which is lost amid larger errors inherent in the lumped system assumption.

The heat transfer model is incorporated into the computer model of the entire blowdown process. For each small timestep in the model blowdown the heat input from the walls is added to the Freon liquid and subtracted from the wall's stored energy. A new mean wall temperature is computed each timestep from the new stored energy and the wall heat capacity.

The Computer Simulation

The venting process is divided into small timesteps. Beginning with the initial conditions (specified system mass, volume, temperature and pressure) and with the assumption of thermodynamic equilibrium at saturation, mass is allowed to vent from the system for the brief timestep according to formulas for fluid flow through an orifice (these governing formulas are listed in Appendix A). The enthalpy of the vented mass at the system's instantaneous thermodynamic state is subtracted from the system's internal energy according to the previously discussed energy balance equation. Once the mass discharge is terminated, heat input from the environment is added to the internal energy and the vented

mass is subtracted from the total system mass. Then a new thermodynamic state is computed, saturated liquid-vapor equilibrium is re-established and all system properties are respecified. The process is repeated until the system pressure reaches atmospheric pressure.

The following assumptions are made for the simulated blowdown.

1. The fluid in the system and in the exit stream is always at thermal equilibrium at saturation.
2. The two-phase column is a uniform mixture.
3. Two-phase flow through the orifice is homogeneous flow with a slip ratio of one (1).
4. The two-phase exit flow has a quality equal to that of the boiling column in the system.
5. Two-phase exit flow ceases when the boiling liquid column subsides from the orifice.
6. The equation of state for real gases developed by Martin and Hou [17] (modified by the thesis author as described in Appendix B) is used to model Freon-12 vapor properties.
7. Empirical correlations based on the published properties of Freon-12 [18] are used to model liquid properties.

Three cases of the model are compared for the 100% liquid fill of each orifice size test. An adiabatic blowdown is simulated as a reference in addition to simulations of the plexiglas and aluminum wall tests. The calculated total heat inputs from the vessel walls for the various modeled tests are plotted versus time in Figure 48. Comparisons of theoretical calculations to the corresponding experimental processes are presented in Figures 49. through 57.

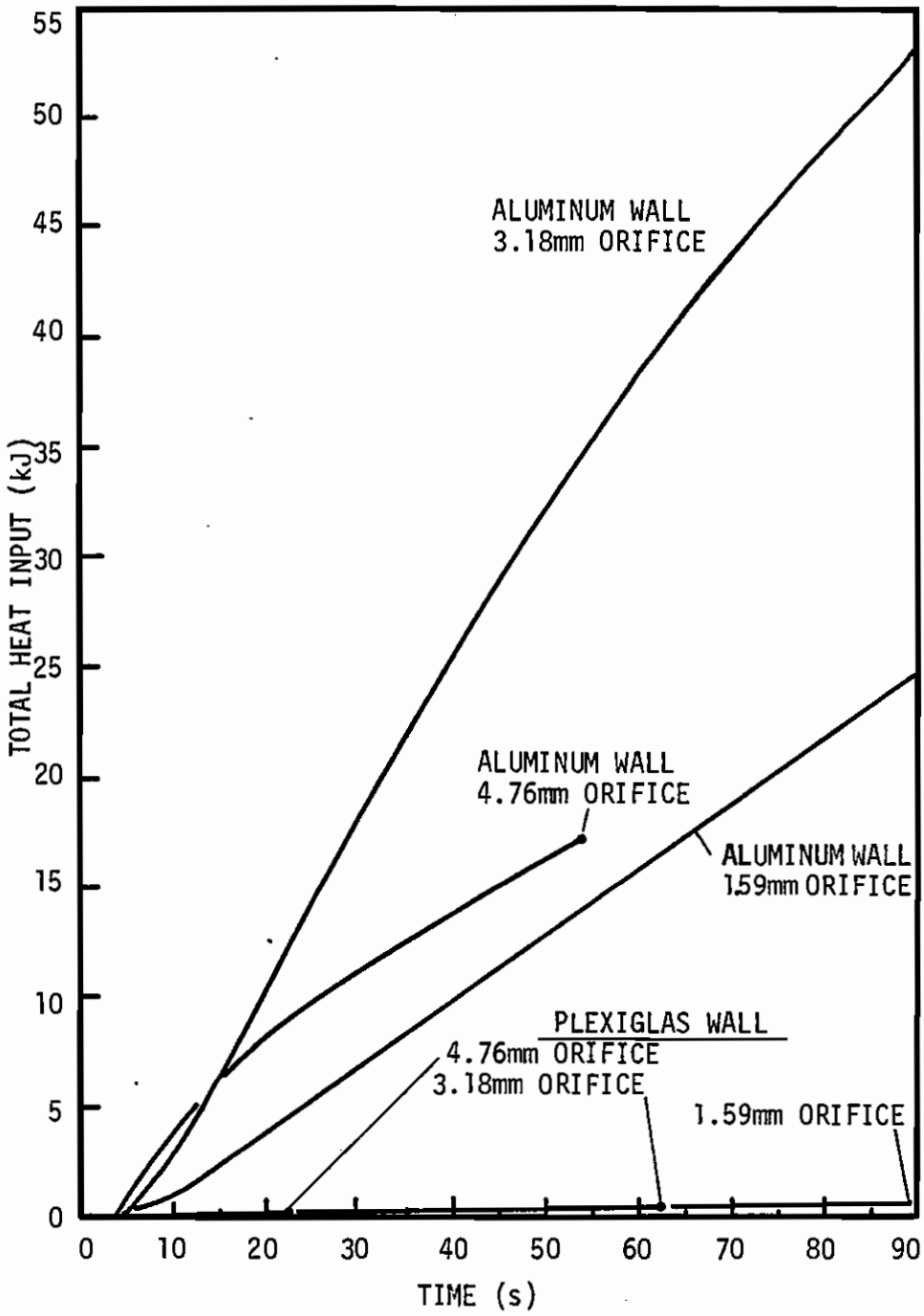

Figure 48. Total Theoretical Heat Input To Fluid Versus Time for the 100% Liquid Fill Tests. (To find heat input in BTU, divide plotted value by 1.056.)

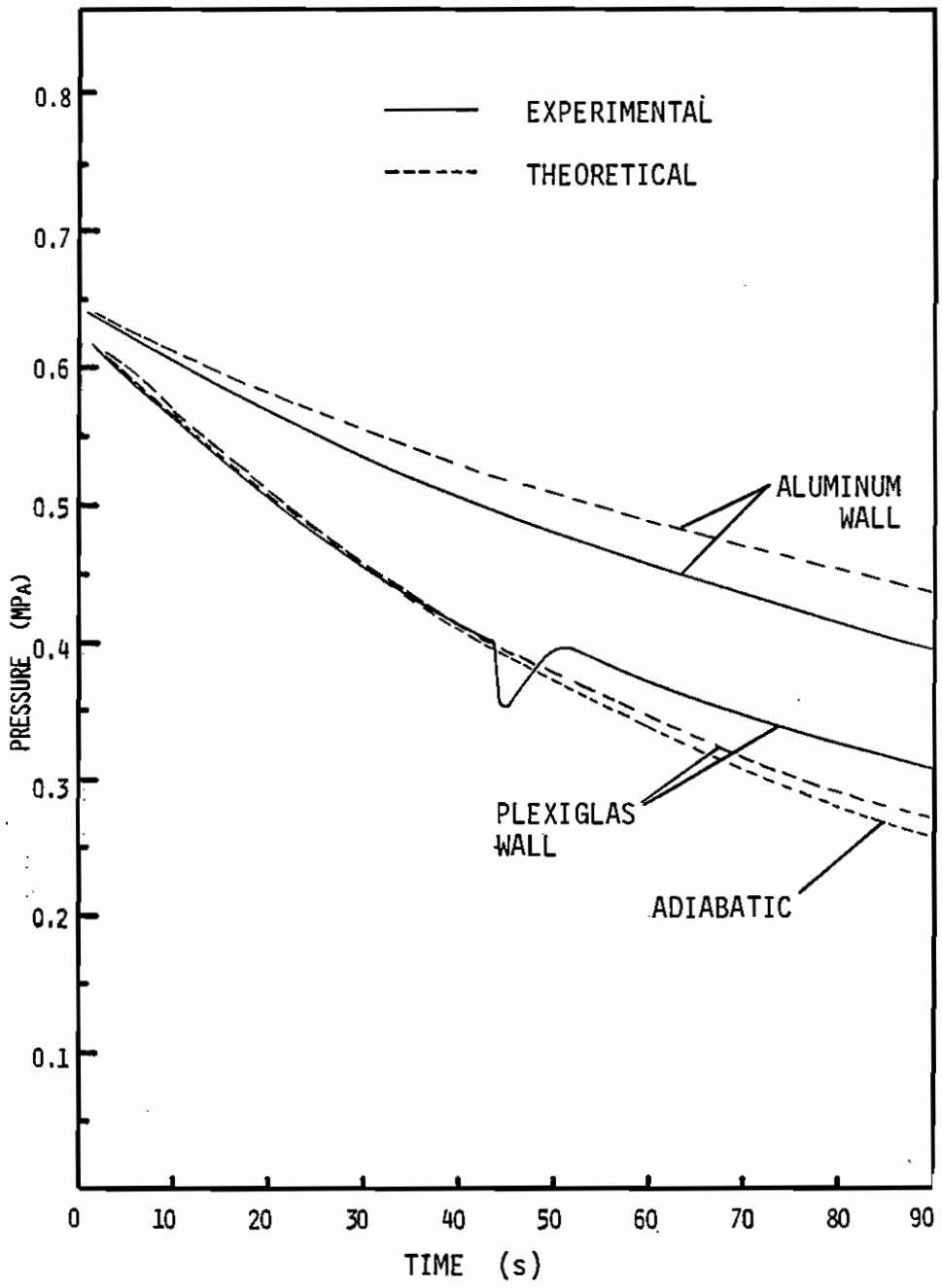

Figure 49. Theoretical and Experimental Pressure Decay: 1.59 mm orifice, 100% liquid fill tests.

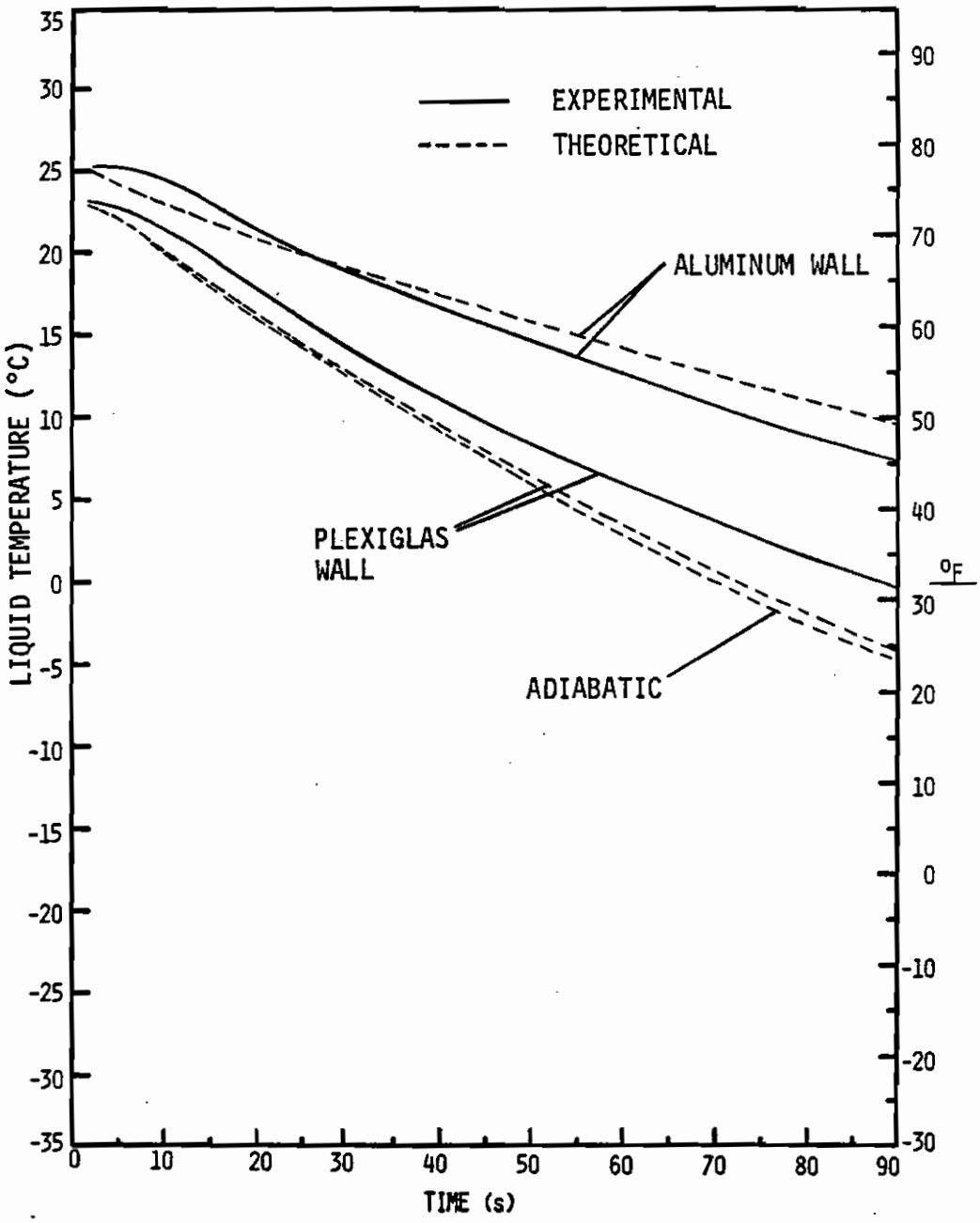

Figure 50. Theoretical and Experimental Temperature Decay: 1.59 mm orifice, 100% liquid fill tests.

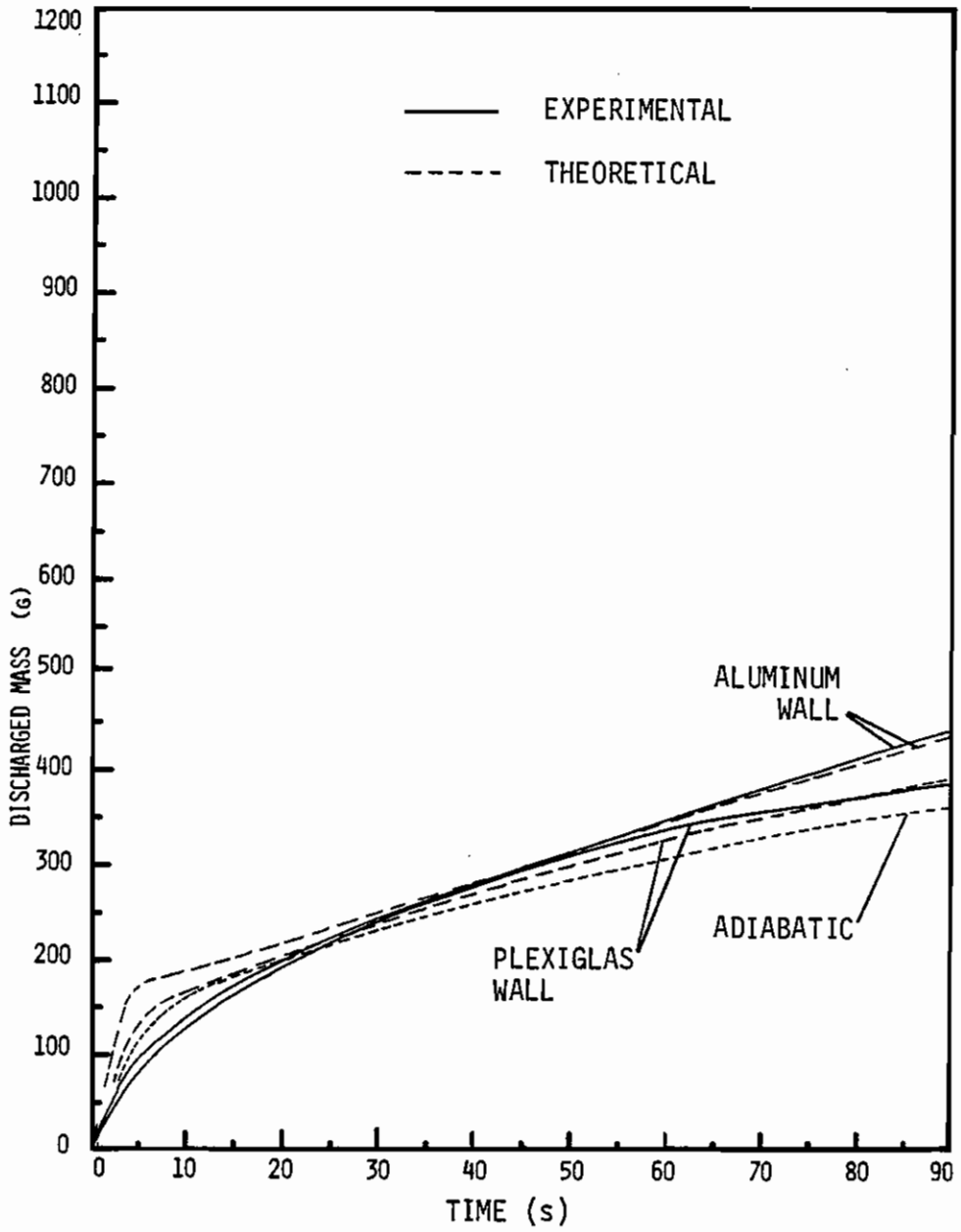

Figure 51. Theoretical and Experimental Mass Discharge: 1.59 mm orifice, 100% liquid fill tests.

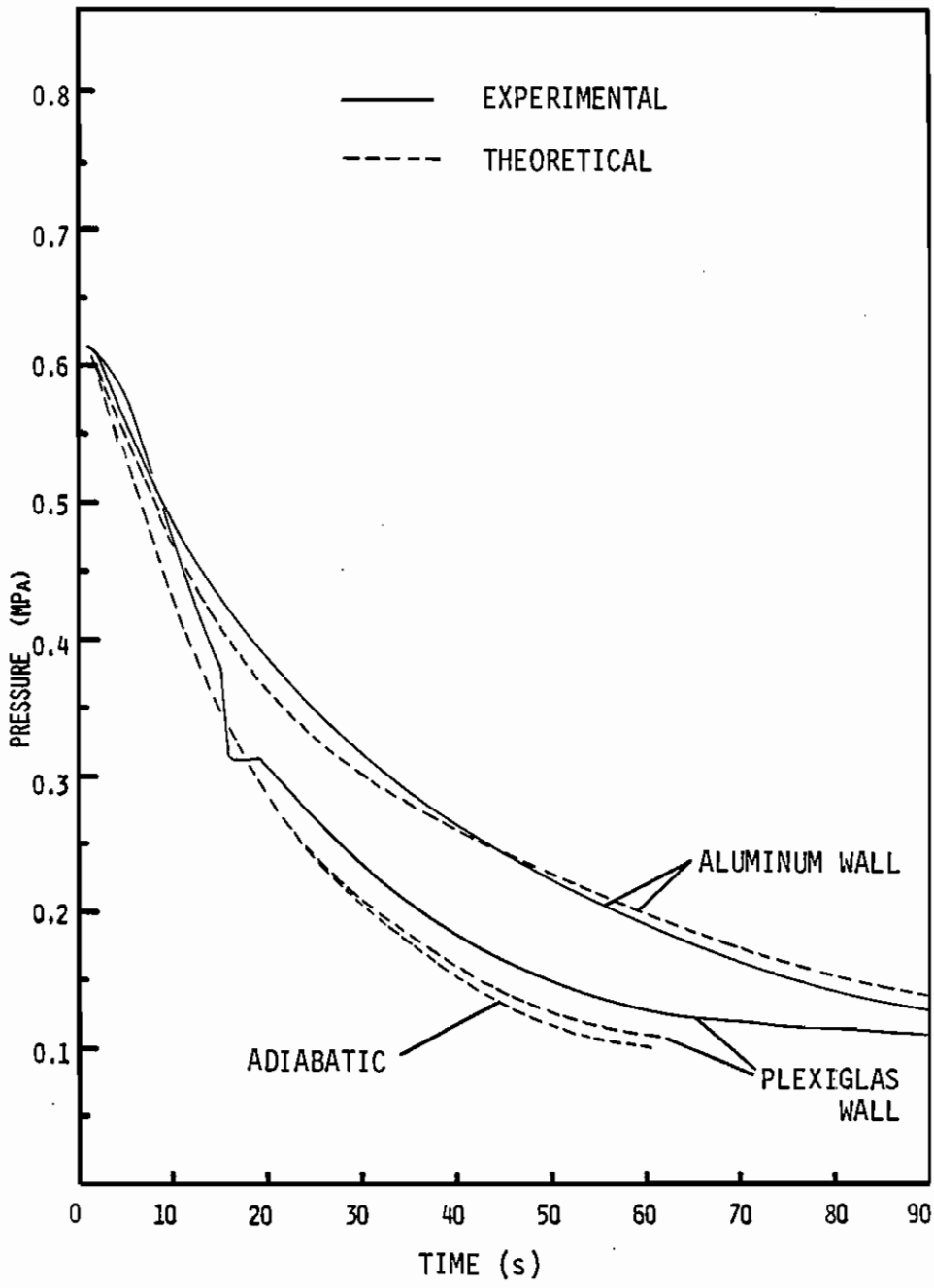

Figure 52. Theoretical and Experimental Pressure Decay: 3.18 mm orifice, 100% liquid fill tests.

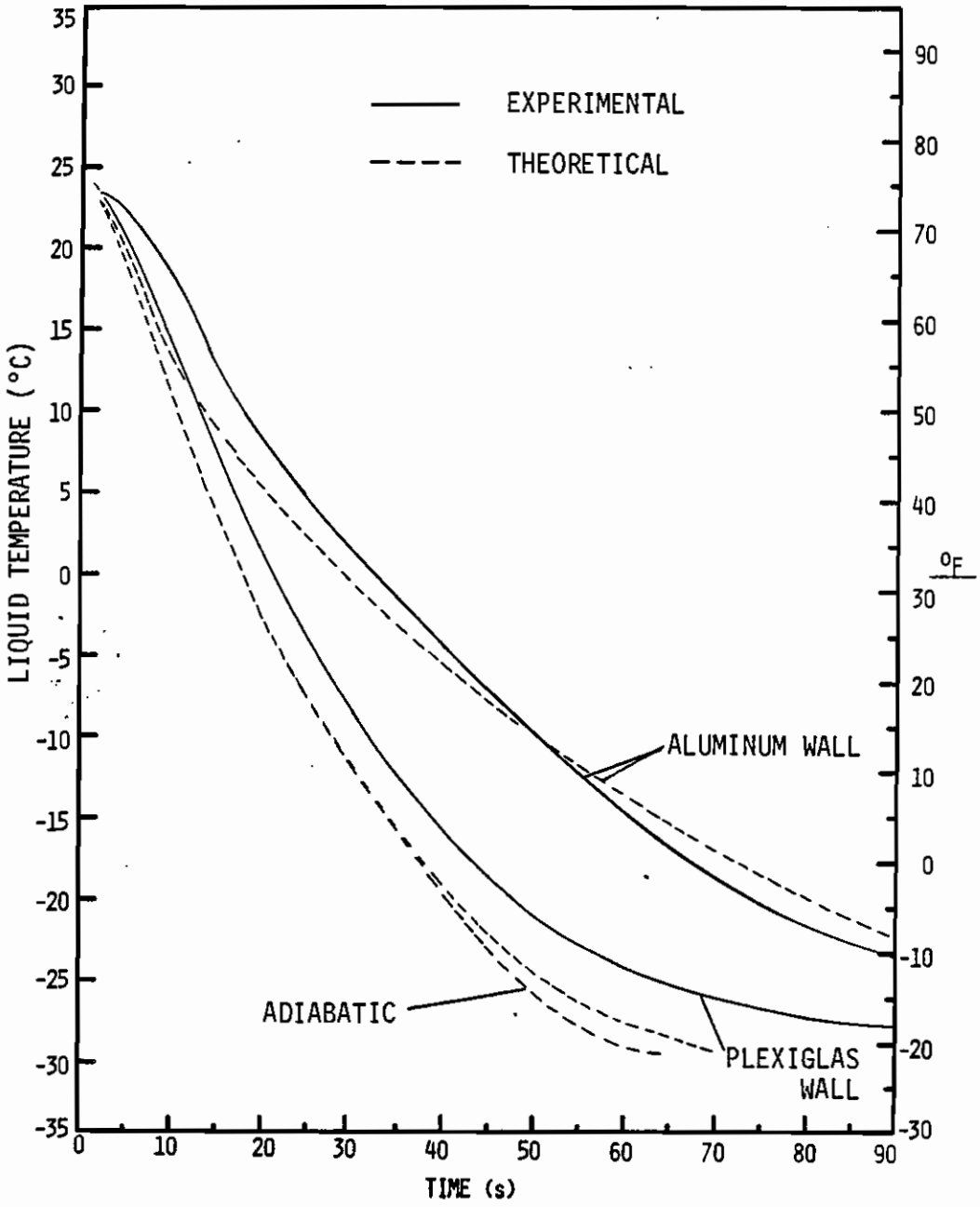

Figure 53. Theoretical and Experimental Temperature Decay: 3.18 mm orifice, 100% liquid fill tests.

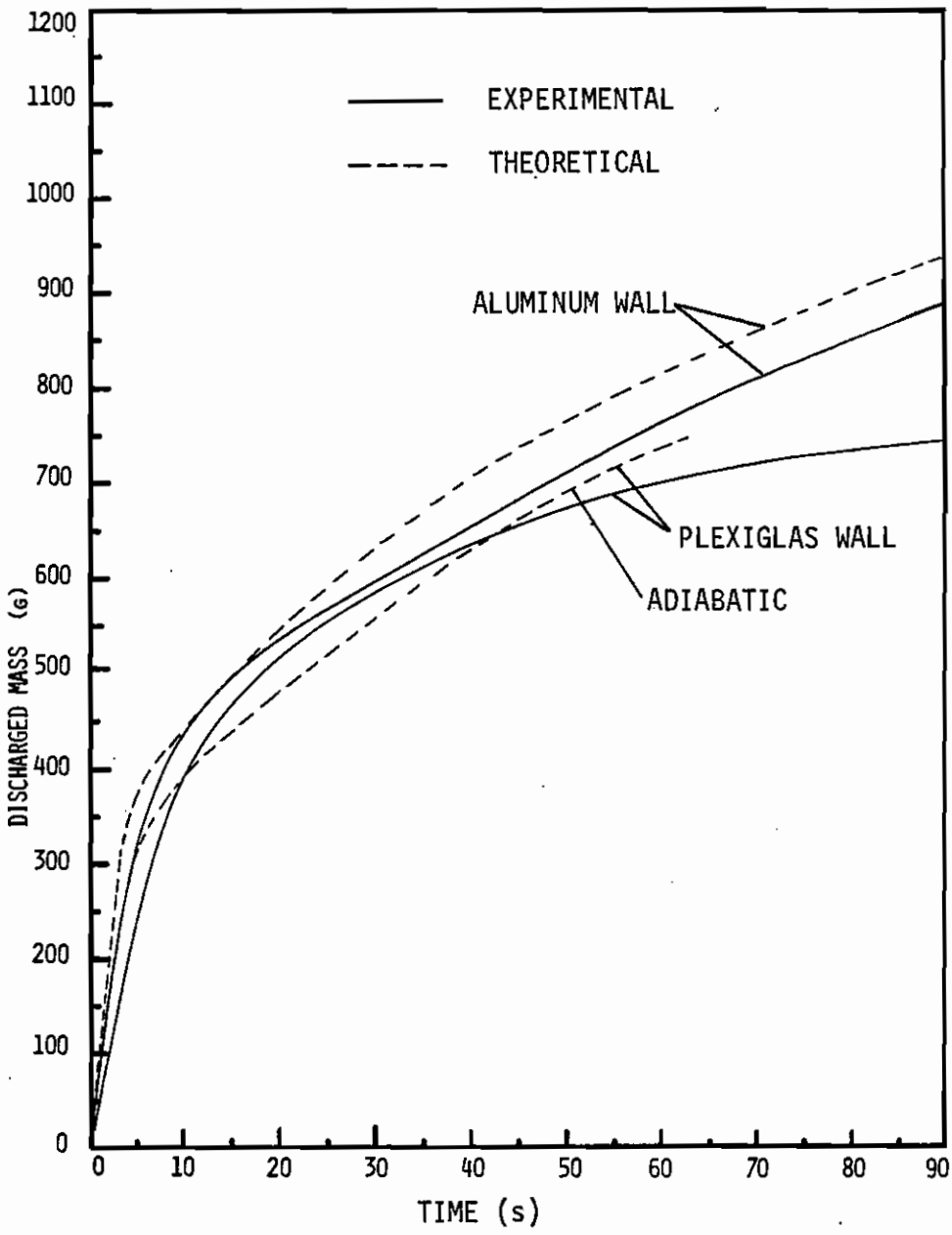

Figure 54. Theoretical and Experimental Mass Discharge: 3.18 mm orifice, 100% liquid fill tests.

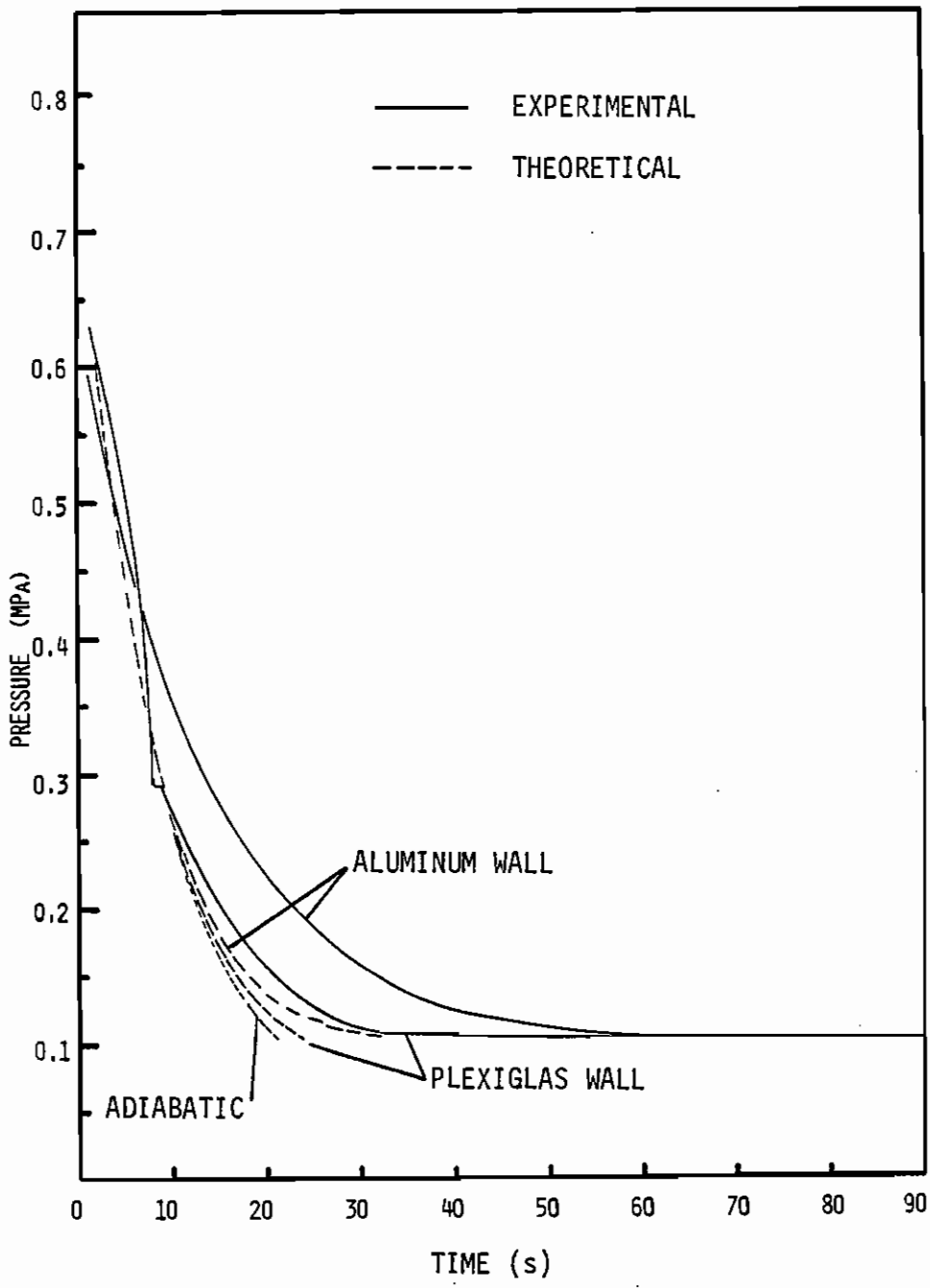

Figure 55. Theoretical and Experimental Pressure Decay: 4.76 mm orifice, 100% liquid fill tests.

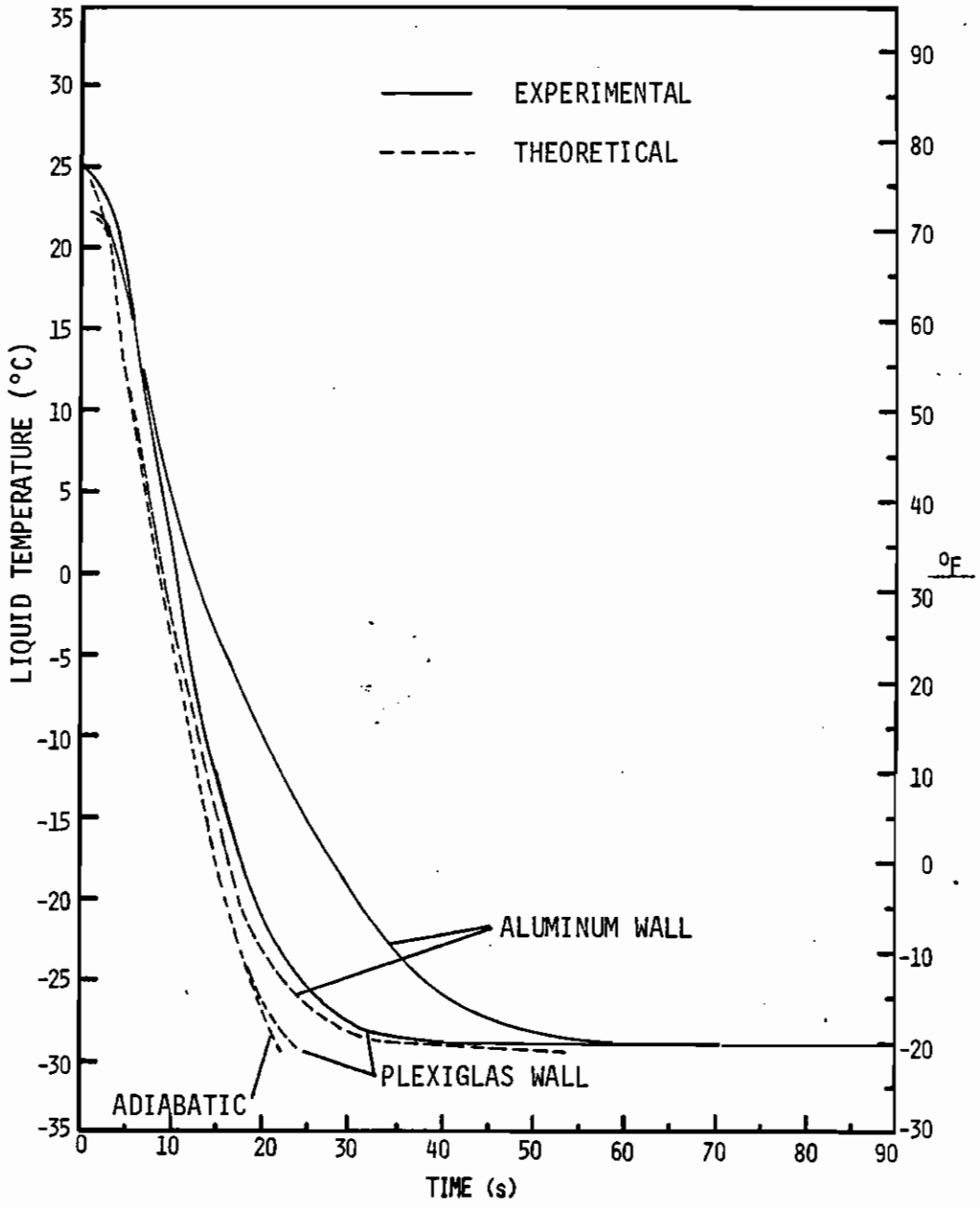

Figure 56. Theoretical and Experimental Temperature Decay: 4.76 mm orifice, 100% liquid fill tests.

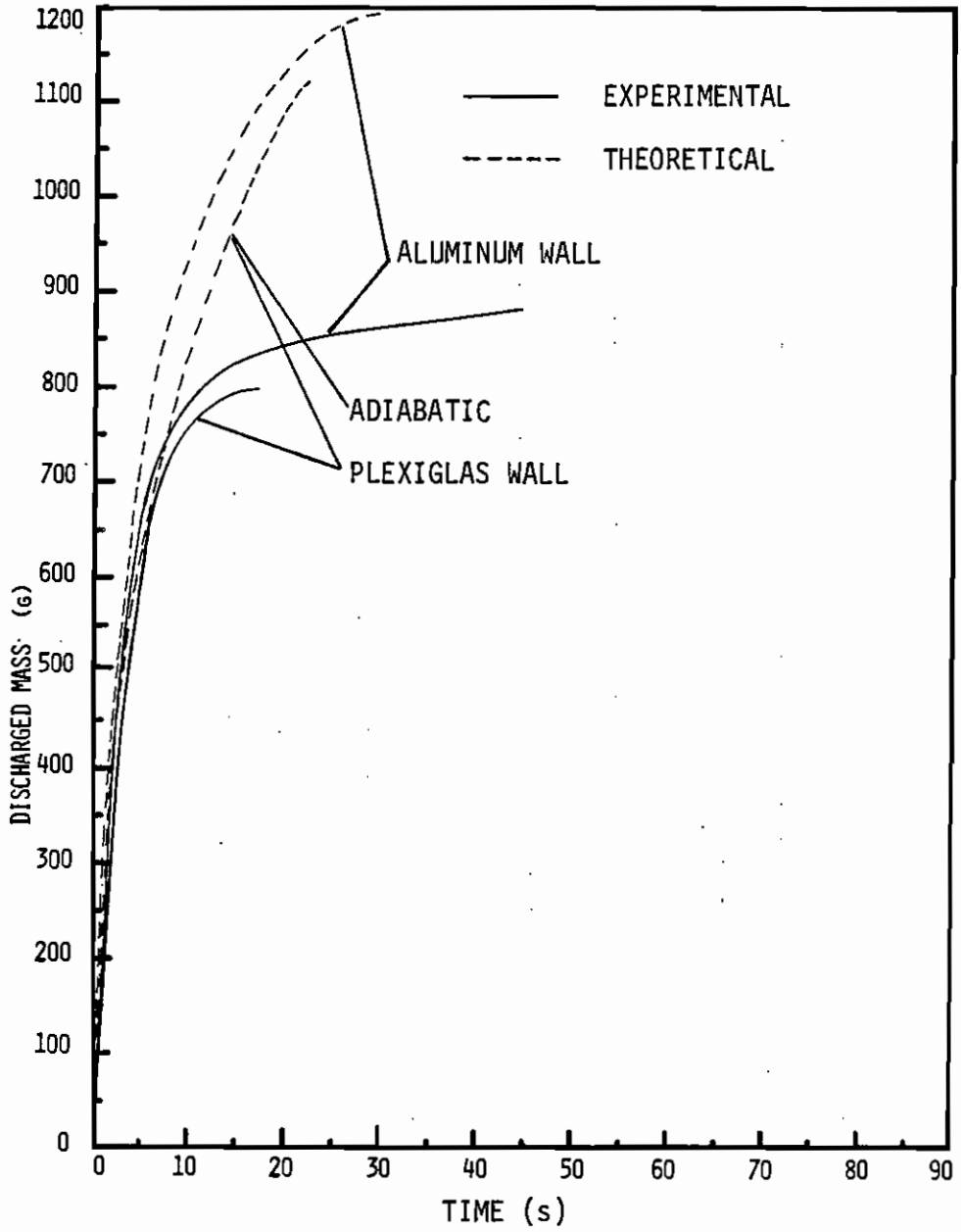

Figure 57. Theoretical and Experimental Mass Discharge: 4.76 mm orifice, 100% liquid fill tests.

For each orifice size test the pressure and temperature decays are retarded more as more energy is transferred to the fluid from the walls, as expected. The mass discharge rate, however, increases with additional heat input. This results from the consistently higher system pressure in higher heat input tests at any given time during the blowdown. The pressure, temperature and system mass profiles of the plexiglas wall model are only slightly different than those of the adiabatic model. The system property profiles of the aluminum wall model are significantly higher than either the plexiglas wall model or the adiabatic model. This corresponds well to the relative magnitudes of the heat input for the different tests, plotted in Figure 48.

Comparison of Individual Tests

The basic heat transfer model appears to follow the experimental results fairly well for the 1.59 mm orifice tests. Since pressure and temperature are not independent for a saturated fluid, the pressure and temperature graphs present nearly the same information. The model slightly underpredicts the thermodynamic state for the plexiglas wall test and overpredicts it for the aluminum wall test. The model accurately follows the experimentally measured mass discharge except for early in the two-phase discharge when the model's assumption of homogeneity is most in error.

For the 3.18 mm orifice tests the model predicts the system's thermodynamic state well, particularly for the aluminum wall test. For the plexiglas wall test the model seems to consistently underestimate the degree of heat input to the system and therefore underpredicts system pressure and temperature. As the blowdown progresses the model tends to

overpredict the mass discharged from the vessel.

For the 4.76 mm orifice tests the model again slightly underestimates the heat input in the plexiglas wall test. In the aluminum wall test, however, it grossly underestimates the heat input and therefore the system's instantaneous thermodynamic state. The mass discharge is predicted well during two-phase discharge, supporting the assumption of homogeneous flow. However, when vapor alone flows through the orifice the mass discharge is greatly overpredicted.

It is suspected that the thermal gradient in the vapor region and the consequent density gradient (lower vapor density near the orifice) hypothesized earlier may induce the model's overestimation of the mass discharge rate in the 3.18 and 4.76 mm orifice cases (the thermal gradient does not develop as rapidly in the 1.59 mm orifice tests). Assuming saturation throughout the vessel, the model would vent higher density vapor than should actually exist at the top of the chamber.

VI. CONCLUSION

The most significant conclusion that can be drawn from the application of this simple computer model is that the blowdown process can be accurately simulated by straightforward application of thermodynamic and fluid dynamic principles. The entire process can be treated as a mass and energy balance problem. The crucial points to be considered in the development of a theoretical blowdown model are as follow.

1. A precise equation of state must be developed for both the liquid and the vapor phases.
2. The correct two-phase flow model of the exit flow must be applied. This requires determination of the flow regime at all times during the blowdown.
3. Although detailed knowledge of the quality distribution throughout the chamber is not necessary, the flow quality through the exit section must be accurately determined.
4. The height of the boiling column should be known at all times since it influences exit conditions (through two-phase exit flow early in the blowdown and through the linear vapor region thermal gradient later).
5. The heat transfer to the system must be modeled, particularly nucleate boiling heat transfer at the walls of the vessel. This also includes modeling transient temperature distributions in the vessel's walls.
6. Nonequilibrium effects such as liquid superheating or subcooling and especially the thermal gradient in the vapor space must be accounted for.

The moderate success of the present model in predicting experimental results implies that the assumption of homogeneous two-phase exit flow may be sufficiently accurate for future application. The assumption of thermodynamic equilibrium in the boiling fluid column is based on experimental observations. Other assumptions require varying degrees of refinement to properly model the actual discharge of flashing fluids from finite vessels.

The experimental results presented in this report can be used as a basis for checking the accuracy of predictive models. The plexiglas wall tests, with their low environmental heat transfer rates, can be assumed adiabatic with small induced error (see Figures 49. through 57., pages 100 through 108) until relatively late times in the blowdowns. This is especially true in the 3.18 and 4.76 mm orifice tests.

REFERENCES

1. Tanger, G. E., Vachon, R. I. and Pollard, R. B.,"Pool Boiling Response to Pressure Decay," Proceedings of the 3rd International Heat Transfer Conference, Chicago, 1966, Vol. 4, pp. 38-43.

2. Ordin, P. M., Weiss, S. and Christenson, H., "Pressure-Temperature Histories of Liquid Hydrogen under Pressurization and Venting Conditions," Advances in Cryogenic Engineering, Vol. 5, Plenum Press, Inc., New York, 1960.

3. Clark, J. A., Van Wylen, G. J. and Fenster, S. K., "Transient Phenomena Associated with the Pressurized Discharge of a Cryogenic Liquid From a Closed Vessel," Advances in Cryogenic Engineering, Vol. 5, Plenum Press, Inc., New York, 1959.

4. Gühler, M., Hannemann, R. and Sallet, D., "Unsteady Two-Phase Blowdown of a Flashing Fluid from a Finite Reservoir," Proc. of the ICHMT International Seminar, Dubrovnik, Yugoslavia, 1978.

5. Sallet, D. W., Palmer, M. E. and Rod, S. R., "The Nonsteady Flow of Fluids from Pressure Vessels," Dynamics of Fluid-Structure Systems in the Energy Industry, M. K. Au-Yang and S. J. Brown, editors, ASME, PVP-39, New York, N. Y., 1979.

6. Sallet, D. W., Palmer, M. E., Rod, S.R., Nastoll, W. and Gühler, M., "The Discharge of a Flashing Fluid Through Tubes," Proceedings of the 2nd Multi-Phase Flow and Heat Transfer Symposium, University of Miami, 1979.

7. Howell, J. R. and Bell, K. J., "An Experimental Investigation on the Effect of Pressure Transients on Pool Boiling Burnout," Chemical Engineering Progress Symposium Series-Houston, Vol. 59, 1963, pp. 88-94.

8. Grolmes, M. A. and Fauske, H. K., "Axial Propagation of Free Surface Boiling into Superheated Liquids in Vertical Tubes," Proc. of 5th International Heat Transfer Conference, Tokyo, 1974, Vol. 4, pp. 30-34.

9. Tatom, J. W., Brown, W. H., Knight, L. H. and Coxe, E. F., "Analysis of Thermal Stratification of Liquid Hydrogen in Rocket Propellant Tanks," Advances in Cryogenic Engineering, Vol. 9, Plenum Press, Inc., New York, 1962, pp. 265-272.

10. Bailey, T. E. and Fearn, R. F., "Analytical and Experimental Determination of Liquid Hydrogen Temperature Stratification," Advances in Cryogenic Engineering, Vol. 9, Plenum Press, Inc., New York, 1964, pp. 254-264.

11. Wallis, Graham B., One-Dimensional Two-Phase Flow, McGraw-Hill Book Co., New York, N. Y., 1969.

12. Peebles, F. N. and Garber, H. J., "Studies on the Motion of Gas Bubbles in Liquids," Chemical Engineering Progress, Vol. 49, 1953, pp. 88-97.

13. Plexiglas, Product Bulletin PL-783e, Rohm & Haas Co., 1975.

14. Ozisik, M. Necati, Basic Heat Transfer, McGraw-Hill Book Co., New York, 1977.

15. Rohsenow, W. M., " Method of Correlating Heat Transfer Data for Surface Boiling Liquids," Transactions of the ASME, Vol. 74, 1952, pp. 969-975.

16. McAdams, W. H., Heat Transmission, McGraw-Hill Book Co., New York, 1954.

17. Martin, J. J. and Hou, Y. C., "Development of an Equation of State for Gases," A.I.Ch.E. Journal, Vol. 1, No. 2, 1955, pp. 142-151.

18. Thermodynamic Properties of Freon-12, Product Bulletin T-12, E. I. DuPont de Nemours & Co., Inc., 1956.

APPENDIX A. Governing Formulas of the Blowdown Model

The equations governing the flow of vapor and liquid through the exit section in the blowdown simulation are presented below. During two-phase discharge a modified version of the Bernoulli equation is employed. For homogeneous flow of a liquid-vapor mixture in thermal equilibrium the equation becomes

$$\dot{m} = c'A(2\cdot\bar{\rho}[P_{system} - P_{atm}])^{0.5} ,$$

where $c' = 0.62$ (valve coefficient for a square-edged orifice),

A = geometric orifice area,

$\bar{\rho} = (x/\rho_g + [1-x]/\rho_l)^{-1}$,

and x = flow quality.

This equation assumes steady flow. In the present model steady flow equations are applicable since properties of the system are held constant during each small timestep. Between timesteps new values for system properties are calculated.

The Bernoulli equation also assumes an incompressible fluid. For the early stages of the blowdown the flow is mostly liquid ($x \simeq 0.005$), so the assumption of incompressibility introduces relatively minor errors. In the absence of more detailed information on flow properties necessary for precise flow modeling, this approach appears sufficiently accurate for a first approximation. No attempt was made to model a low quality two-phase flow "choked" regime.

The equations for pure vapor flow are adapted directly from standard gas dynamics formulas. Assuming isentropic flow through the

orifice (valid in the absence of shock waves or major flow restrictions), the mass flow rate in the case of choked flow is given by

$$\dot{m} = \frac{A^* p_o}{\sqrt{\frac{ZR}{g_c} T_o}} \sqrt{k \left(\frac{2}{k+1}\right)^{\frac{k+1}{k-1}}}$$

where the compressibility factor Z is introduced to account for real gas effects according to the relation

$$Pv = ZRT$$

The area A^* is the effective area of the orifice under choked conditions and k is the ratio of specific heats, c_p/c_v.

When the exit flow is subsonic the mass flow rate is given by

$$\dot{m} = \frac{A p_o}{\sqrt{\frac{ZR}{g_c} T_o}} \sqrt{\frac{2k}{k-1} \left[\left(\frac{p}{p_o}\right)^{\frac{2}{k}} - \left(\frac{p}{p_o}\right)^{\frac{k+1}{k}}\right]}$$

The criterion by which the vapor flow regime is determined at the start of a new calculation loop is the ratio of the system pressure, p_o to the environmental pressure, p^*. For choked flow to exist the pressure in the reservoir must be

$$p_o \geq \frac{p^*}{\left(\frac{2}{k+1}\right)^{\frac{k}{k-1}}}$$

A new system temperature is computed at the end of each timestep by an iterative process. The specific internal energies of the vapor and liquid are functions of temperature. Trial temperature are used in the equation

$$E_{system} = m_{system}(x \cdot u_g(T) + [1-x] \cdot u_f(T)) \quad ,$$

until the trial system internal energy equals (within a predetermined error) the system internal energy calculated from the mass and enegy balance equations.

The new system pressure is calculated from the Clausius-Clapyron equation:

$$dP = (h_{fg}/[T \cdot v_{fg}]) \cdot dT \qquad (T \text{ in } °K) \quad ,$$

where in the case of the model dP and dT are the incremental changes in pressure and temperature for one calculation loop. As the blowdown proceeds the timestep is modified as required to assure that the Clausius-Clapyron equation remains valid (i.e. $dP \ll P$ and $dT \ll T$).

APPENDIX B. APPLICATION OF THE MARTIN - HOU EQUATION OF STATE TO THE GENERATION OF PRESSURE-VOLUME-TEMPERATURE DATA FOR PURE SATURATED VAPOR

In their original paper Martin and Hou developed an equation of state of the form:

$$P = \frac{RT}{V-b} + \frac{A_2+B_2T+C_2e^{kT/T_c}}{(V-b)^2} + \frac{A_3+B_3T+C_3e^{kT/T_c}}{(V-b)^3} + \frac{A_4}{(V-b)^4} + \frac{B_5T+C_5e^{kT/T_c}}{(V-b)^5}$$

where the A, B and C coefficients and the constants 'b' and 'k' can be determined by a method outlined in the article [17]. To determine the appropriate coefficients the following input is required:

1. the critical properties of the material under study; critical pressure, temperature and specific volume.
2. a point on the vapor pressure curve.
3. the Boyle temperature.
4. a temperature T', determined empirically by the authors and subsequently read from a graph in their article.
5. a factor β, also read from a graph in the article.
6. the gas constant, R, for the material.

For this investigation a computer program was written which employs the outlined method to generate a first approximation of the constants and coefficients required by the equation of state, compare computed pressures to a set of experimentally determined P-V-T data and adjust the factors T', T_B and the exponential factor k to achieve the minimum error. Thus an optimized equation of state, typically with an average error less than 0.1% is generated. The details of the computer program's operation follow.

The program first reads the input data. There is in reality no freedom of choice in selection of the critical properties. The vapor pressure data point is used to calculate the derivative:

$$\left(\frac{dP}{dT}\right)_{V_{crit}}$$

which in turn is used to determine the coefficients A_3 and B_3. The data point should be chosen relatively near the critical point to closely approximate the slope of the pressure curve along the critical isometric. However, the deviation is small and the ultimate effect of lowering the test temperature is the very slight raising of the vapor pressure calculated from the equation of state near the critical point. As an example, for Freon-12, lowering the test temperature by 5° F below T_{crit} (a change of 1%) raises the value of B_3 by 0.2%, A_3 by 0.06% and the vapor pressure near the critical point by 0.001%. Thus the choice of the pressure curve data point is not crucial since the later optimization of other parameters will compensate for small perturbations of the calculated pressure that choices of different pressure data points induce.

The Boyle temperature (T_B) varies for different gases but is typically about 2.1 to 2.5 times the critical temperature. Since T_B is usually not known to great accuracy it was chosen as one of the parameters to be varied in search of the best fit of the equation of state to experimental data. For points along the saturated vapor curve raising T_B raises the computed pressure at high temperatures and densities (approaching the critical point) and lowers very slightly the pressure at low temperatures and densities. The initial value of T_B chosen for our calculations was 2.3 X T_{crit}.

The "best" value of the parameter T' varies for different gases but, as was found by Martin and Hou, it remains near 0.80 times the critical temperature. The initial value of T' was therefore chosen as 0.80 X T_{crit} and was then varied systematically to find the "best" value. Raising T' lowers the computed pressure all along the saturation curve but the effect is most pronounced at high temperatures and densities. In fact, all manipulation of parameters had greater effect at higher temperatures and densities, which is reasonable since the deviation from perfect gas behavior is more pronounced there and the contributions of the correction terms in the equation of state become more significant.

The factor β was empirically fitted by Martin and Hou as a function of the compressibility factor Z at the critical point:

$$\beta = -31.883 \times Z_{crit}^2 + 20.533 \times Z_{crit} \qquad \text{where } Z_{crit} = \frac{P_{crit} V_{crit}}{R T_{crit}}$$

β was not altered during the optimization procedure.
In Martin and Hou's paper [17] the exponential factor 'k' was a constant equal to -5.475. To arrive at this value the authors optimized their equation of state by varying k while holding all other parameters constant for the seven compounds they investigated (CO_2,H_2O, N_2, etc.). Their result was duplicated in our calculations for CO_2, which tends to verify the method, but there is no assurance that other compounds would be best fit by the same value of k. Thus k was the third and final parameter varied in our optimization. Raising the value of k raises computed pressures at low temperatures and densities but lowers pressures at high temperatures and densities.

The optimization procedure was implemented by minimizing the average error of a set of experimental data points on the saturated vapor curve for the material under study. The number of data points employed was usually around 20 for economy of computer time considering the fairly large number of calculations required for each data point in each iteration. Only one parameter at a time was varied since the effect of each on the equation of state is complex and so trying to simultaneously optimize all three would slow convergence and increase the risk of non-convergence through interfering effects. In terms of percentage change in computed pressure induced by a given percentage change in a parameter, T' had the greatest influence, followed in order by T_B and k. The latter two parameters had an "influence" about an order of magnitude less than that of T' and on this basis the order of optimization was chosen as T',T_B,k. The optimization procedure was tried with the other possible permutations of T',T_B and k (e.g.,T',k,T_B and T_B,k,T') but the originally chosen sequence did indeed yield the best overall accuracy. The results of the optimization are presented below for eight materials for which accurate P-V-T data was available.

Table B-1. Results of First Set of Trial Optimizations

MATERIAL	T'	T_B	k	average % deviation
carbon dioxide	.7960	2.197	-5.475	0.61%
chlorine	.7565	2.161	-4.487	0.01%
Freon-12	.7990	2.137	-5.634	0.04%
Freon-22	.8020	2.254	-5.126	0.05%
butadiene	.7931	1.885	-4.487	0.08%
methyl chloride	.8110	1.885	-5.031	0.13%
sulfur dioxide	.8070	1.885	-4.532	0.18%
ammonia	.8304	1.885	-5.776	0.73%

Conclusion:

The systematic optimization of the three parameters T',T_B and k appears sufficient to produce an equation of state that is consistently accurate to within ±1% of experimental data on the saturated vapor curve. In the cases of butadiene, methyl chloride, sulfur dioxide and ammonia, the same values of T_B probably indicate that the optimization was terminated at the maximum allowed number of iterations rather than at the best value of T_B. Future trials with a lower initial value of T_B or more allowed iterations may improve the accuracy for these compounds (all these compounds currently have accuracies that are noticably higher than the others, though still within the typical error originally anticipated by Martin and Hou).

One important feature of this optimization routine is its ability to fit data on specific regions on the saturation curve. By selecting the data points in a particular region, the user can optimize the equation of state for that region, gaining additional accuracy there (at the expense of accuracy in regions that are not of particular interest).

It is conceivable that if additional accuracy is require beyond the best values of T',T_B and k, that optimization can be done for other parameters (e.g.; β, vapor pressure test point for dP/dT calculation) but note that the accuracy of the equation of state is ultimately limited by the accuracy of the experimental data used to optimize it.

APPENDIX C. Listing of the Computer Program

The computer model of the nonsteady blowdown of a flashing fluid from a finite reservoir is listed herein. In actual practice the modeling method is more important than the details of the program presented here. A flowchart of the program is included as Figure C-1.

Figure C-1. Flowchart of the Blowdown Model Process.

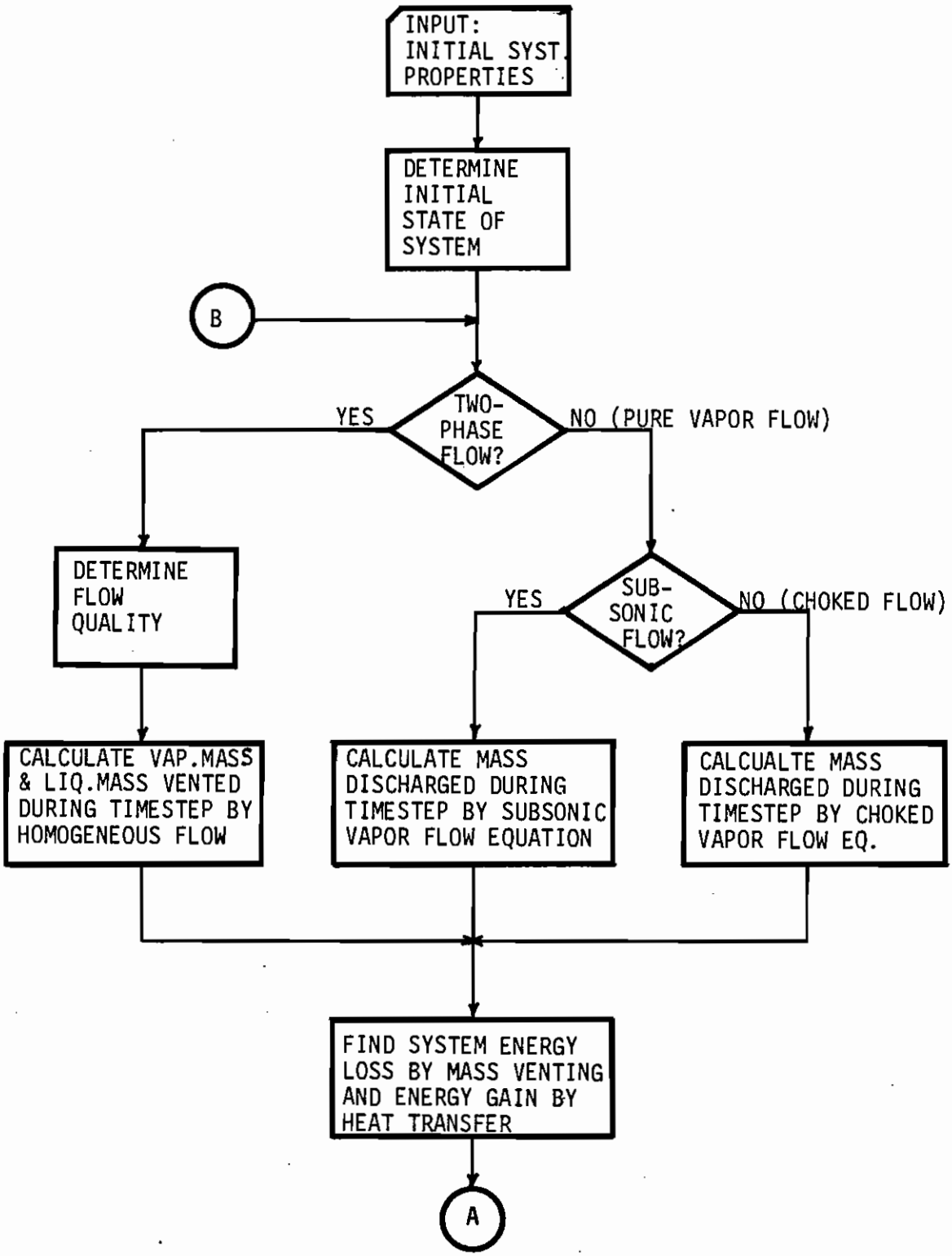

Figure C-1. Flowchart of the Blowdown Model (continued).

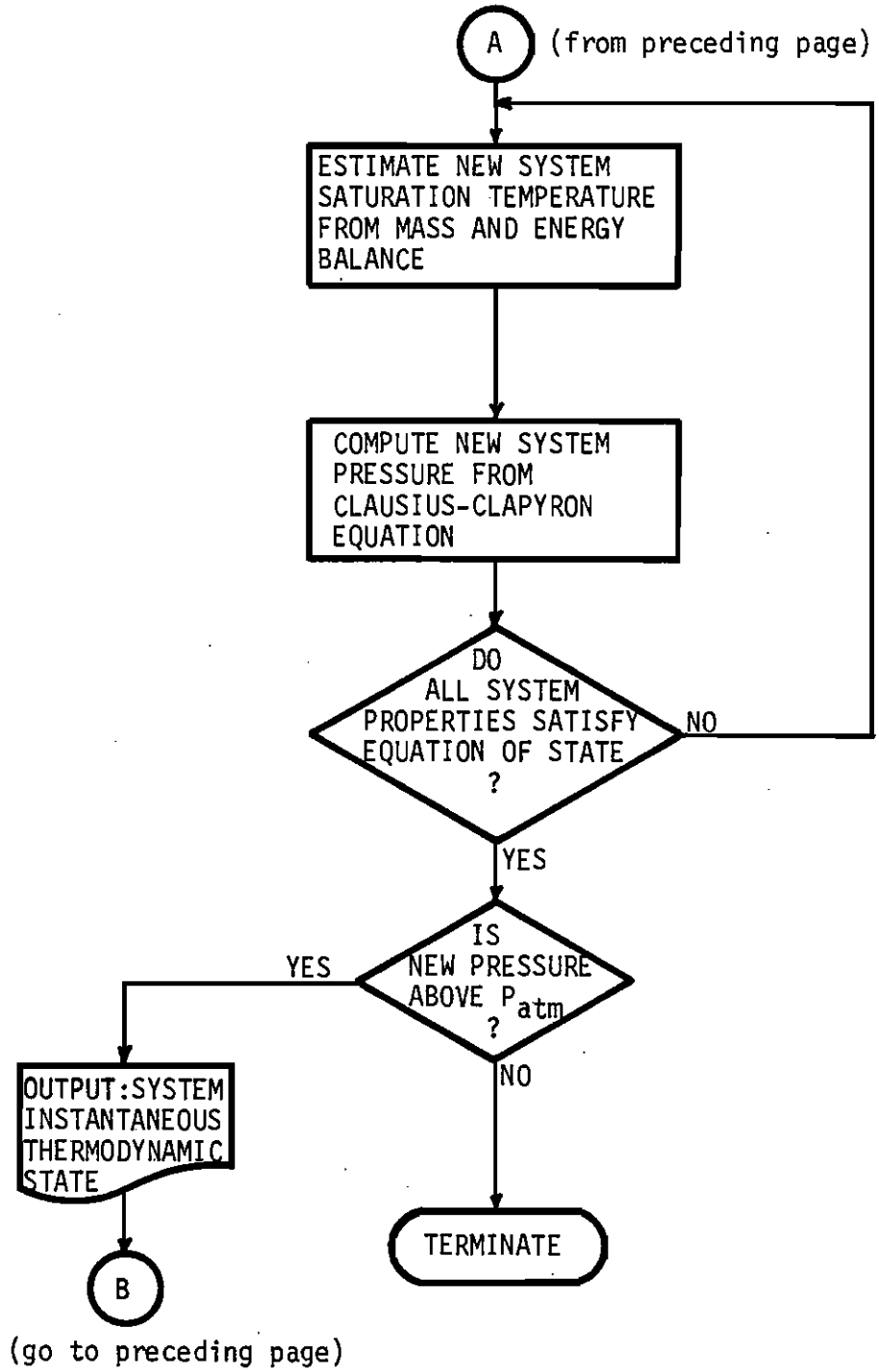

```
-RALPH,FIS BLODON
C             THIS PROGRAM CALCULATES SYSTEM TEMPERATURE AND PRESSURE
C             AND MASS FLOW AS A FUNCTION OF TIME FOR A SINGLE-COMPONENT,
C             TWO-PHASE (VAPOR/LIQUID) SYSTEM VENTING TO THE ATMOSPHERE
C             THROUGH AN ORIFICE.  THIS MODEL ASSUMES THAT EQUILIBRIUM
C             BETWEEN THE PHASES IS MAINTAINED.
C
C            'REQUIRED INPUT)
C            CARD 1)  NAME OF THE SUBSTANCE UNDER STUDY (M1 THROUGH M8)
C            CARD 2)  MOLECULAR WEIGHT OF SUBSTANCE (WT) /
C                       TOTAL VOLUME OF CLOSED SYSTEM (VOL) /
C                       AMBIENT PRESSURE  (PATM)
C                     INITIAL SYSTEM PRESSURE (P) /
C                       INITIAL SYSTEM TEMPERATURE (T) /
C                       INITIAL MASS OF LIQUID IN SYSTEM (ML)
C                     PHYSICAL CROSS-SECTIONAL AREA OF ORIFICE (ASTAR) /
C                       VALVE COEFFICIENT FOR ORIFICE (VC) /
C                       ISENTROPIC EXPANSION COEFFICIENT (K)
C                     COMPRESSIBILITY FACTOR (Z)  (ESTIMATE TO START RUN)/
C                     MAXIMUM QUALITY OF 2-PHASE COLUMN (HIQUAL)
C            CARDS 3,4 + 5)  COEFFICIENTS FOR THE MARTIN-HOU EQUATION OF
C                            STATE FOR THE SUBSTANCE UNDER STUDY.
C            CARD 6) CRITICAL PRESSURE (PC),(PSIA) /
C                    CRITICAL VOLUME (CV), (CU.FT./LBM) /
C                    CRITICAL TEMPERATURE (TC),(DEG. F) /
C                    MARTIN-HOU EXPONENTIAL FACTOR (Y) /
C                    MARTIN-HOU T- FACTOR (TP) /
C                    BOYLE TEMPERATURE (TB), (OPTIMIZED FOR M.H. FIT)
C             CARD 7) COEFFICIENTS FOR THE LIQUID SPECIFIC VOLUME FUNC.
C             CARD 8) TOTAL WINDOW HEAT CAPACITY (CWIN), (BTU/DEG C) /
C                       WINDOW CONDUCTIVITY (XKWIN), (BTU/FT/S/DEG F) /
C                       WINDOW VOLUME (VWIN),  (CU FT) /
C                     TOTAL  WALL  HEAT CAPACITY (CWALL),(BTU/DEG C) /
C                      WALL   CONDUCTIVITY (XKWALL) (BTU/FT/S/DEG F) /
C                      WALL   VOLUME (VWALL), (CU FT)
C
C             OUTPUT)  TIME  (SECONDS)
C                      TIMESTEP  (SECONDS)
C                      PRESSURE  (PSIA) --SYSTEM PRESSURE
C                      TEMP  (DEGREES F) --SYSTEM TEMPERATURE
C                      TOT MASS (LBM) --TOTAL MASS IN SYSTEM
C                      LIQ MASS (LBM) --TOTAL LIQUID MASS IN SYSTEM
C                      VAP MASS (LBM) --TOTAL VAPOR MASS IN SYSTEM
C                      MASS FLO (G/S) --INSTANTANEOUS MASS FLOW RATE
C                      SYS ENERGY (BTU) -- TOTAL SYSTEM INTERNAL ENERGY
C                      HEAT IN (BTU) -- HEAT INPUT DURING TIMESTEP
C                      TOT HEAT (BTU)--TOTAL HEAT INPUT FROM WALLS
C  ***********************************************************************
C
      DIMENSION A(5),B(5),C(5),F(5)
      IMPLICIT DOUBLE PRECISION (A-H,O-Z)
      DOUBLE PRECISION K,KSTAR,M,ML,MV,MV1,LSPV
      COMMON A,B,C,Y,TP,TB,PC,CV,TC,R,D,F,WT
      HFG(X)=.687996492E+02-.110037256*X-.17298907E-03*X*X
      LSPV(X)=.11021757E-01+.12912381E-04*X+.355661376E-07*X*X
  200 FORMAT(95H   MOL WT      VOLUME      AMB PRES    SYS PRES    SYS TEMP
     1  LIQ MASS  VALV AREA  VALV COEF      K ,18H          COMPR (Z)/)
  300 FORMAT(2X,11F11.5)
  310 FORMAT(8A6)
```

```
  350 FORMAT(1H1,-MATERIAL *** -,8A6//)
  400 FORMAT(120H0   TIME        TIMESTEP   PRESSURE    TEMP       TOT MAS
     1S   LIQ MASS    VAP MASS    MASS FLO  SYS ENERGY  HEAT IN   TOT HEAT)

C             READ INPUT AND INITIALIZE  VARIABLES AS NECESSARY

      READ(5,310) M1,M2,M3,M4,M5,M6,M7,M8
      INPUT WT,VOL,PATM,P,T,ML,ASTAR,VC,K,Z,HIQUAL
      INPUT (A(I),B(I),C(I),I=1,5),PC,CV,TC,Y,TP,TB
      INPUT(F(I),I=1,5)
      INPUT CWIN,XKWIN,VWIN,CWALL,XKWALL,VWALL
      WRITE(6,350)M1,M2,M3,M4,M5,M6,M7,M8
      WRITE(6,200)
      WRITE(6,300) WT,VOL,PATM,P,T,ML,ASTAR,VC,K,Z
      WRITE(6,400)
      PC=PC/14.696
      TC=TC+459.69
      TWIN=T
      TWALL=T
      SCOND=0.
      R=.73/WT
      D=(31.883*PC*CV/R/TC-5.533)*CV/15.
      Q=T+459.69
      S=P/14.696
      VVAP=VSPV(Q,S)
      VLIQ=LSPV(T)

C             DETERMINE INITIAL PHASE EQUILIBRIUM CONDITIONS

      VL=VLIQ*ML
      VV=VOL-VL
      MV=VV/VVAP
      M=ML+MV
      HRGAS=HVAP(S,VVAP,Q)
      UVAP=HRGAS-S*VVAP*2.721316
      UTOT=(HRGAS-HFG(T)-S*VLIQ*2.721316)*ML+UVAP*MV

C             DETERMINE INITIAL TIMESTEP

      TAU=2.
      DM =.02*MV
      DTAU= DM/ASTAR/2.54/VC/P/SQRT(WT/Z/Q)
      WRITE(6,300) TAU,DTAU,P,T,M,ML,MV,DM,UTOT,XCOND,SCOND

C             TIMESTEP LOOP (IN WHICH CALCULATIONS OF INCREMENTAL MASS
C             FLOW AND NEW EQUILIBRIUM CONDITIONS ARE MADE)

      DO 80 JJ=1,300

C             DETERMINE FLOW REGIME

      IF(P.LT.14.8) GO TO 90
      QUAL=MV/M
      IF(QUAL.GT.HIQUAL) GO TO 60

C             TWO-PHASE FLOW. HOMOGENEOUS MODEL

      DENAV=M/VOL
      DM=DTAU*96.2606*ASTAR*SQRT(DENAV*(P-PATM))*VC
```

```
      DMV=QUAL*DM
      DL=DM-DMV
      GO TO 3
   60 K=CPCV(S,VVAP,Q)

C             CRITP = SUBSONIC/CHOKED  FLOW TRANSITION CRITERION FOR
C             VAPOR FLOW (ONE PHASE)

      CRITP=((K+1.)/2.)**(K/(K-1.))
      IF(P/PATM.LT.CRITP) GO TO 20

C             CHOKED FLOW

      KSTAR=K*(2./(K+1.))**((K+1.)/(K-1.))
      GO TO 30

C             SUBSONIC FLOW

   20 KSTAR=((PATM/P)**(2./K)-(PATM/P)**((K+1.)/K))*2.*K/(K-1.)
   30 DMV=68.0666*ASTAR*DTAU*DSQRT(KSTAR*P/VVAP)*VC
      DM=DMV

C             DETERMINE INCREMENTAL CHANGE IN SYSTEM TEMPERATURE.
C            (CALCULATION OF NEW EQUIL. TEMP. FROM ENERGY & MASS BALANCE)

      DL=0.
    3 CONTINUE
      M=M-DM
      ML=ML-DL
      MV1=MV-DMV
      HRGAS=HVAP(S,VVAP,Q)
      HTLIQ=VL/.03048
      AWIN=.5208*HTLIQ
      AWALL=.2292*HTLIQ
      QWIN=XKWIN*DTAU*(TWIN-T)/VWIN*AWIN*AWIN
      QWALL=XKWALL*DTAU*(TWALL-T)/VWALL*AWALL*AWALL
      XCOND=QWIN+QWALL

C             XCOND IS THE TOTAL HEAT INPUT FROM THE VESSEL WALLS.

      UTOT=UTOT-(HRGAS-HFG(T))*DL-HRGAS*DMV+XCOND
      SCOND=SCOND+XCOND
      TWIN=TWIN-QWIN/CWIN
      TWALL=TWALL-QWALL/CWALL
      DT=.1
      T2=T
      VFG=VVAP-VLIQ
      HHFG=HFG(T2)
      DO 10 I=1,40

C             DETERMINE INCREMENTAL CHANGE IN SYSTEM PRESSURE USING
C             CLAUSIUS-CLAPYRON EQUATION

      DP=HHFG/VFG/Q/.18509*DT
      P=P-DP
      T2=T2-DT
      Q=T2+459.69
      S=P/14.696
      VVAP=VSPV(Q,S)
```

```
      VLIQ=LSPV(T2)
      DMV2=(VOL-VLIQ*ML-WVAP*MV1)/(WVAP-VLIQ)
      HRGAS=HVAP(S,WVAP,Q)
      UTEST=(HRGAS-HFG(T2)-S*VLIQ*2.721316)*(ML-DMV2)+(HRGAS-S*WVAP*2.72
     11316)*(MV1+DMV2)
      IF(ABS(UTEST-UTOT).LT.0.00005*UTOT) GO TO 15
      IF(UTEST.GT.UTOT) GO TO 10
      T2=T2+DT
      P=P+DP
      DT=DT*.2
   10 CONTINUE
   15 CONTINUE
      MV=MV1+DMV2
      ML=ML-DMV2
      IF(ML.LT.0.) GO TO 90
      VL=VLIQ*ML
      VV=VOL-VL
      DT=T2-T
      T=T2
      VVAP=WVAP
      TAU=TAU+DTAU
      DM=DM/DTAU
      WRITE(6,300) TAU,DTAU,P,T,M,ML,MV,DM,UTOT,XCOND,SCOND

C           ADJUST TIMESTEP, IF NECESSARY, TO INSURE THAT EQUILIBRIUM
C           ASSUMPTION REMAINS VALID AND THAT TIMESTEP IS NOT SO SMALL
C           THAT IT UNDULY INCREASES COMPUTATION TIME.

      IF(DT.GT.0.) GO TO 90
      IF(DT/Q.GT.-.0005) GO TO 23
      IF(DT/Q.LT.-.005) GO TO 22
      GO TO 40
   22 DTAU=DTAU/2.
      GO TO 40
   23 DTAU=DTAU*1.5
   40 CONTINUE
   80 CONTINUE
   90 CONTINUE
      WRITE(6,300) TAU,DTAU,P,T,M,ML,MV,DM,UTOT,XCOND,SCOND
      STOP
      END
```

```
-RALPH,FIS VSPV
      FUNCTION VSPV(T,P)
C  ***********************************************************************
C  *  THIS PROGRAM COMPUTES THE SPECIFIC VOLUME OF A VAPOR ASSOCIATED    *
C  *  WITH A GIVEN TEMPERATURE AND PRESSURE ON THE SATURATION CURVE.     *
C  *  THE MARTIN-HOU EQUATION OF STATE IS USED.                          *
C  ***********************************************************************
      DIMENSION A(5),B(5),C(5),E(5)
      IMPLICIT DOUBLE PRECISION (A-H,O-Z)
        COMMON A,B,C,Y,TP,TB,PC,CV,TC,R,D,E,WT
      EX=DEXP(Y*T/TC)
      DV=.05
      V=1.05*R*T/P
      DO 70 J=1,100
      V=V-V*DV
      VD=V-D
      PTEST=(((((B(5)*T+C(5)*EX)/VD+A(4))/VD+(A(3)+B(3)*T+C(3)*EX))/VD+(
     1A(2)+B(2)*T+C(2)*EX))/VD+R*T)/VD
      IF(DABS(PTEST/P-1.).LT.0.00001) GO TO 60
      IF(P-PTEST) 20,60,70
   20 V=V+V*DV
      DV=DV/5.
   70 CONTINUE
   60 VSPV=V
      RETURN
      END
```

```
-RALPH,FIS HVAP
      FUNCTION HVAP(P,V,T)
C
C             THIS PROGRAM COMPUTES THE VAPOR ENTHALPY FOR A REAL GAS.
C
      IMPLICIT DOUBLE PRECISION (A-H,O-Z)
      DIMENSION A(5),B(5),C(5),E(5)
            COMMON A,B,C,Y,TP,TB,PC,CV,TC,R,D,E,WT
      RR=1.9869/WT
      W=V-D
      HIG=(((E(5)*T+E(4))*T+E(3))*T+E(2))*T+E(1)
      Z=Y/TC
      E=DEXP(Z*T)
      H=0.
      DO 10 I=2,5
      H=H+(A(I)+C(I)*(1.-Z*T)*E)/FLOAT(I-1)/W**(I-1)
   10 CONTINUE
      HVAP=HIG+(P*V+H)*2.721316-RR*T
      RETURN
      END
```

```
-PALPH,FIS CPCV
      FUNCTION CPCV(P,V,T)
C
C             THIS PROGRAM CALCULATES THE RATIO OF SPECIFIC HEATS (CP/CV)
C             OF A REAL GAS.
C
      IMPLICIT DOUBLE PRECISION (A-H,O-Z)
      DIMENSION A(5),B(5),C(5),F(5)
          COMMON A,B,C,Y,TP,TB,PC,CV,TC,R,D,F,WT
      RR=1.9869/WT
      W=V-D
      CPIG=((4.*F(5)*T+3.*F(4))*T+2.*F(3))*T+F(2)
      CVIG=CPIG-RR
      Z=Y/TC
      E=DEXP(Z*T)
      CV=C(2)/W+C(3)/2./W/W+C(5)/4./W**4
      CV=CVIG-T*Z*Z*E*CV*2.721316
      CP=RR*T/W/W
      DO 20 I=2,5
      CP=CP+(A(I)+B(I)*T+C(I)*E)*FLOAT(I+1)/W**(I+1)
   20 CONTINUE
      Z=(((B(5)-C(5)*Z*E)/W/W+B(3)-C(3)*Z*E)/W+B(2)-C(2)*Z*E)/W/W+RR/W
      CP=CV+T*Z*Z/CP*2.721316
      CPCV=CP/CV
      RETURN
      END
```